Reactivity and Structure of Supported Nickel Phosphides (Ni_2P) in Deep Hydrodesulfurization Catalysis

Yong-Kul Lee

Dissertation submitted to the faculty of Virginia Polytechnic Institute and State University in partial fulfillment of the requirement for the degree of

Doctor of Philosophy
in
Chemical Engineering

S. Ted Oyama, Chairman

David F. Cox

Rickey M. Davis

Brian E. Hanson

Amadeu K. Sum

December 16, 2004

Blacksburg, Virginia

Keywords: Nickel phosphide, HDS, HDN, 4,6-DMDBT, EXAFS, FTIR

Reactivity and Structure of Supported Nickel Phosphides (Ni_2P) in Deep Hydrodesulfurization Catalysis

by

Yong-Kul Lee

Chemical Engineering

Abstract

This dissertation describes preparation and characterization of Ni_2P catalysts and their application in deep hydrodesulfurization (HDS) of a model sulfur compound, 4,6-dimethyldibenzothiophene (4,6-DMDBT), one of the most refractory S-compounds. This topic is of great importance in addressing recently enacted environmental regulations limiting the sulfur content in fuels. The work carried out includes synthesis of Ni_2P on different siliceous supports, SiO_2, MCM-41, and ultra-stable Y zeolite (USY). It also includes determining the characteristics of the supported Ni_2P catalysts with a wide range of techniques: X-ray powder diffraction (XRD), transmission electron microscopy (TEM), Fourier transform infrared (FTIR) and X-ray absorption fine structure (XAFS) spectroscopy. The use of these techniques allowed better understanding of the nature of the active sites as well as the effect of supports. Activity tests were conducted in the HDS of 4,6-DMDBT and the HDN of quinoline. The performance of the catalysts will be compared to that of a

conventional sulfide hydrotreating catalyst, Ni-Mo-S/Al_2O_3. Investigation of the reaction mechanism in the hydrodenitrogenation (HDN) of 2-methylpiperidine together with in situ FT-IR measurements were conducted to understand how catalyst properties affect activity and selectivity.

To my mother In-Sill Park

and

my family Sun-Gwang and Juwon

Acknowledgements

"I will give you thanks, for you answered me; you have become my salvation [Psalm 118:23]"

I would like to express my sincere gratitude to my advisor, Dr. S. Ted Oyama for his guidance and careful advice. I am deeply grateful for his continuous support and encouragements. I also appreciate the efforts made by the committee members Dr. Cox, Dr. Davis, Dr. Hanson, and Dr. Sum.

During the last five years, our research group (Environmental Catalysis and Nanomaterials Laboratory) in close cooperation with the Surface Science Laboratory group has provided me with a unique educational environment and helped me broaden my academic and professional perspectives. I would like to thank to our past and current group members for their help: Corey Reed, Doohwan Lee, Juan Bravo, Xianqin Wang, Wang-Jae Chun, Yunfeng Gu, Yuying Shu, Yan Xi, Pelin Hacarlioglu, Travis Gott, and Hankwon Lim. I thank the Chemical Engineering Department staff, Riley Chan, Chris Moore, Diane Cannaday, and Michael Vaught for their support and help.

I am grateful to Pastor Chung, brothers and sisters in the Korean Baptist Church of Blacksburg, and I would like to give special thanks to the bible study group for our fellowship in Jesus Christ.

Words cannot express how grateful I am to my family. I would like to express my sincere appreciation to my mother, In-Sill Park, for her prayers and all the sacrifices she made throughout her life for the family. Much appreciation goes to my brother, In-Kul, for his understandings and encouragements.

Profound and tender love from my heart goes to my wife, Sun-Gwang. She has been standing by me during the rough times, and she has supported me in every aspect of my work. Special thoughts go to my child, Juwon.

Finally, I would like to share the joy of this small achievement with my father who rests in heaven with the Lord.

Table of Contents

Chapter 3

The Nature of a SiO_2-Supported Ni_2P Catalyst for Hydrotreating: EXAFS and FTIR studies

Chapter 4

A Novel Nickel Phosphide (Ni_2P) Catalyst Supported on KUSY Zeolite for the Hydrodesulfurization of 4,6-DMDBT

Chapter 5

Mechanism of Hydrodenitrogenation on Phosphides and Sulfides

List of Tables

List of Figures

List of Schemes

List of Abbreviations

- BET – Brunauer-Emmett-Teller
- BJH - Barrett-Joyner-Halenda
- BT/MBT/DMBT/TMBT- benzothiophene/methyl-/dimethyl-trimethylbenzothiophene
- DBT – dibenzothiophene
- DMBCH - dimethylbicyclohexane
- 3,3-DMBP - 3,3-dimethylbiphenyl
- 4,6-DMDBT – 4,6-dimethyldibenzothiophene
- DMDS - dimethyldisulfide
- DDS – direst desulfurization
- EXAFS – extended X-ray absorption fine structure
- FTIR – Fourier transform infrared
- HDN – hydrodenitrogenation
- HDS – hydrodesulfurization
- HYD / deHYD – hydrogenation / dehydrogenation
- ICP-AES - inductively coupled plasma-absorption emission spectroscopy
- MCHT - methylcyclohexyltoluenes
- 4-MDBT – 4-methyldibenzothiophene
- TEM - transmission electron microscopy
- TPD - temperature-programmed desorption
- TPR – temperature-programmed reduction
- XRD – X-ray diffraction

Chapter 1

Introduction

1.1. Growing Importance of Deep Hydrodesulfurization (HDS)

Because of their high energy densities and convenient physical form, petroleum products are presently being consumed in vast quantities, and this usage continues to grow at alarming rates. This high consumption is having a major impact on the global environment [1]. Transportation fuels, the major petroleum products, are receiving high scrutiny, because the pollution in exhaust gases is difficult to control [2]. Pollutants of major concern in exhaust gases include SO_x, CO, NO_x, particulates, trace elements, olefins, aromatic hydrocarbons, and their interaction products. One key feature in environmental control is the level of SO_x in the exhaust, as it contributes to acid rain, poisons catalysts in catalytic converters, and participates in the cycle of atmospheric gas chemistry that leads to ozone production and smog [3,4].

Table 1.1 Sulfur limit of gas oil

	1990-1994	1995-2000	Post 2000
USA	500 ppm	500 ppm	15 ppm by 2006 [5]
Europe	500 ppm	500 ppm	10 ppm by 2011 [6]
Japan	0.2 wt%	500 ppm	50 ppm by 2005 [6]

Although great improvements have been made in catalytic converters in gasoline-powered vehicles and exhaust control devices for diesel-fueled vehicles, further development in these areas is limited. Industrialized countries have lowered the allowed sulfur content of gas oil to 500 ppm in the mid 1990s, and will lower the limit to less than 50 ppm in the near future, as summarized in Table 1.1. Considering that the sulfur level in a typical gas oil is 2 wt% (2000 ppm) a reduction to 10 ppm will require 99.95% HDS. For these resons a new generation of high activity hydroprocessing catalyst is needed. The transition metal phosphides offer this possibility.

1.2. Limitations in Conventional HDS Processes

Standard hydrodenitrogenation/hydrodesulfurization (HDN/HDS) catalysts consist of MoS_2-type phases supported on γ-Al_2O_3 promoted by Co or Ni. There are many different kinds of sulfur compounds present in the gas oil fraction, such as alkyl-substituted benzothiophenes (BT) and dibenzothiophenes (DBT). The most refractory sulfur compounds are high molecular weight dibenzothiophenes that contain side chains in positions close to the sulfur atom such as 4-methyldibenzothiophene (4-MDBT) and 4,6-dimethyldibenzothiophene (4,6-DMDBT) [7]. The difficulty of S removal from those alkyl substituted DBT derivatives is due to the steric hindrance caused by the alkyl groups substituted on carbon positions 4 and/or 6 in DBT. Considering that more than 99.9 % of the refractory sulfur compounds will have to be further desulfurized to reduce the sulfur content of the current 500 ppm S to the new standards of 10 and 15 ppm S for the Europe and United States, it is essential to desulfurize alkyl substituted DBT derivatives effectively

in order to achieve deep HDS. The problem is compounded by the nitrogen compounds [48], which are known inhibitors of desulfurization.

Much research on deep HDS has employed 4-methyl DBT and/or 4,6-DMDBT as model compounds [7,8,10,23,33,46]. In general, as illustrated in Scheme 1.1 there are two reaction pathways for the HDS of 4,6-DMDBT, [8,9]. The first pathway is the direct desulfurization (DDS, hydrogenolysis route), in which the sulfur atom is extracted from the heterocycle without prior hydrogenation of either benzene ring, to produce 3,3-dimethylbiphenyl (BP). The second pathway is the hydrogenation route (HYD), in which partial or total hydrogenation of one of the rings occur prior to sulfur removal to form 4,6-dimethyl-tetrahydro or hexahydro-DBT. This is followed by desulfurization to give methylcyclohexyltoluene (MCHT) and dimethylbicyclohexane (DMBCH) by further hydrogenation. Previous studies on conventional Co-Mo and Ni-Mo sulfide catalysts have shown that the HDS of unsubstituted DBT proceeds mostly via direct desulfurization. For the alkyl substituted DBT (4,6-DMDBT) the rate of direct desulfurization is diminished, whereas the rate of HDS via the hydrogenation pathway is relatively unaffected [10].

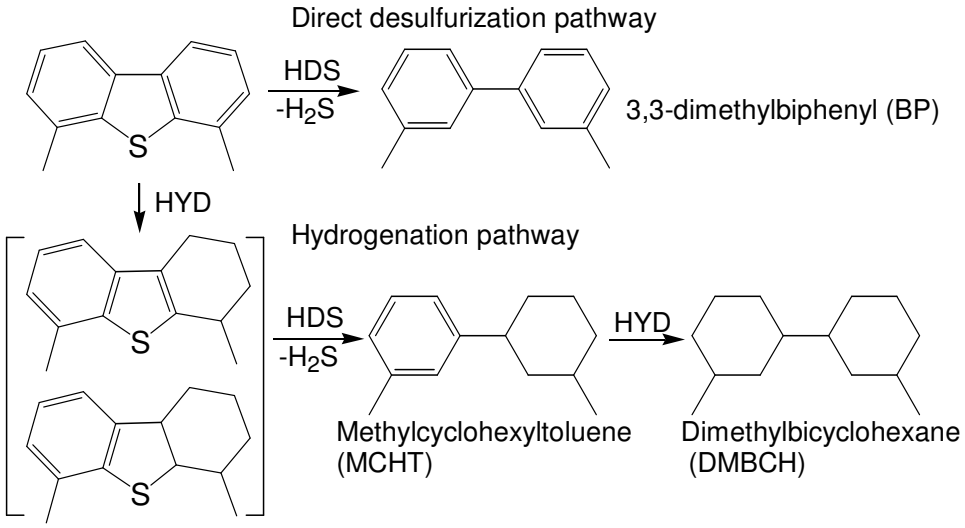

Scheme 1.1. Reaction scheme for hydrodesulfurization of 4,6-DMDBT.

Conventional Ni-Mo-S/Al_2O_3 catalysts, which exhibit relatively high hydrogenation activity, have a higher activity for the HDS of 4,6-DMDBT via the HYD route than conventional Co-Mo-S/Al_2O_3 catalysts which desulfurize primarily via the DDS route. The Ni-Mo-S/Al_2O_3 catalysts, however, exhibit lower HDS activity than the Co-Mo-S/Al_2O_3 catalysts in the presence of high concentration of aromatics and nitrogen compounds, due to the inhibition caused by those compounds [10,11]. For this reason, gas oil refining currently operates mostly with Co-Mo-S/Al_2O_3 catalysts at moderate temperatures (340-360 ^oC) and pressures (3.0-5.0 MPa). Nonetheless, these conditions are unable to achieve the low sulfur specification of gas oil of less than 15 ppm S [10,11]. Increasing the temperature to achieve higher HDS rates causes degradation of the produced oil due to unwanted side reactions. Thus, the required reduction in sulfur will have large consequences for refineries and

significant resources will have to be devoted to improve the processes. The development of more effective HDS catalysts is greatly needed.

1.3. Metal Phosphides as a New Catalyst Group for Hydrotreating

There are many approaches to obtain better catalysts by changing active components and/or supports. Work on alternative hydroprocessing catalysts to the widely used sulfides includes research on transition-metal carbides, nitrides, phosphides, and noble metals [12-17]. Transition-metal phosphide catalysts have been studied in hydrogenation reactions [24-27] but research focused on their hydrotreating activities has been carried out only recently [15-23]. Metal phosphides are categorized into three groups according to the atomic ratio of metal to phosphorus [28]. The structural features and properties of phosphides are summarized in Table 1.2. Recently, the preparation of transition metal phosphides by temperature programmed reduction (TPR) of oxidic precursors (metal phosphates) has been demonstrated to be possible at moderately high temperature (500 - 600 ^{o}C) [15].

Table 1.2 Properties of metal phosphides

Monophosphides M_xP_y (x=y)	Metal-rich phosphides M_xP_y (x>y)	P-rich phosphides M_xP_y (x<y)
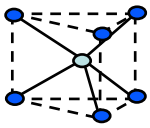 6-fold trigonal coordination around P	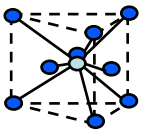 9-fold tetrakaidecahedral coordination around P	Various structures with P-P chains
MoP, WP, TiP, VP, CrP, MnP, FeP, CoP, RuP, ZrP	Ni_2P, Fe_2P, Co_2P, Ti_5P_3, Ru_2P	PdP_2, NiP_2, ZnP_2, TiP_2, CdP_2, CuP_2, CdP_4
High hardness and resistance to oxidation at high temp	High thermal and electrical conductivities	Unstable to reversion to mono- or metal-rich phosphides on heating

Table 1.3 Structure of Ni_2P

Unit cells		
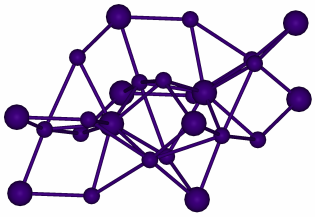 [111]	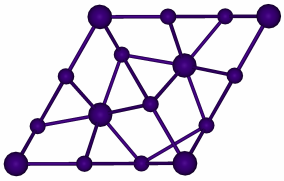 [001]	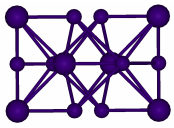 [100]
 P Ni		
Structural type: Fe_2P type (hexagonal $P\bar{6}2m$), a = b = 5.859Å, c=3.382 Å		

Recent studies have shown that MoP, WP, Ni_2P and Co_2P catalysts are very active for both HDS and HDN of petroleum feed stocks [15, 29,31,33]. The group 6 metal

phosphides (MoP and WP) were more active for HDN of quinoline than sulfides and stable during reaction and under H_2S. It has been shown that MoP is well dispersed on the support SiO_2 (200 m^2g^{-1}) and has four times higher activity in the HDS of thiophene than MoS_2/Al_2O_3 [30], measured at 643 K under atmospheric pressure. Iron group phosphides were also applied in hydrotreating reactions. Previous studies of the group 6 metal phosphide catalysts in the HDS of dibenzothiophene (3000 ppm S) and the HDN of quinoline (2000 ppm N) revealed that the overall activity was in the order: Fe_2P/SiO_2 < CoP/SiO_2 < MoP < WP < Ni_2P/SiO_2, in which the comparison was made based on equal chemisorption sites (70 μmol of CO for the phosphides and atomic oxygen for a Ni-Mo-S/Al_2O_3 catalyst) loaded in the reactor at 643 K and 3.1 MPa [31,32].

Further studies of the effect of phosphorus content for Ni_2P/SiO_2 catalysts with varying atomic ratio of Ni to P in the oxidic precursors [33] revealed that a sample with excess P (initial Ni/P ratio =1/2) gave more dispersed and stable phases with higher activity (HDS conversion of 100% and HDN conversion of 81%) than samples with lower P content. A study of the electronic properties of SiO_2 supported Ni_2P, MoP, and MoS_2 catalysts has been made using density functional calculations [34]. In this study, the amount of electron density of the metal in the phosphides followed the order, MoS_2/SiO_2 < MoP/SiO_2 < Ni_2P/SiO_2, which correlated well with the thiophene HDS activities of the catalysts. It was noted that the electron transfer from the metal cation of the catalysts could enhance HDS activity to the nonmetal by facilitating the dissociation of H_2 and the adsorption of thiophene [34,35].

The results above suggest that Ni_2P catalysts are promising in the deep HDS area where considerable improvements in activity are required. Therefore, this research concentrates mostly on the Ni_2P catalysts for the HDS of 4,6-DMDBT.

1.4. High Surface Area Supports: MCM41 and Ultra-Stable Y (USY) Zeolite

MCM-41 is a mesoporous molecular sieve that is characterized by a hexagonal array of uniform mesopores, a narrow pore size distribution ranging from 1.5 to 10.0 nm, and high surface area of over 1000 m^2g^{-1}, and thermal stability [36]. The mesopores feature of MCM-41 allow easy diffusion of catalyst precursors and polyaromatic sulfur compounds during HDS reactions, which might result in useful catalysts for deep HDS and HDN [37,38].

Zeolites are crystalline aluminosilicates with a microporous structure (pores < 2 nm), which makes them very suitable for separation processes or shape selective catalysis. Zeolite Y is one member of this class of compounds which is widely used for a number of industrial catalytic applications, such as catalytic cracking, hydrocracking, aromatic alkylation, and alkane hydroisomerizations, because of its acidic properties and stability [39]. Modifications of either the structure (pore system) or the acidic properties of the zeolite Y have been made to increase the accessibility of larger molecules and to alter the chemical characteristics of the material. Much improvement in accessibility has been achieved by post-synthesis modification of Y zeolite with hydrothermal treatments (steaming) and/or acid leaching [40]. These treatments generate mesopores (2-50 nm in diameter) by extraction of aluminum from the zeolite lattice, thus causing partial collapse of the framework. It was found that thermal stability of the zeolite is enhanced after the

modification, and that is why the modified zeolite Y is called ultra stable zeolite Y (USY). Acidity can also be modified using cation exchange. Among the cations applied, potassium is known to be highly effective for poisoning acid sites as shown by a reduction in the cracking of gas oil [41]. USY has been widely used in the refining industry [39] because of its well-developed mesoporous structure and moderate acidity.

In this research the supports, SiO_2, MCM-41 and KUSY, have been employed to increase the dispersion of the Ni_2P and to determine whether any enhancements can be obtained from support interactions.

1.5. HDN Mechanism Study

The nitrogen present in gas oil is contained in heterocyclic compounds, which are composed of one or two ring N-compounds in the light fraction (< 340 ^oC, boiling point) and asphaltenes in the heavy fraction [42]. The nitrogen content in crudes is much lower than the sulfur content (in general 5 to 20 times lower). However, the N-compounds have lower reactivity than the S-compounds and strongly inhibit HDS by competitive adsorption on the active sites [42,43]. For these reasons, considerable attention will be paid to HDN, particularly with simultaneous deep HDS.

The HDN of heterocyclic N-compounds generally involves the following reactions: (i) hydrogenation of the N ring, (ii) cleavage of a C-N bond to form an amine intermediate, and (iii) hydrogenolysis of the amine to hydrocarbons and ammonia [43]. Much research has been carried out on the study of the C-N bond cleavage step using model N-compounds [44,45,46]. As an example of a model compound, 2- methylpiperidine, a primary product of

the HDN of 2-methylpyridine, will be employed in this dissertation. The HDN of 2-methylpiperidine is generally considered to occur through ring-opening by Hofmann elimination (E2) or by nucleophilic substitution (S_N2). Scheme 1.2 shows these two main routes for the HDN of 2-methylpyridine.

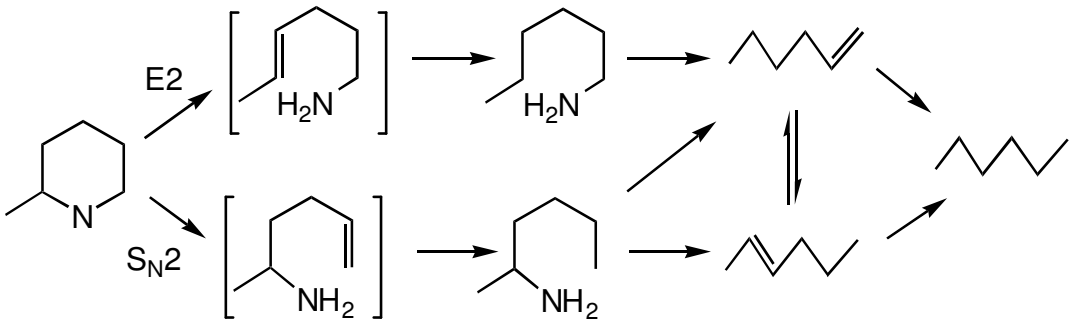

Scheme 1.2. Reaction scheme for the HDN of 2-methylpyridine.

The dinuclear elimination (E2) occurs by attack of a base (^-SH) on the hydrogen atoms at β positions to the nitrogen atom. This results in formation of an olefin and displacement of the nitrogen as an amine. The elimination is favored by β hydrogen atoms [47].

The dinuclear nucleophilic substitution (S_N2) occurs by attack of a nucleophile (HS^-) on a carbon atom at a position α to the nitrogen atom [48]. For 2-methylpyridine the 2-position is blocked and attack occurs through the sterically accessible 6-position. The result is 2-aminohexane as a primary product.

By following the formation of the primary products it will be possible to determine which mechanism is favored for the phosphide. Again, comparison will be made to sulfides

catalysts to determine whether the nature of reactive surfaces is similar or completely different.

1.6. Goals

The primary goals of this research are to develop highly active Ni_2P catalysts, characterize the catalysts, and examine activities in deep HDS and HDN reactions. In order to achieve these goals the following tasks have been carried out:

- Synthesis of Ni_2P catalysts on various supports with different surface area
- Synthesis of high surface area material MCM-41 and use of SiO_2 and K-ion exchanged USY zeolite as supports for the Ni_2P catalyst
- Characterization of supported Ni_2P catalysts with CO chemisorption, N_2 physisorption, TEM to obtain physical properties such as active site density, surface area, pore volume, and morphology
- XRD and EXAFS measurements to identify the structure of Ni_2P catalysts
- EXAFS simulation to determine structural parameters in the Ni_2P
- FTIR measurements to investigate surface properties of Ni_2P catalysts with the probe molecules CO, pyridine, and piperidine
- Activity tests in HDS of 4,6-DMDBT, HDN of quinoline, and hydrogenation of tetralin for Ni_2P catalysts and a commercial Ni-Mo-S/Al_2O_3 catalyst
- Investigation of inhibition effects of aromatic (tetralin), nitrogen (quinoline) and sulfur (dimethyldisulfide) compounds on the HDS of 4,6-DMDBT for Ni_2P catalysts and a commercial Ni-Mo-S/Al_2O_3 catalyst

- Activity test in HDN of 2-methylpiperidine with varying residence time for Ni_2P catalysts and a commercial Ni-Mo-S/Al_2O_3 catalyst
- In situ FTIR measurements with 2-methylpiperidine as a probe molecule for Ni_2P catalysts and a commercial Ni-Mo-S/Al_2O_3 catalyst

.

1.7. Dissertation Overview

Chapter 1 describes the background, objectives and dissertation overview.

Chapter 2 presents the preparation of well dispersed Ni_2P catalysts on high surface area SiO_2 and MCM-41 supports and the effect of dispersion of Ni_2P particles on structure and catalytic activities. It also includes the investigation of inhibition effects of aromatic (tetralin), nitrogen (quinoline) and sulfur (dimethyldisulfide) compounds on the HDS of 4,6-DMDBT for Ni_2P catalysts and a commercial Ni-Mo-S/Al_2O_3 sample. X-ray absorption spectroscopy is used to characterize the structural properties of the dispersed Ni_2P particles.

Chapter 3 presents the synthesis, characterization, and catalytic activity in the HDS of 4,6-DMDBT of the Ni_2P/SiO_2 catalyst. Structural and surface properties of the Ni_2P/SiO_2 catalyst are investigated by X-ray absorption spectroscopy and FTIR measurements of CO and pyridine adsorption. It is found that that the Ni_2P/SiO_2 catalyst exhibits a bifunctional nature with metallic properties and mild acidity, which is related to the high catalytic activity in the HDS of 4,6-DMDBT via the hydrogenation pathway and the resistance to N-compounds.

Chapter 4 presents the synthesis of Ni_2P catalysts on KUSY support with varying Ni_2P loadings and initial Ni/P ratios and reports their effect on the structural and catalytic properties of the Ni_2P catalysts. The catalytic activity and stability of Ni_2P/KUSY catalysts are greatly affected by the initial Ni/P ratio and reach a maximum at a Ni/P ratio of 1/2.

Chapter 5 provides a review in HDN mechanisms and reports the HDN mechanism study of 2-methylpiperidine for both Ni_2P and commercial Ni-Mo-S/Al_2O_3 catalysts. The nature of the intermediates on these catalysts is characterized by in situ FTIR measurements with 2-methylpiperidine as a probe molecule.

Chapter 6 presents the conclusions of this research.

References

1. J. G. Speight, The Chemistry and Technology of Petroleum, 2nd ed., Dekker, New York, 1991.
2. A. C. Stern, R. W. Boubel, D. B. Turner, and D. L. Fox, Fundamentals of Air Pollution, 2nd ed., Academic Press, Orlando, FL, 1984.
3. H. Topsøe, B. S. Clausen, and F. E. Massoth, Hydrotreating Catalysis, Springer-Verlag, New York, 1996.
4. J. M. Thomas, and W. J. Thomas, Principles and Practice of Heterogeneous Catalysis, VCH, New York, 1997.
5. U. S. EPA Document, Federal Register. 66 (12), 2001, p.5006.
6. R. Shafi, and G. I. Hutchings, Catal. Today 59 (2000) 423.
7. H. Schulz, W. Böhringer, F. Ousmanov and P. Waller, Fuel Proc. Tech. 61 (1999) 5.
8. D. D. Whitehurst, T. Isoda, and I. Mochida, Adv. Catal. 42 (1998) 345.
9. K. Segawa and S. Satoh, Stud. Surf. Sci. Catal. 127 (1999) 129.
10. K. G. Knudsen, B. H. Cooper, and H. Topsøe, Appl. Catal. A 189 (1999) 205.
11. I. V. Babich and J. A. Moulijn, Fuel, 82 (2003) 607.
12. J. C. Schlatter, S. T. Oyama, J. E. Metcalfe, and J. M. Lambert, Ind. Eng. Chem. Res. 27 (1988) 1648.
13. H. Abe, T. K. Cheung, and A. T. Bell, Catal. Lett. 21 (1993) 11.

14. S. T. Oyama (Ed.), The Chemistry of Transition Metal Carbides and Nitrides, Blackie Academic and Professional, London, 1996.

15. W. Li, B. Dhandapani, and S. T. Oyama, Chem. Lett. (1998) 207.

16. W. Qian, Y. Yoda, Y. Hirai, A. Ishihara, and T. Kabe, Appl. Catal. A, 184 (1999) 81.

17. A. M. Venezia, V. La Parola, G. Deganello, B. Pawelec, and J. L. G. Fierro, J. Catal. 215 (2003) 317.

18. C. Stinner, R. Prins, and Th. Weber, J. Catal. 191 (2000) 438.

19. C. Stinner, R. Prins, and Th. Weber, J. Catal. 202 (2001) 187.

20. P. Clark, W. Li, and S. T. Oyama, J. Catal. 200 (2001) 140.

21. S. T. Oyama, P. Clark, V. L. S. Teixiera da Silva, E. J. Lede, and F. G. Requejo, J. Phys. Chem. B, 105 (2001) 4961.

22. C. Stinner, Z. Tang, M. Haouas, Th. Weber, and R. Prins, J. Catal. 208 (2002) 456.

23. S. T. Oyama,; P. Clark, X. Wang, T. Shido, Y. Iwasawa, S. Hayashi, J. M. Ramallo-Lopez, and F. G. Requejo, J. Phys. Chem. B, 106 (2002) 1913.

24. N. P. Sweeny, C. S. Rohrer, and O. W. Brown, J. Am. Chem. Soc. 80 (1958)799.

25. E. L. Muetterties, and J. C. Sauer, J. Am. Chem. Soc. 96 (1974) 3410.

26. F. Nozaki, and R. Adachi, J. Catal. 40 (1975) 166.

27. F. Nozaki, and M. Tokumi, J. Catal. 79 (1983) 207.

28. D. E. C. Corbridge, “Phosphorus : an outline of its chemistry, biochemistry, and technology” Amsterdam, New York, Elsevier, 1990.

29. S. T. Oyama, J. Catal. 216 (2003) 343.

30. D. C. Phillips, S. J. Sawhill, R. Self, and M. E. Bussell, J. Catal. 207 (2002) 266.

31. P. Clark, and S. T. Oyama, J. Catal. 218 (2003) 78.

32. P. Clark, X. Wang, and S. T. Oyama, J. Catal. 207 (2002) 256.

33. S. T. Oyama, X. Wang, .Y.-K. Lee Bando, and F. G. Requejo, J. Catal. 210 (2002) 207.

34. J. A. José A. Rodriguez, J.-Y. Kim, J. C. Hanson, S. J. Sawhill, and M. E. Bussell, J. Phys. Chem. B, 107 (2003) 6276.

35. J. A. Rodriguez, J. Phys. Chem. B, 101 (1997) 7524.

36. K. S. W. Sing, D. H. Everett, R. A. W. Haul, L. Moscou, R. A. Pierotti, J. Rouquerol, and T. Siemieniewska, Pure Appl. Chem. 57 (1985) 603.

37. U.T. Turaga, C. Song / Catalysis Today 86 (2003) 129.

38. U.T. Turaga, C. Song, Prepr. Div. Pet. Chem. Am. Chem. Soc. 46 (2001) 275.

39 J. Scherzer, "Octane Enhancing Zeolite FCC Catalysts." Dekker, New York, 1990.

40 J. Scherzer, ACS Symp. Ser., 248 (1984) 157.

41 R. Kumar, W.C. Cheng, K. Rajagopalan, A.W. Peters, and P. Basu ,.J. Catal. 143 (1993) 594.

42. S. Kasztelan, T. des Courières and M. Breysse, Catal. Today 10 (1991) 443.

43. G. Perot, Catal. Today 10, 447 (1991).

44. J. Sonnemans, W. J. Neyens, and P. Mars, J. Catal. 34 (1974) 230.

45. H. Schulz, M. Schon, and N. M. Rahman, Stud. Surf. Sci. Catal. 27, (1986) 201.

46. M. Egorova and R. Prins J. Catal. 224 (2004) 278.

47. J. L. Portefaix, M. Cattenot, M. Guerriche, J. Thivolle-Cazat, and M. Breysse, Catal. Today 10 (1991) 473.

48. M. Egorova, Y. Zhao, P. Kukula, and R. Prins, J. Catal. 206 (2002) 263.

Chapter 2

The Effect of Reaction Conditions on the Hydrodesulfurization of 4,6-DMDBT on Nickel Phosphide Catalysts Supported on High Surface Area Siliceous Supports

2.1. Introduction

Environmental regulations for reducing motor vehicle emissions has put considerable pressure on the refining industry worldwide to produce cleaner fuels, and has motivated much research for the development of new hydrotreating catalysts. Nickel phosphide (Ni_2P) is a novel catalyst for deep hydrotreating and have received much attention due to their high activity for hydrodesulfurization (HDS) and hydrodenitrogenation (HDN) of petroleum feedstocks [1-4].

Previous studies of silica-supported Ni_2P employed a low surface area (90 $m^2 g^{-1}$) support [4,5,6]. It is the objective of this work to investigate a high surface area silica (350 $m^2 g^{-1}$) and a mesoporous siliceous material (790 $m^2 g^{-1}$) as supports. Particular attention is placed on understanding the effect of nitrogen, sulfur and aromatic compounds on the catalytic behavior, as these compounds are reported to inhibit HDS. The present study also includes the use of X-ray absorption fine structure (XAFS) spectroscopy to study the structure of the finely dispersed phosphide phases before and after reaction. As will be shown, the samples after use show evidence for the formation of a surface phospho sulfide phase of very high activity.

2.2. Experimental

2.2.1. Synthesis of Supported Ni_2P Catalysts

Commercial SiO_2 supports (Cabot, Cab-O-Sil) of low surface area (L-90, 90 $m^2 g^{-1}$) and high surface area (EH-5, 350 $m^2 g^{-1}$) were used as received. A mesoporous MCM-41 silica support was synthesized following a literature procedure [7]. The chemicals used in the synthesis were colloidal silica (HS-40, Fluka), cetyltrimethylammonium bromide (CTMABr, 99%, Aldrich) and tetramethylammonium hydroxide (TMAOH, 25 wt% aqueous solution, Aldrich). The TMAOH and CTMABr were added to deionized water with stirring at 300 K until the solution became transparent, then the colloidal silica was added to the solution with stirring for 1 h and the resulting reaction gel was aged for 24 h at 323 K. The molar composition was 1.0 SiO_2 : 0.19 TMAOH : 0.27 CTMABr : 40 H_2O. After aging, the mixture was reacted for 48 h at 393 K in a Teflon-lined stainless steel autoclave. The product was filtered, washed with distilled water, dried in air at 393 K, and finally calcined at 623 K for 8 h.

The supported Ni_2P catalysts were prepared with excess phosphorus (Ni/P=1/2) and a loading of 1.16 mmol Ni/g support (12.2 wt.% Ni_2P/SiO_2). Previous studies [4,6] had shown that this composition and loading level gave high activity and stability in hydroprocessing reactions. Samples prepared with low surface area silica (L90) were denoted as Ni_2P/SiO_2-L and samples prepared with the high surface area silica (EH5) were denoted as Ni_2P/SiO_2-H. The synthesis of the catalyst involved two steps and was described elsewhere [4]. Briefly, in the first step, a supported nickel phosphate precursor was prepared by incipient wetness impregnation of a solution of nickel nitrate and ammonium phosphate,

followed by calcination at 673 K. In the second step, the supported metal phosphate was reduced to a phosphide by temperature-programmed reduction (TPR). In the TPR procedure, which was also used to determine the reduction characteristics of the material, 0.20 g of material was loaded in a quartz glass u-tube reactor and the effluent was monitored by a mass spectrometer (Ametek/Dycor MA100). In catalyst preparation, larger batches using up to 5.50 g of supported nickel phosphate were prepared in a similar manner by reduction to 873 K, 883 K, and 893 K for Ni_2P/SiO_2-L, Ni_2P/SiO_2-H, and Ni_2P/MCM-41, respectively. The hydrogen flow rate was set at 1000 μmol s^{-1} (1500 cm^3 (NTP) min^{-1}) per g of sample. At the end of the temperature program the sample was cooled to room temperature in helium and was passivated under 0.5 % O_2/He for 6 h.

2.2.2. Characterization of Samples

X-ray diffraction (XRD) patterns of both the freshly prepared and used samples were obtained with a Scintag XDS-2000 powder diffractometer operated at 45 kV and 40 mA using Cu K_α monochromatized radiation (λ = 0.154178 nm). CO chemisorption uptakes were obtained on passivated, air-exposed samples rereduced in hydrogen for 2 h at 723 K, and were used as the basis for hydroprocessing tests. Pulses (5.6 μmol) of CO at room temperature (300 K) were passed over the sample to measure the total, dynamic gas uptake. A Micromeritics ASAP 2010 micropore size analyzer was used to measure the N_2 adsorption/desorption isotherms at 77 K in the samples. Before the measurements, the passivated samples were degassed at 403 K for 12 h. The calculation of the pore size distribution (PSD) was performed using the Barrett-Joyner-Halenda (BJH) formula [8]. The specific surface area of the sample was calculated from the linear portion of BET plots (P/Po

= 0.01–0.10), and the cumulative surface area of the mesopores was obtained from PSD curves. The chemical composition of the samples was determined by inductively coupled plasma-absorption emission spectroscopy (ICP-AES) (Spectro Analytical Instruments, Model Spectroflame FTMO A85D). For complete dissolution of the samples, aqua regia digestion was carried out with heating in a microwave oven (EthosPlus, Milestone).

X-ray absorption (XAS) spectra at the Ni K edge (8.333 keV) of reference and catalyst samples were recorded in the energy range 8.233 to 9.283 keV using synchrotron radiation at the National Synchrotron Light Source (NSLS) at Brookhaven National Laboratory (BNL), beamline X18B. The X-ray ring at the NSLS has a flux of 1×10^{10} photons s^{-1} at 100 mA and 2.5 GeV. The monochromator is equipped with a Si (111) channel-cut single crystal and has an energy range capability of 5.8 to 40 keV. The crystal was detuned slightly to prevent glitches due to harmonics. Extended X-ray absorption fine structure spectra (EXAFS) were recorded at ambient temperature in transmission mode using ionization chambers for the detection of primary (I_0, 100 % N_2) and transmitted (I_t, 75 % N_2, balance Ar) beam intensities. Bulk reference samples were diluted with BN (0.1 g catalyst + 0.3 g BN). The obtained EXAFS data were analyzed by Winxafs 97. In order to fit the experimental EXAFS spectra for the fresh and used samples, the theoretical EXAFS equation for Ni_2P was used to calculate phase shifts and amplitude functions of Ni_2P, using FEFF 8.0 code [9]. Fitting was then carried out for the fresh samples using the three dominant shells (2 Ni-P at 0.2266 nm, 4 Ni-P at 0.2457 and 4 Ni-Ni at 0.2678 nm), using a reducing factor (S_o^2), fixed as 0.90, a value obtained by fitting the Ni-Ni contribution in Ni foil. Fitting was also carried out for the used samples using three dominant shells (2 Ni-P at 0.2266 nm, 6 N-S at 0.2369 and 2 Ni-Ni at 0.2613 nm) of which phase shifts and amplitude

functions were calculated with FEFF 8.0 code from Ni_2P [9] and NiS [10]. Again, the reducing factor (S_o^2), was fixed as 0.90, during the fitting.

2.2.3. Activity Test for HDS

Hydrotreating was carried out at 3.1 MPa (450 psig) at two different temperatures, 573 K (300 ^oC) and 613 K (340 ^oC) in a three-phase upflow fixed-bed reactor. The feed liquid was prepared by combining different quantities of tetralin (Aldrich, 99%), n-tridecane (Alfa Aesar, 99%), quinoline (Aldrich, 99%), 4,6-dimethyldibenzothiophene (4,6-DMDBT, Fisher, 95%), dimethyldisulfide (DMDS, Aldrich, 99%), and n-octane (Aldrich, 99%). The liquid was delivered at 0.0833 $cm^3\ s^{-1}$ (5 $cm^3\ h^{-1}$) using a liquid pump along with 100 μmol s^{-1} (150 cm^3 (NTP) min^{-1}) hydrogen flow. Liquid product compositions were determined with a Hewlett Packard 5890A gas chromatograph, equipped with a 50 m dimethylsiloxane column having 0.32 mm i.d. (Chrompack, CPSil 5B), on samples collected at 4- to 5-h intervals. Reaction products were identified by matching retention times with commercially available standards, as well as by GC/MS analysis. The GC/MS combined a Fisons Carlo Erba 8060 series gas chromatograph, using a HP-5MS 5% phenylmethylsiloxane stationary phase, with a VG Quattro triple quadrupole mass spectrometer operated in the electron impact–positive ion mode. Quantities of catalysts loaded in the reactor corresponded to the same amount of CO or atomic oxygen uptake (70 μmol), and were 2.80 g for the Ni_2P/SiO_2–L catalyst, 2.3 g for the Ni_2P/SiO_2-H catalyst, 1.70 g for the Ni_2P/MCM-41 catalyst and 0.83 g for the Ni-Mo-S/Al_2O_3 catalyst, with corresponding liquid hourly space velocity (LHSV) of 0.65, 0.80, 1.10, and 4.0 h^{-1}. For the hydroprocessing reaction the passivated phosphide

catalysts were pretreated for 2 h at 623 K in 100 μmol s^{-1} (150 cm^3(NTP) min^{-1}) of H_2, and the sulfide catalyst was pretreated at 578 K for 2 h with 100 μmol s^{-1} of 10 % H_2S/H_2 at a pressure slightly above 1 atm. The experiments were long (~ 200 h) and, for each change in composition or temperature, the reaction system was allowed to run for 40-50 h to establish steady-state. The results of several measurements were averaged. After the runs, the reactors were cooled down to 327 K and n-hexane was introduced though the reactors at a rate of 10 cm^3 h^{-1} for 12 h. The wet catalysts samples were then collected and stored in n-hexane in order to avoid air-exposure. They were moved to reactors in hexane for drying and transferred to glass cells for EXAFS analysis also without exposure to the environment. The 4,6-dimethyldibenzothiophene (4,6-DMDBT) molecule undergoes HDS via two parallel reaction pathways: (i) direct desulfurization (DDS) leading to the formation of 3,3-dimethylbiphenyl (3,3-DMBP) and (ii) pre-hydrogenation followed by desulfurization (HYD) giving first 4,6-tetrahydro- and hexahydrodibenzothiophenes, which are further desulfurized to methylcyclohexyltoluenes (MCHT) and dimethylbicyclohexyls (DMBCH).

In this study, the HDS conversion and the selectivities are defined as

$$HDS\ Conversion\,(\%) = 100\times\left(1-\frac{MCHT + DMBCH + 3{,}3DMBP}{4{,}6DMDBT_{in}}\right)$$

$$HYD\ Selectivity\,(\%) = 100\times\left(\frac{MCHT + DMBCH}{4{,}6DMDBT_{in} - 4{,}6DMDBT_{out}}\right)$$

$$DDS\ Selectivity\,(\%) = 100\times\left(\frac{3{,}3DMBP}{4{,}6DMDBT_{in} - 4{,}6DMDBT_{out}}\right)$$

As will be discussed, the selectivities are approximate as there is interconversion between dimethylbiphenyl and the cyclohexylbenzene through hydrogenation and dehydrogenation reactions. However, these reactions are relatively slow, and the

compounds are not equilibrated.

2.3. Results

2.3.1. Structural Characterization of Supported Ni_2P Catalysts

Figure 2.1 shows the TPR profiles of the calcined phosphate precursors of the Ni_2P/SiO_2-L, Ni_2P/SiO_2-H, and Ni_2P/MCM-41. The TPR profiles for NiO/SiO_2-L and PO_x/SiO_2-L are also shown as references. For the supported Ni_2P catalyst samples a distinct reduction peak at around 850 K is observed with the peak maximum being shifted to higher temperature with increase of the surface area of the support. The NiO/SiO_2-L is reduced at a low temperature of around 570 K, while PO_x/SiO_2-L over a broad temperature range of 800-1050 K.

Figure 2.2 shows the powder XRD patterns of the freshly prepared and used silica-supported Ni_2P catalyst samples and of a bulk Ni_2P reference material. The XRD patterns confirm that Ni_2P is formed on both SiO_2 supports, with the signals being more broadened for Ni_2P/SiO_2-H than for Ni_2P/SiO_2-L.

Figure 2.3 shows the powder XRD patterns of the calcined MCM-41 support and of the freshly prepared and used Ni_2P/MCM-41 catalysts. They display the characteristic peaks of the MCM-41 support, with diffraction lines from the (100), (110), (200), and (210) planes of the hexagonal phase [7]. For the Ni_2P/MCM-41 samples the peaks of MCM-41 are retained, although at reduced peak intensity, but no signals originating from Ni_2P are observed.

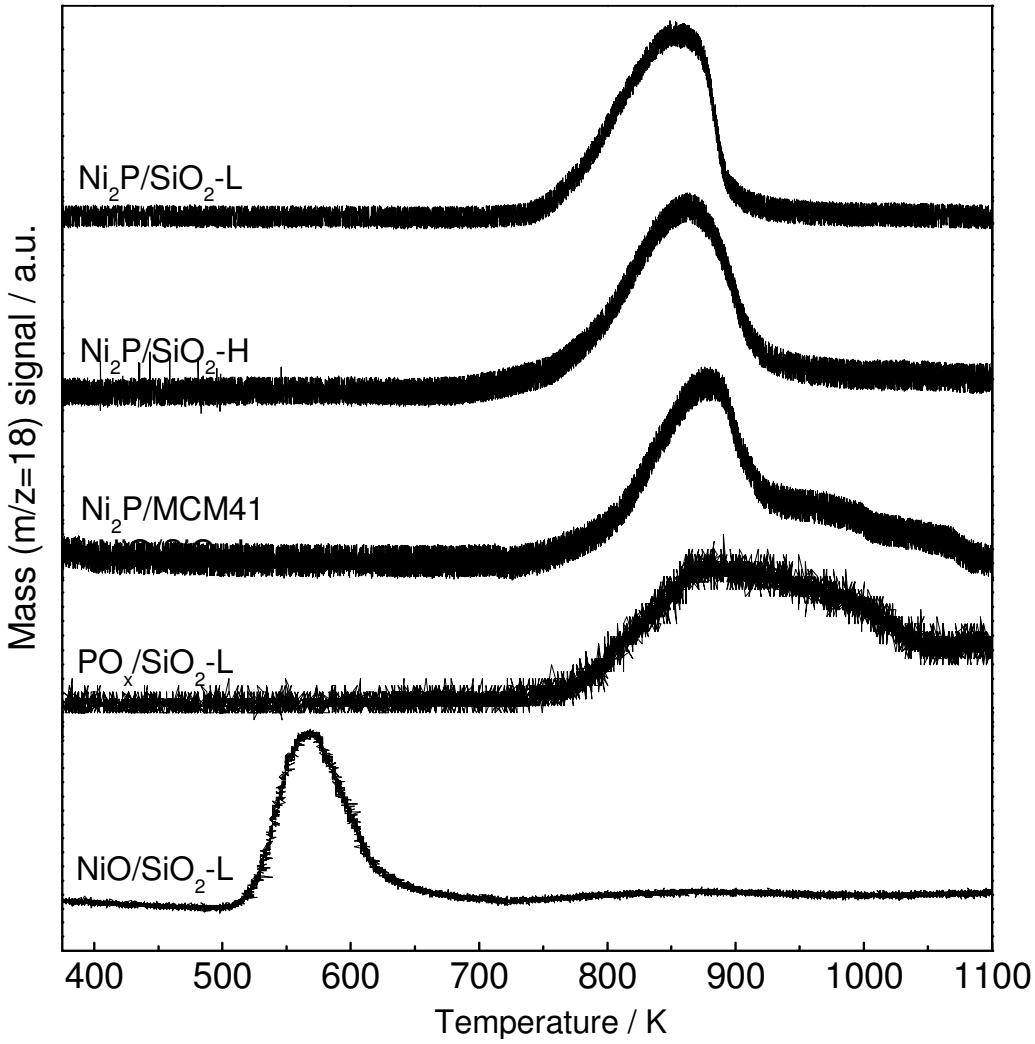

Figure 2.1. TPR profiles of supported Ni_2P catalysts and reference samples.

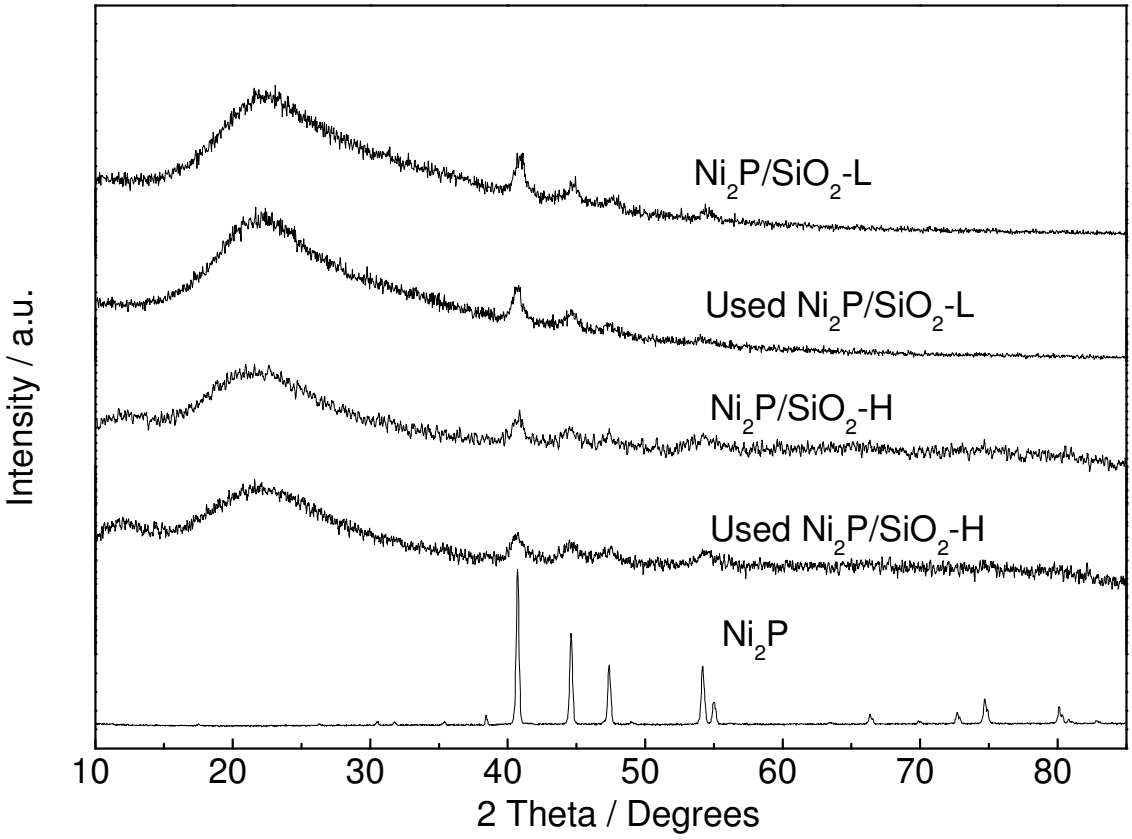

Figure 2.2. XRD profiles of the SiO_2 supported Ni_2P catalysts.

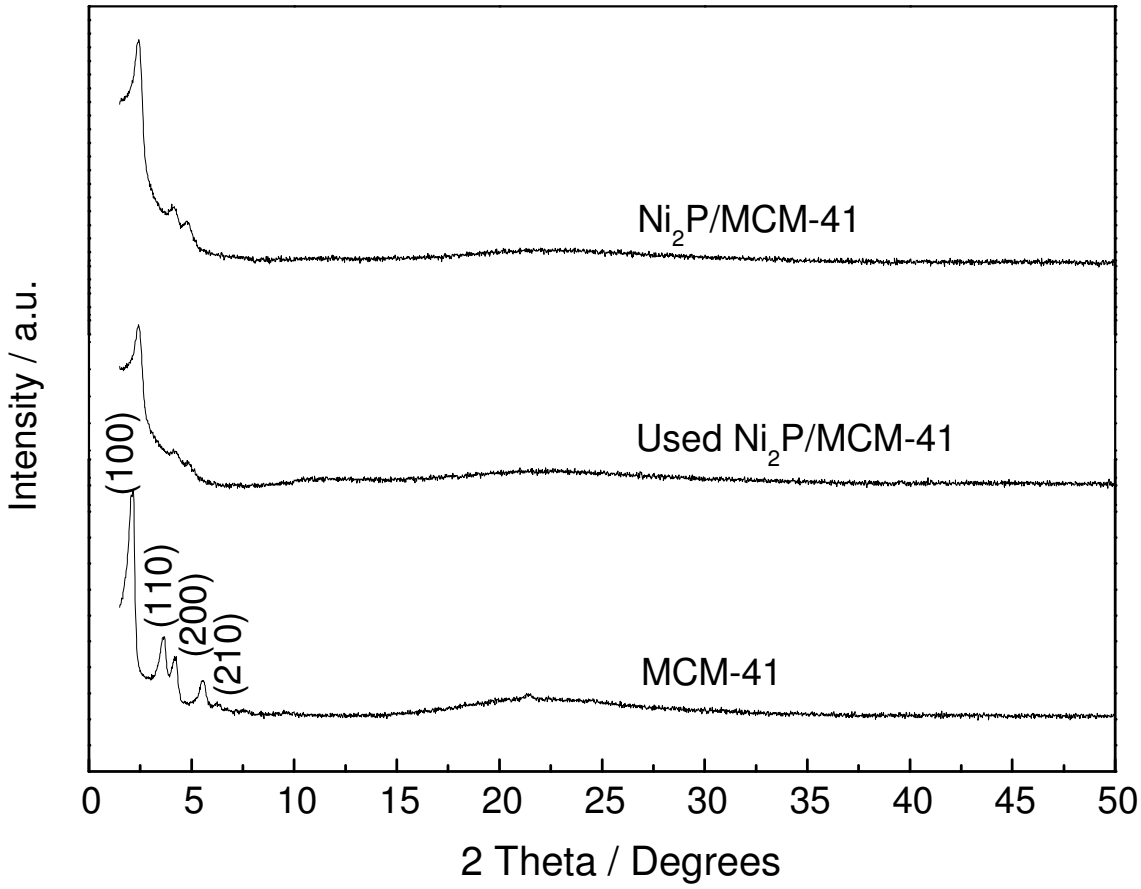

Figure 2.3. XRD profiles of the MCM-41 supported Ni_2P catalyst.

Table 2.1 summarizes the physical properties of the supported Ni_2P catalyst samples. For the freshly prepared samples, the amount of CO uptake increases with the surface area of the support. For the used samples the amount of CO uptake was lower than for the fresh samples, with the reduction more severe for higher S exposures. The BET surface area and pore volume for the Ni_2P/MCM-41 were much lower than those of the calcined MCM-41.

Table 2.1 Physical properties of the Ni_2P catalysts

Sample	Condition	CO uptake / μmol g^{-1}	N_2 adsorption	
			BET area / m^2 g^{-1}	Pore volume / cm^3 g^{-1}
SiO_2-L	-	-	92	-
Ni_2P/SiO_2-L	Fresh	25	88	-
Ni_2P/SiO_2-L	Used [a]	19	85	-
Ni_2P/SiO_2-L	Used [b]	9	86	-
SiO_2-H	-	-	350	-
Ni_2P/SiO_2-H	Fresh	33	240	-
Ni_2P/SiO_2-H	Used [b]	25	233	-
MCM-41, calcined	-	-	789	0.71
Ni_2P/MCM-41	Fresh	41	487	0.41
Ni_2P/MCM-41	Used [c]	35	412	0.34

[a] 0.35 % S in feed, [b] 0.65 % S in feed, [c] 1.05 % S in feed

Table 2.2 gives the nickel, phosphorous, and sulfur concentrations of the samples before and after reaction, and the molar ratios of P to Ni and S to P, as determined by ICP-AES. All of the samples were prepared with an initial Ni/P ratio of 1/2. In all cases the freshly prepared samples were found to have phosphorus contents that were smaller than the initial value, with Ni/P ratios ranging from 1/0.76 to 1/1.113. During reaction, the samples underwent further loss in P to give Ni/P ratios of 1/0.607, 1/0.716, 1/0.894 for Ni_2P/SiO_2-L,

Ni_2P/ SiO_2-H and Ni_2P /MCM-41, respectively. More P content remained for the samples with higher dispersion. Sulfur was found to be associated with the catalysts after reaction.

Table 2.2 Elemental analysis results

Sample	Condition	Molar ratio		
		P / Ni	S / Ni	S / P
Ni_2P (bulk)		0.49		
Ni_2P/SiO_2-L	Fresh	0.760	-	
Ni_2P/SiO_2-L	Used [a]	0.607	0.101	0.166
Ni_2P/SiO_2-L	Used [b]	0.601	0.178	0.296
Ni_2P/SiO_2-H	Fresh	0.963	-	
Ni_2P/SiO_2-H	Used [b]	0.716	0.157	0.219
Ni_2P/MCM-41	Fresh	1.113		
Ni_2P/MCM-41	Used [c]	0.894	0.171	0.191

[a] 0.35 % S in feed, [b] 0.65 % S in feed, [c]1.05 % S in feed

Figure 2.4 shows the N_2 adsorption and desorption isotherms for the calcined MCM-41 and Ni_2P/MCM-41 samples, and in the inset, the pore size distribution for the MCM-41. These isotherms are of Type IV in the IUPAC classification, which are indicative of the characteristic mesoporous nature of MCM-41. Introduction of Ni_2P in MCM-41 results in the overall N_2 adsorbed volume to be lowered.

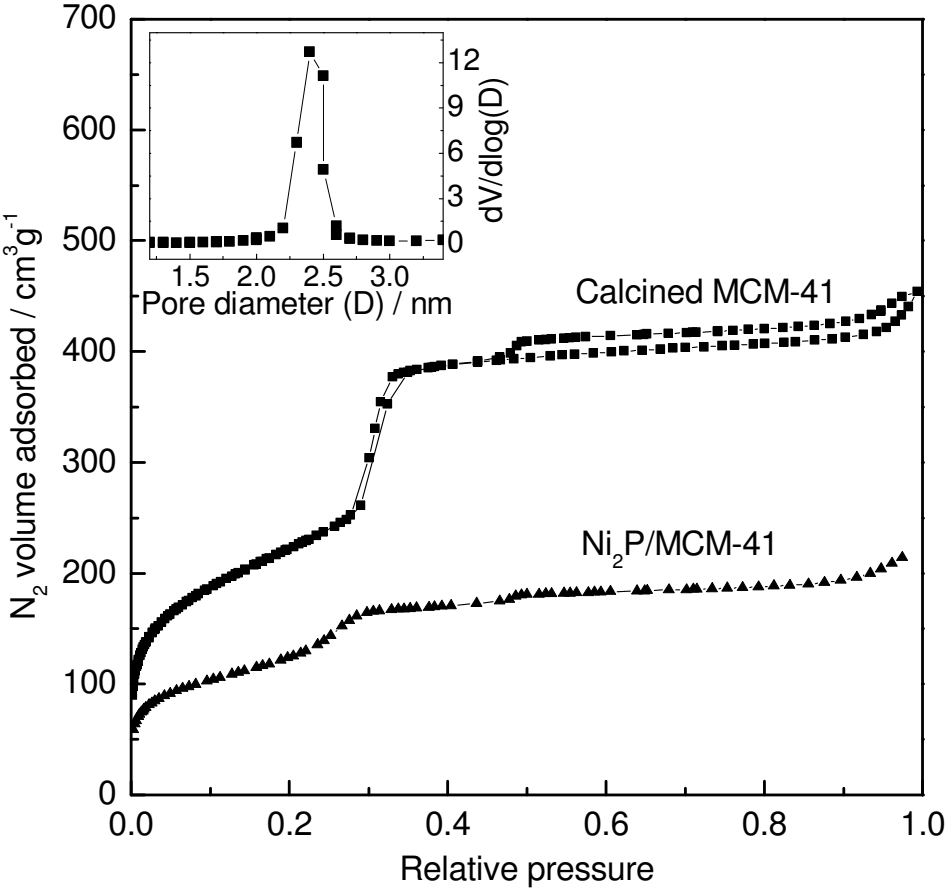

Figure 2.4. N_2 adsorption and desorption profiles of MCM-41 samples

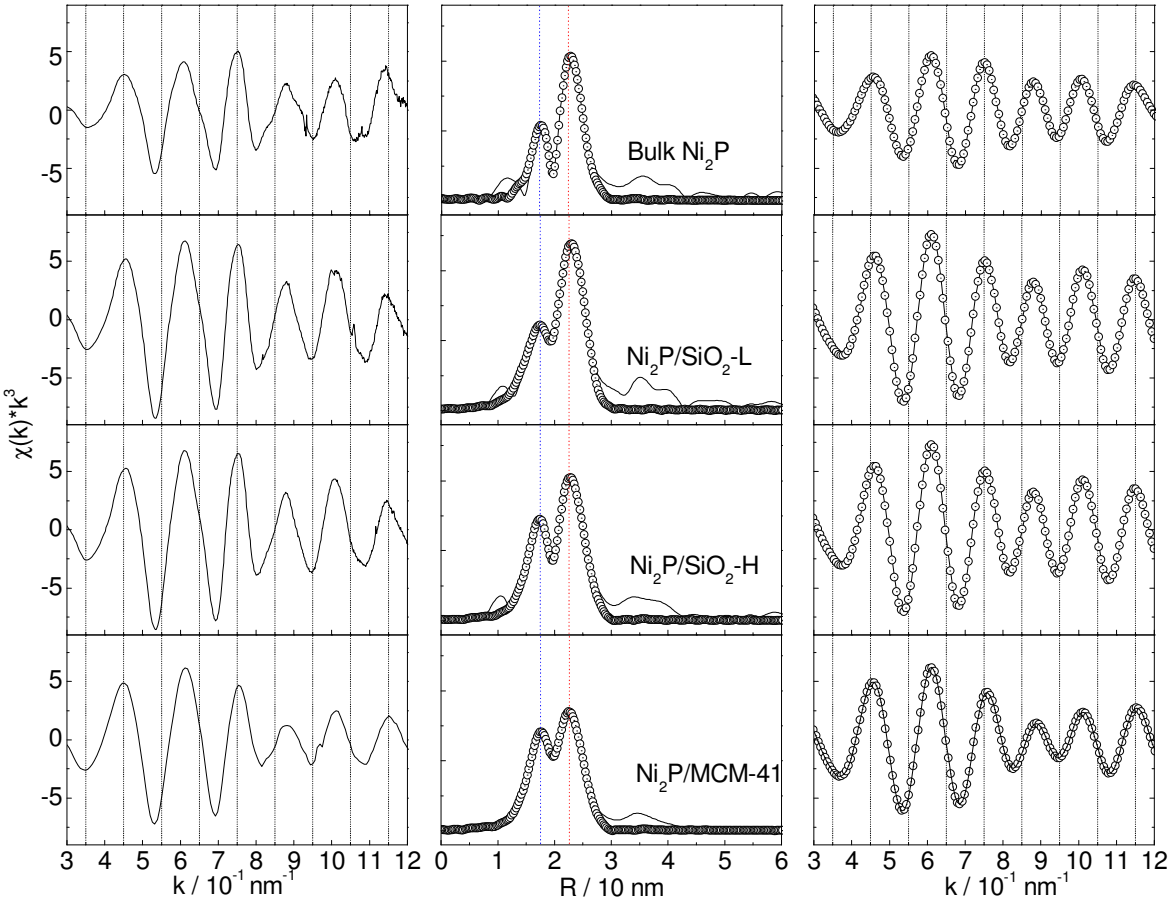

Figure 2.5. EXAFS analysis results for the fresh samples. The solid lines are the experimental curves and the circles are calculated points.

Figure 2.5 shows the Ni K-edge EXAFS spectra, Fourier transforms and Fourier filtered EXAFS spectra of the freshly prepared samples before reaction and a bulk reference Ni_2P sample. For the bulk Ni_2P the Fourier transform gives two main peaks, a smaller peak at 0.171 nm, and a larger peak at 0.228 nm. For the supported Ni_2P samples there are also two main peaks located at almost the same positions as those of the bulk Ni_2P reference, but with the larger peak weakened and broadened as the surface area of the support increases.

Table 2.3 summarizes the curve-fitting results of the EXAFS spectra for the freshly prepared Ni_2P samples, the reference experimental bulk Ni_2P sample and crystallographic Ni_2P standard data from the literature [9]. For the bulk Ni_2P the coordination numbers of the first (Ni(I)-P) and third (Ni-Ni) shell are in good agreement with those of the standard Ni_2P with the bond lengths being slightly lowered, while the coordination number of the second shell (Ni(II)-P) is much lower than that of reference Ni_2P (1.75 vs. 4.0). For the supported Ni_2P samples in the first shell the Ni(I)-P coordination number remains constant at around 2.0, with the bond distance being lowered. In the second shell the Ni(II)-P coordination number increases with increase of catalyst dispersion, while the bond distance decreases. In the third shell the Ni-Ni coordination number decreases with catalyst dispersion (3.43, 3.05, and 2.88 for Ni_2P/ SiO_2-L, Ni_2P/ SiO_2-H, and Ni_2P/MCM-41, respectively), while the bond distance increases slightly.

Table 2.3 Curve-fitting results for Ni_2P catalysts

Samples	Ni-P								Ni-Ni (I, II)				R(%)
	Ni-P (I)				Ni-P (II)								
	CN	R / nm	σ^2 / 10^{-5} nm^2	ΔE / eV	CN	R / nm	σ^2 / 10^{-5} nm^2	ΔE / eV	CN	R / nm	σ^2 / 10^{-5} nm^2	ΔE / eV	
Ni_2P Feff reference	2	0.22662			1	0.23688			4	0.26783			
Ni_2P (bulk)	2.0	0.2253	3.00	0.420	1.750	0.2401	0.499	0.423	3.99	0.2644	6.00	1.798	0.48
Ni_2P / SiO_2-L	1.99	0.2234	4.900	-2.397	2.57	0.2399	6.352	-2.392	3.43	0.2612	8.001	-0.389	0.962
Ni_2P / SiO_2-H	1.98	0.2225	6.420	-4.260	3.191	0.2383	8.460	-4.261	3.05	0.2625	8.159	-1.156	1.048
Ni_2P / MCM-41	1.99	0.2210	2.884	-0.448	3.482	0.23753	4.361	-0.381	2.88	0.2631	8.477	-2.290	1.249

ΔR filtered = 0.1427 - 0.27598 nm, $S_o^2 = 0.9$

$$Residual\,(R,\%) = \left(\frac{\sum_{i=1}^{N} \left| y_{\exp}(i) - y_{theo}(i) \right|}{\sum_{i=1}^{N} y_{\exp}(i)} \right) \times 100$$

Figure 2.6 shows the Ni K-edge EXAFS spectra, and Fourier transforms of the used samples after the reaction test with comparison also made to those of bulk Ni_2P and NiS/SiO_2-L. For the used Ni_2P/SiO_2-L samples which were tested under either 0.35 % S or 0.65 % S in the feed for 300 h, the Fourier transforms give two overlapping peaks with the second peak being weakened and widened, compared to those of the freshly prepared sample. A similar result is observed for the used Ni_2P/MCM-41 tested under 1.0 S % in the feed, with the second peak being more broadened. For the sulfided NiS/SiO_2-L sample a single Ni-S feature can be observed in the EXAFS spectrum with a peak at 0.18 nm.

Table 2.4 summarizes the curve-fitting results of the EXAFS spectra for the used Ni_2P samples and the NiS/SiO_2-L reference. For the NiS there is only one kind of Ni site which is surrounded by 6 S atoms at 0.2395 nm and the fitting gives a reasonable coordination number and bond length of 5.7 and 0.2390 nm, respectively. For the used Ni_2P samples the coordination number in the first shell (Ni-P) remains constant at around 2.0, with the bond distance being lowered for the used Ni_2P/MCM-41. In the second shell (Ni-S) the coordination number and bond length were found to be similar to that of NiS/SiO_2-L, particularly for the Ni_2P/SiO_2-L tested under 0.65 S %. For the third shell corresponding to a Ni-Ni bond the parameters for the coordination number and bond length were decreased in all cases compared to that of the fresh samples, and relatively higher values of the Debye-Waller factor were obtained.

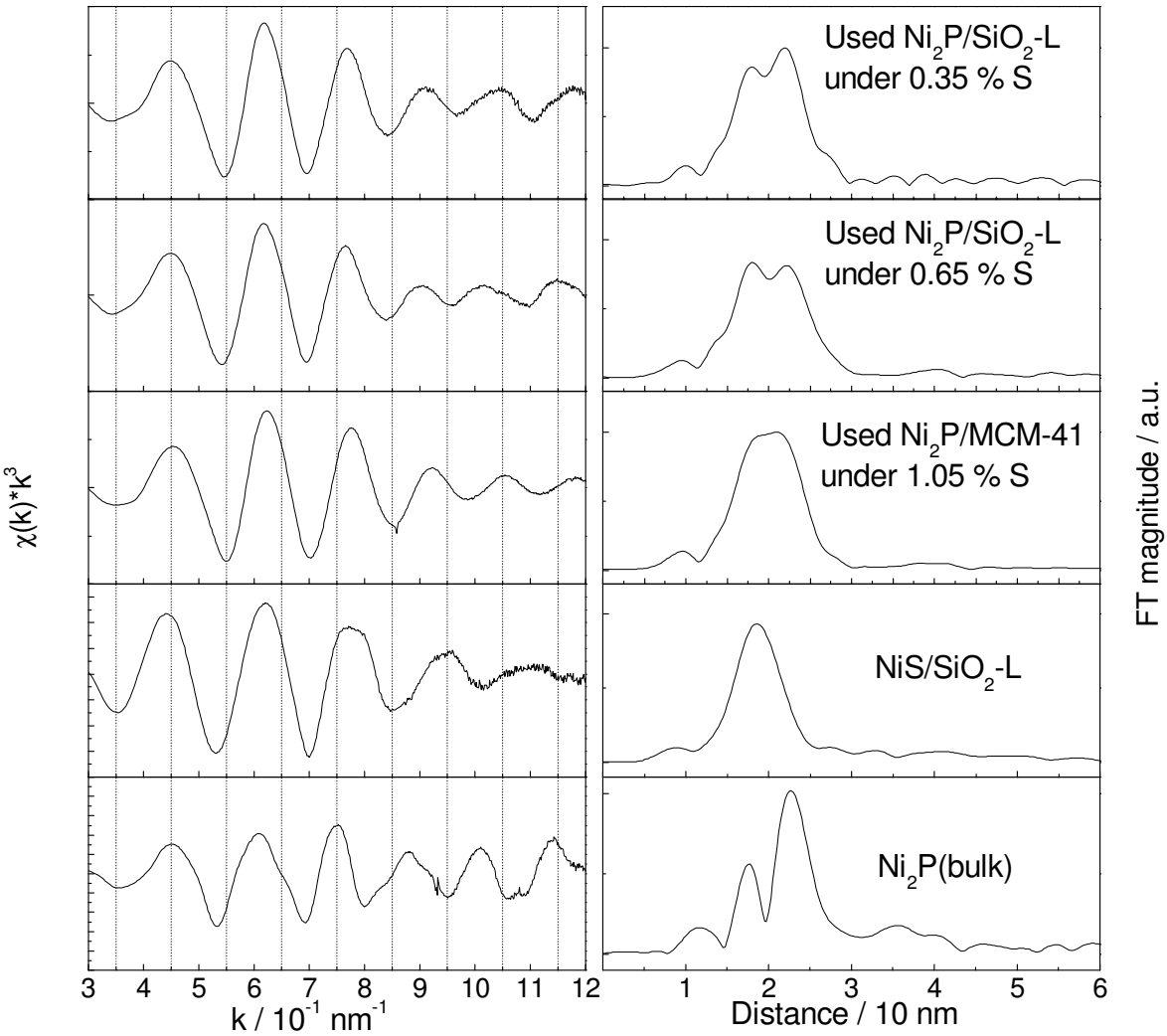

Figure 2.6. EXAFS analysis results for the used samples.

Table 2.4 Curve-fitting results for used Ni_2P catalysts

Used Samples	Ni-P				Ni-S				Ni-Ni				R(%)
	CN	R / nm	σ^2 / 10^{-5} nm^2	ΔE / eV	CN	R / nm	σ^2 / 10^{-5} nm^2	ΔE / eV	CN	R / nm	σ^2 / 10^{-5} nm^2	ΔE / eV	
Feff reference	2	0.22662			6	0.2395			2	0.26131			
NiS [a] / SiO_2-L					5.70	0.2390		5.764					2.23
Ni_2P [b] / SiO_2-L	1.90	0.2260	4.024	-1.034	4.154	0.2375	1.3346	-1.034	2.98	0.2569	10.42	-1.034	1.83
Ni_2P [c] / SiO_2-L	2.03	0.2263	6.739	-0.734	5.373	0.2391	4.838	-0.734	2.577	0.2583	12.58	-0.734	1.11
Ni_2P [d] / MCM41	1.89	0.2225	6.79	-1.987	2.249	0.2361	4.813	-1.987	2.142	0.2547	11.70	-1.987	0.99

ΔR filtered = 0.1380 - 0.2589 nm, $S_o^2 = 0.9$, [a] sulfided under 10 %H_2S/H_2 for 2 h at 400 ^oC, [b] tested under 0.35% S, [c] tested under 0.65% S, [d] tested under 1.05 % S in feed

2.3.2. Activity Test for HDS of 4,6-DMDBT

Figure 2.7 shows the HDS conversion and product selectivities for the Ni_2P/SiO_2-L and Ni_2P/SiO_2-H samples toward the DDS and HYD pathways of 4,6-DMDBT as a function of time on stream. Various liquid feeds with different composition were introduced in sequence in the course of the reaction test. Initially, 4,6-DMDBT dissolved in tridecane was introduced alone (Fig. 2.7 A) at 573 K (300 ^{o}C). For both catalysts the HDS conversion was high and stable at 97-99% and the selectivity favored the HYD pathway (95 %) over the DDS pathway (5 %). After 40 h on stream time 0.3 % S (as DMDS) was added to the feed (Fig. 2.7 B), and this resulted in a small drop in conversion for the Ni_2P/SiO_2-L catalyst. After 85 h 1% tetralin was also introduced (Fig. 2.7 C), but this gave no distinctive change in the HDS results. After 135 h 0.02 % N was added (Fig. 2.7 D) and this led to a decrease by 22 % in HDS conversion for Ni_2P/ SiO_2-L and by 12 % for Ni_2P/ SiO_2-H, respectively. After 185 h the level of sulfur was increased to 0.6 % S (as DMDS) and the tetralin and N were stopped (Fig. 2.7 E) and this led to an enhancement in HDS conversion but the levels of HDS conversion were lower than those with 0.3 % S (as DMDS) in the feed. It is interesting to note that the product selectivities remained constant during the course of reaction with the different feeds on stream, particularly at 573 K (300 ^{o}C). After 225 h the temperature was increased up to 613 K (340 ^{o}C) under the same feed (Fig. 2.7 F), and this led to an enhancement in HDS conversion to 96-99 % in both cases and gave rise to a substantial increase in the selectivity for the DDS pathway over the HYD pathway.

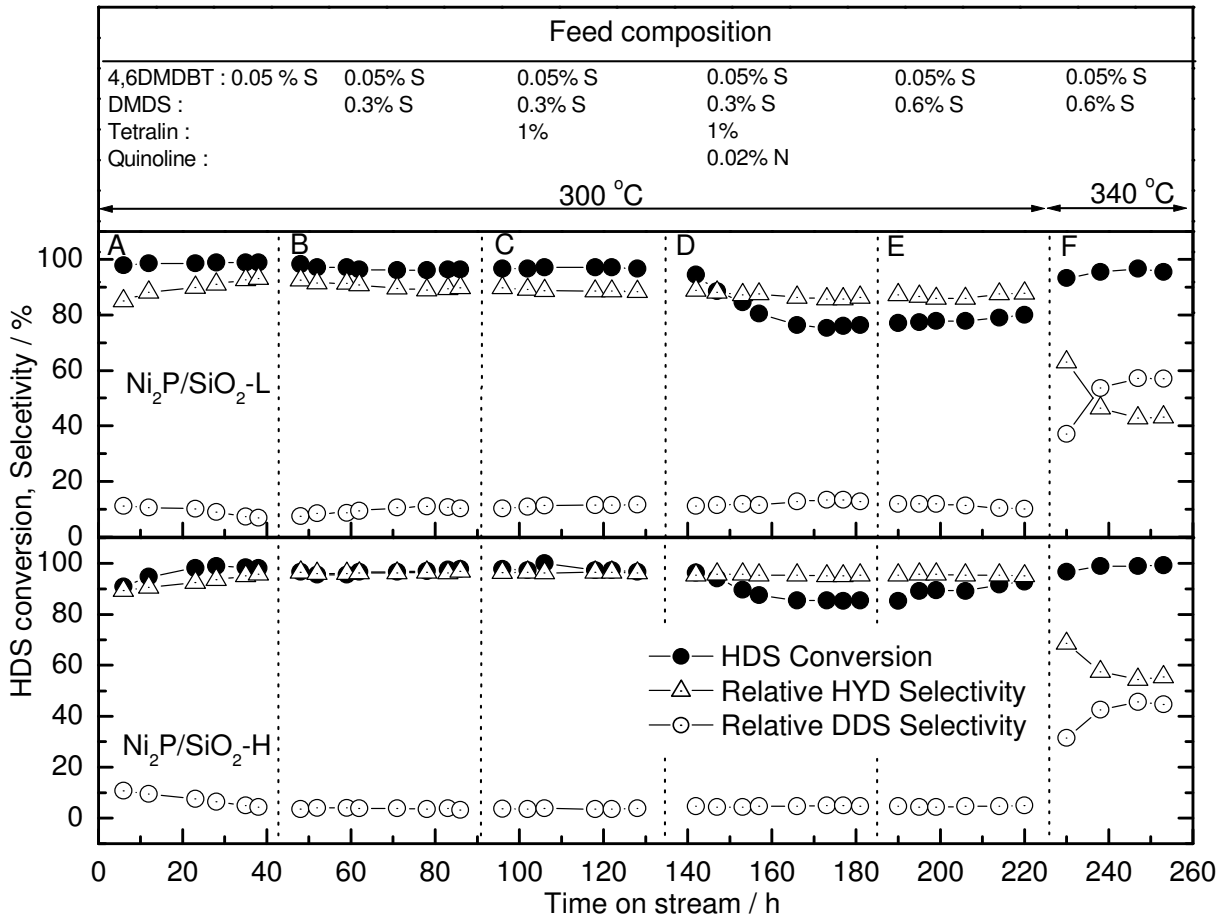

Figure 2.7. Activity test in HDS of 4,6-DMDBT for SiO_2 supported Ni_2P catalysts at 300 °C

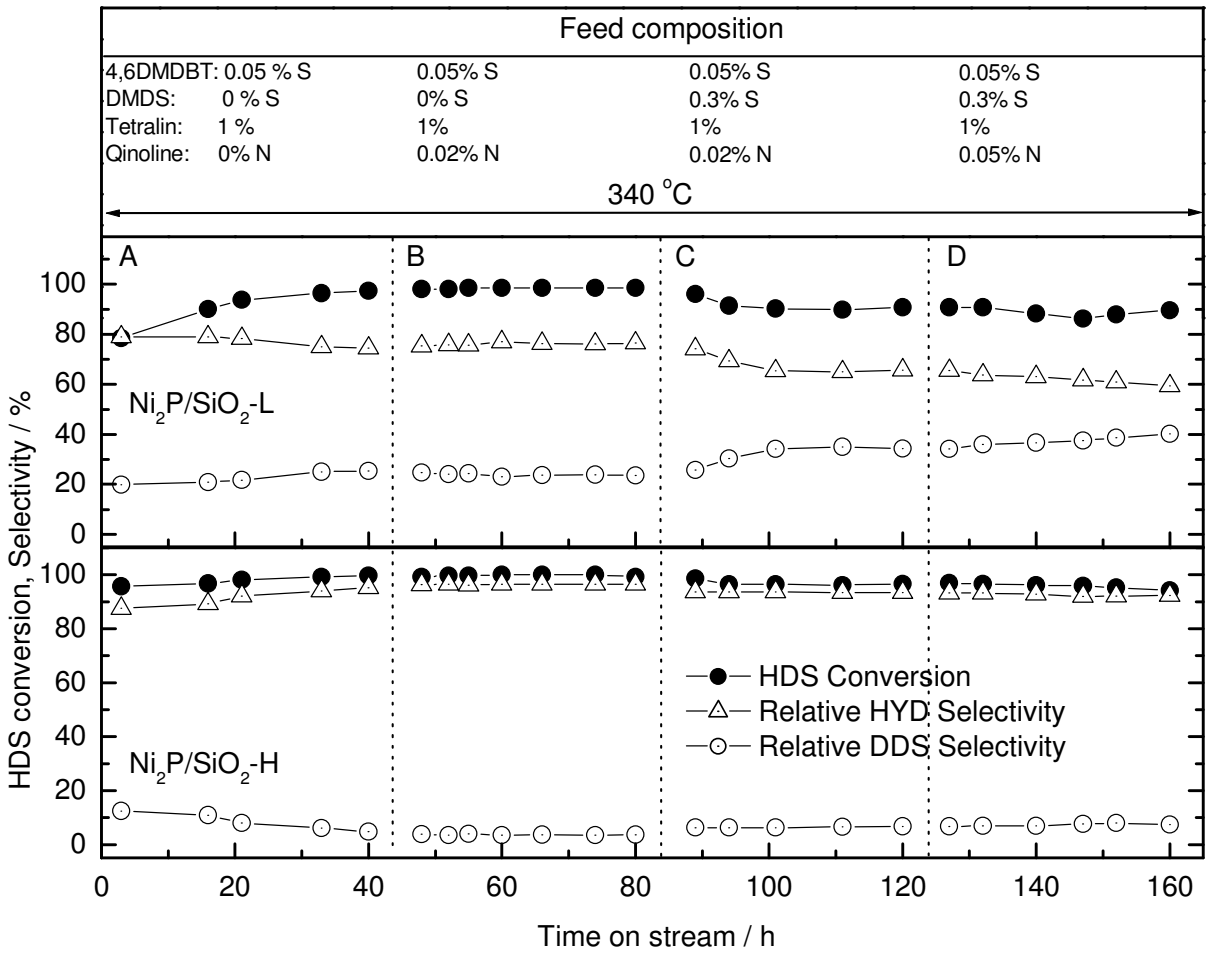

Figure 2.8. Activity test in HDS of 4,6-DMDBT for SiO_2 supported Ni_2P catalysts at 340 °C.

Figure 2.8 shows the result of similar reaction tests carried out at higher temperature, 613 K (340 ^{o}C) again with fresh Ni_2P/SiO_2-L and Ni_2P/SiO_2-H. Again, initially 4,6-DMDBT dissolved in tridecane was introduced at 613 K (340 ^{o}C). In both cases, HDS conversion was high at 98-99% and was stable as observed in the previous run at 573 K (300 ^{o}C). After 45 h on stream, 1% tetralin and 0.02 % N (as quinoline) were added, but this gave no distinctive difference in HDS conversion as well as product selectivities. After 85 h 0.02 % N (as quinoline) and 0.03 % S (as DMDS) were added and this led to a decrease by 9 % in the HDS conversion for Ni_2P/SiO_2-L and by 3 % for Ni_2P/SiO_2-H. After 125 h more quinoline was added to the feed (0.05 % N in total). This gave rise to only a slight decrease in HDS conversion of less than 2 % in both cases with the product selectivity remaining constant.

Figure 2.9 shows similar results at different conditions again for Ni_2P/SiO_2-L and Ni_2P/SiO_2-H at 613 K (340 ^{o}C). The initial feed contained 0.65 % S (0.6 % S as DMDS and 0.05 % S as 4,6-DMDBT) dissolved in tridecane at 613 K (340 ^{o}C). In both cases, HDS conversion was high and stable at 95 - 99 %, while the selectivities were different. The selectivities to HYD and DDS were 43 and 57 % for Ni_2P/SiO_2-L and 58 and 42 % for Ni_2P/SiO_2-H. After 45 h the supply of DMDS was cut off and this led to an increase in selectivity to HYD from 45 to 51% for Ni_2P/SiO_2-L and 58 to 64 % for Ni_2P/SiO_2-H, with the HDS conversion being maintained. After 85 h DMDS, tetralin, and quinoline were reintroduced, and this led to a decrease in HDS conversion from 92 to 69 % for Ni_2P/SiO_2-L and from 98 to 83 % for Ni_2P/SiO_2-H. The selectivity to HYD was also lowered from 51 to 34 % for Ni_2P/SiO_2-L and from 65 to 50 % for Ni_2P/SiO_2-H. After 135 h the N level was increased from 0.02 % to 0.05 % and this led to a slight decrease in HDS conversion for

Ni_2P/SiO_2-L and no change for Ni_2P/SiO_2-H.

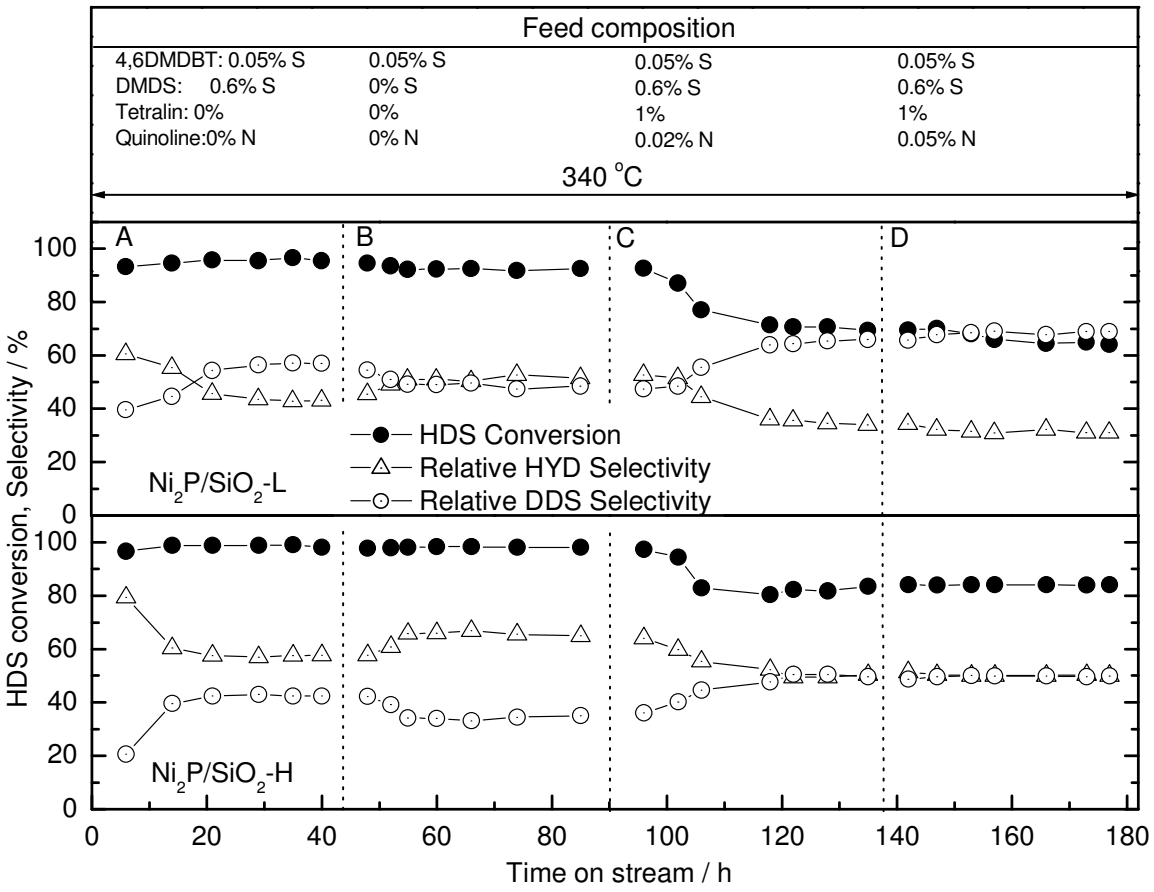

Figure 2.9. Activity test in HDS of 4,6-DMDBT for SiO_2 supported Ni_2P catalysts at 340 °C.

Figure 2.10 shows the HDS conversion of 4,6-DMDBT and the product selectivities toward DDS and HYD for the Ni_2P/MCM-41 and Ni-Mo-S/Al_2O_3 catalyst as a function of time on stream. An initial feed containing 0.35 % S (0.03 % S as 4,6-DMDBT and 0.3 % S as DMDS) dissolved in tridecane was introduced at 573 K (300 ^oC). For Ni_2P/MCM-41 the HDS conversion was high and stable at 99 % with the selectivities being 95 and 5 % toward the HYD and DDS pathways, respectively, while for Ni-Mo-S/Al_2O_3 the HDS conversion and HYD selectivity were low at 61 % and 70 %, respectively. After 40 h N was added and this led to a decrease in HDS conversion for Ni-Mo-S/Al_2O_3 from 61 % to 41 %, and a decrease in HYD selectivity from 70 % to 65 %. For Ni_2P/MCM-41 there was no change in conversion and selectivity. After 81 h the temperature was increased to 613 K under the same feed, which led to an increase in HDS conversion for Ni-Mo-S/Al_2O_3 from 41 % to 75 % with the HYD selectivity being enhanced from 65 % to 75 %. For Ni_2P/MCM-41 the HDS conversion and selectivity remained constant. After 125 h a feed with additional 0.3 % S as DMDS was introduced, which led to an increase of HDS conversion for Ni-Mo-S/Al_2O_3 from 71 % to 80 % with the HYD selectivity being slightly increased from 75 % to 80 %. For Ni_2P/MCM-41 the HDS conversion remained constant but the selectivity to HYD decreased from 93 % to 70 %. After 174 h tetralin was added and N was increased from 0.02 % to 0.05 %, and this led to a decrease in HDS conversion from 98 % to 90 % for Ni_2P/MCM-41 and from 80 % to 68 % for Ni-Mo-S/Al_2O_3. The selectivity to HYD was decreased from 69 % to 65 % for Ni_2P/MCM-41 and 80 % to 73 % for Ni-Mo-S/Al_2O_3. After 214 h the S level was increased from 0.6 % to 1.0 %, and this led to no change in HDS conversion but the HYD selectivity were reduced from 64 to 51 % for Ni_2P/MCM-41. For Ni-Mo-S/Al_2O_3 a further decrease in HDS conversion was observed from 69 % to 65 % with

the resulting selectivites being 70 and 27 % toward HYD and DDS, respectively.

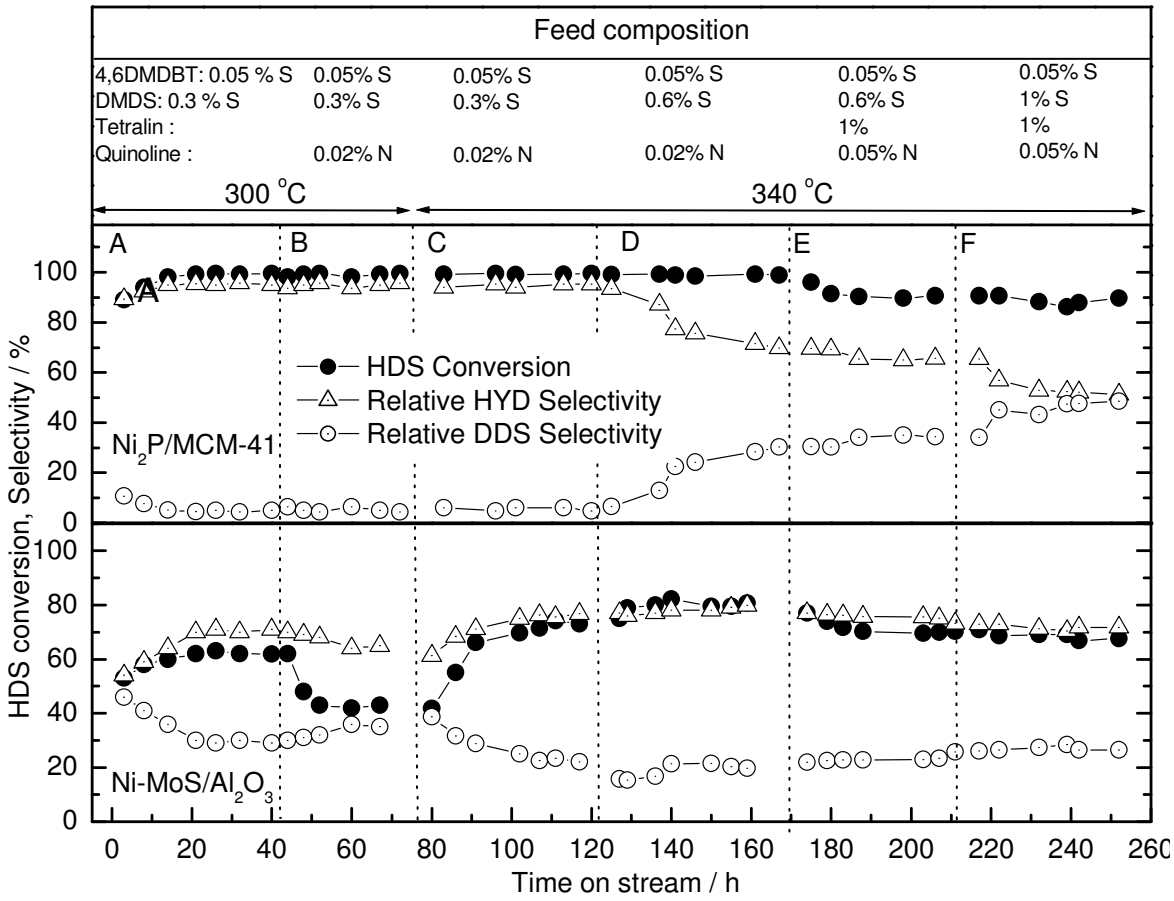

Figure 2.10. Activity test in HDS of 4,6-DMDBT for Ni_2P/MCM-41 and Ni-MoS/Al_2O_3.

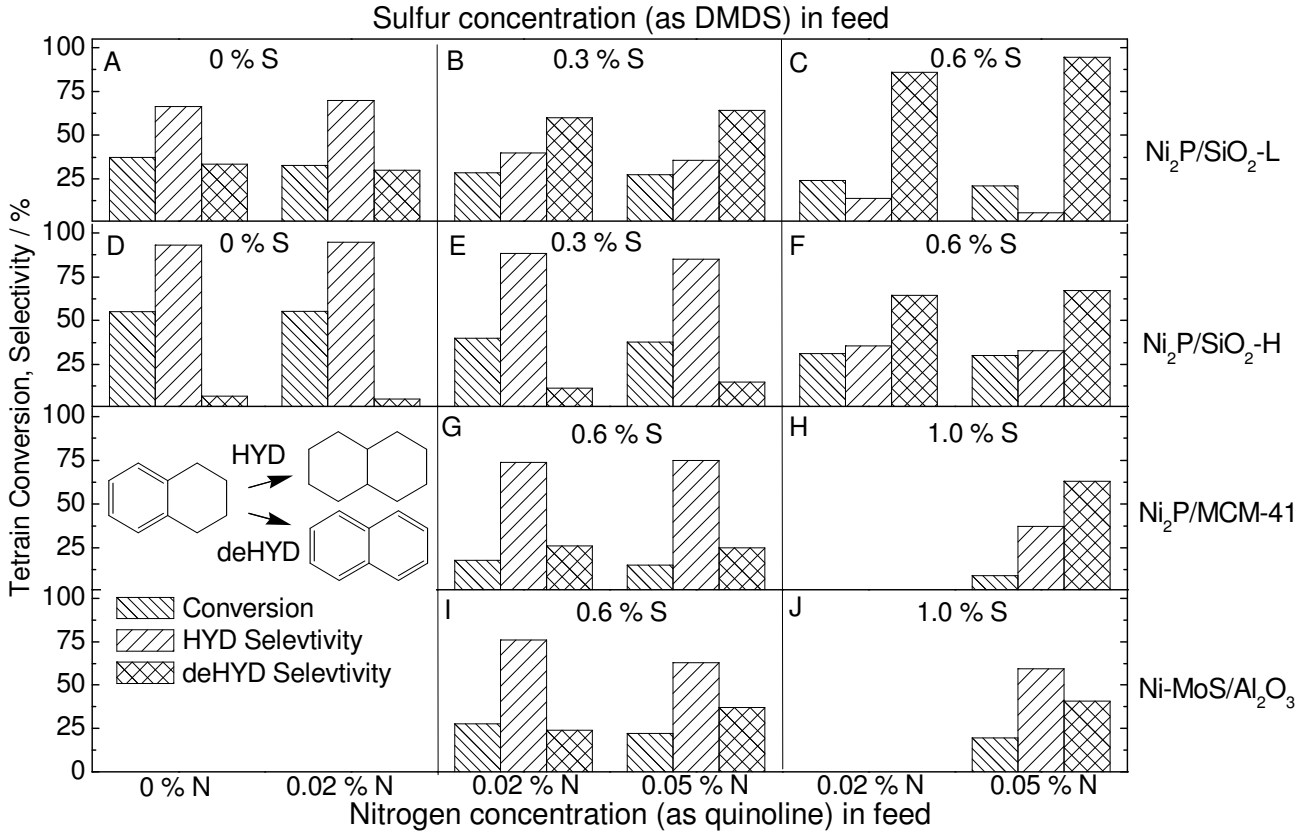

Figure 2.11. Comparison of hydrogenation/dehydrogenation activity for tetralin over Ni_2P/ SiO_2-L, Ni_2P/ SiO_2-H, Ni_2P/ MCM-41 and Ni-MoS/Al_2O_3.

Figure 2.11 shows the conversion and the product selectivities toward hydrogenation (HYD) and dehydrogenation (deHYD) of tetralin as a function of nitrogen (as quinoline) and sulfur (as DMDS) content in the feed for the Ni_2P/SiO_2-L, Ni_2P/SiO_2-H, Ni_2P/MCM-41 and Ni-Mo-S/Al_2O_3 catalysts at 613 K and 3.1 MPa. In all cases 0.05 % S (as 4,6-DMDBT) in tridecane was also introduced. For the Ni_2P/SiO_2-L catalyst the conversion and HYD selectivity of tetralin were 37 % and 66 %, respectively with no DMDS in the feed (Fig. 2.11 A). Introduction of N in the feed led to a slight decrease in tetralin conversion from 37 % to 33 %, but with little change in selectivity. Introduction of 0.3 % S (as DMDS) resulted in a decrease in the conversion from 33 % to 28 % with HYD selectivity being lowered, and further addition of S (0.6 % S as DMDS in total) led to much greater decrease in conversion as well as HYD selectivity (Fig. 2.11 B-C). The same reaction conditions were used with Ni_2P/SiO_2-H, which exhibited better conversion (55 %) of tetralin than Ni_2P/SiO_2-L, and higher HYD selectivity (93 %), particularly under conditions of no DMDS in the feed (Fig. 2.11 D). Addition of DMDS up to 0.3 % S led to a slight decrease in the conversion of tetralin, and further addition of S much lowered the HYD selectivity, but, again, the catalytic behavior was less affected by the N-compound (Fig. 2.11 E-F). The same reaction conditions but even higher amounts of S were used for the Ni_2P/MCM-41 and Ni-Mo-S/Al_2O_3 catalysts. The Ni_2P/MCM-41 showed slightly lower activity with a tetralin conversion of 18 % but high HYD selectivity of 74 % under 0.6 % S (as DMDS) in the feed (Fig. 2.11 G). Further addition of S led to a decrease in conversion as well as HYD selectivity (Fig. 2.11 H). The Ni-Mo-S/Al_2O_3 showed slightly higher activity than Ni_2P/MCM-41 with a tetralin conversion of 27 % (Fig. 2.11 I). Unlike the case of the supported Ni_2P catalysts, further addition of N lowered the tetralin conversion from 29 % to

20 % with the HYD pathway being inhibited (Fig. 2.11 I).

2.4. Discussion

2.4.1. The Nature of Supported Ni_2P Catalysts

Ni_2P [11] adopts a hexagonal structure (Space group: $P_{\bar{6}2m}$, D^2_{3h}, Struckturbericht notation: revised C22) with lattice parameters, a = b = 0.5859 nm, c = 0.3382 nm, in which the Ni atoms form two types of 9-fold arrangements around each P atom. Both 9-fold arrangements consist of a Ni trigonal prism around a P and three additional Ni atoms bonded to the center P through the three rectangular faces of the trigonal prism. There are two types of Ni (denoted as Ni(I), Ni(II)) and P (denoted as P(I), P(II)) sites, which form two different trigonal prisms in Ni_2P. For example, the Ni (I) site is surrounded by 4 P atoms (2 P at 0.2209 nm and 2 P neighbors at 0.2266 nm) and 8 Ni atoms (2 Ni (I) at 0.2613 nm, 2 Ni (II) at 0.2605 nm, and 4 Ni (II) at 0.26783 nm). The Ni (II) site is surrounded by 5 P atoms (1 P at 0.2369 nm, 4 P at 0.2457 nm) and 6 Ni atoms (2 Ni (I) at 0.2605 nm, and 4 Ni (I) at 0.26783 nm).

Ni_2P catalysts were successfully prepared on the SiO_2 and MCM-41 supports. The temperature programmed reduction profile for the calcined nickel phosphate precursors gives a distinctive reduction peak at a moderately high temperature of around 873 K. In the case of PO_x/SiO_2-L a broad reduction feature is observed at high temperature, indicating that the phosphate is difficult to reduce. In the case of NiO/SiO_2-L the reduction occurs at a lower temperature, 570 K, consistent with the known ease of the reducibility of nickel oxide. These results indicate that Ni species in the oxidic precursor are strongly associated with the

P component. Furthermore, the peak maximum of reduction temperature is shifted to slightly higher temperature for the samples with better dispersion, and this implies that smaller particles have stronger interaction with the supports. Such results are commonly found in the case of SiO_2-supported Ni catalysts, in which reduction of well dispersed NiO particles occurs at higher temperature because the interaction between the catalysts and support increases with dispersion [12]. The samples were prepared with excess phosphorus using a P/Ni ratio of 2/1. Elemental analysis shows that there was a loss of the phosphorus during preparation (Table 2.2) with P/Ni ratios of 0.7-0.9, approaching the stoichiometric value of 0.5 for Ni_2P. Previous work had shown that phosphorus is removed as PH_3 during the reduction procedure [4,6]. Elemental analysis revealed that more P remained on the better dispersed supported Ni_2P catalysts (Table 2.2), even though higher temperatures were applied for reducing these well dispersed samples (873, 883, and 893 K for Ni_2P/SiO_2-L, Ni_2P/SiO_2-H, and Ni_2P/MCM-41, respectively). This suggests that there are stronger interactions between Ni and P in the smaller particles. On the SiO_2 supports characteristic XRD signals of Ni_2P are clearly visible (Fig. 2.2), although the overall peak intensity is lowered for the higher surface area support (SiO_2-H). The broader, less intense Ni_2P XRD peak in the Ni_2P/SiO_2-H material indicates a higher dispersion of the phosphide phase, as also indicated by the high CO uptake compared to the Ni_2P/SiO_2-L sample (Table 2.1). In the case of the Ni_2P/MCM-41 sample XRD shows retention of the peaks of the MCM-41 support, although somewhat attenuated, and no peaks due to Ni_2P. The retention of the MCM-41 peaks indicates that the framework structure does not deteriorate seriously during the synthesis steps which include calcination at 673 K followed by reduction at 893 K. The lack of XRD signals for Ni_2P is probably due to line-broadening caused by highly dispersed

particles.

EXAFS analysis is particularly useful for characterizing the highly dispersed phase on the supports with large surface area. Fourier transform EXAFS spectra for the supported Ni_2P catalysts show two overlapping peaks in the region 0.15-0.30 nm. A simple analysis of the spectra was precluded because it was not possible to extract directly from the experimental spectra the phase shifts and backscattering amplitude functions needed for the fits due to the insufficient separation of the peaks corresponding to the Ni and P neighbors and the possible superposition in the second shell of both the Ni and the P contributions. The spectrum of the reference Ni_2P compound was therefore first simulated with Feff, with structural parameters obtained from the literature [9]. The Feff simulation (circles in Fig. 2.5) allowed the assignment of those peaks that appeared in the Fourier transform. The first small peak centered at 0.180 nm was due to P neighbors at 0.2209 and 0. 2266 nm and the second larger peak centered at 0.230 nm was due to a mixed feature of P neighbors at 0.2369 and 0.2457 nm and of Ni neighbors at 0.26783 nm. Since the number of independent fitting parameters is limited by 12 as given by the formula [13], $N_{ind} = 2 \cdot \Delta k \cdot \Delta R / \pi + 2$, a three-shell analysis is permissible. For the curve fittings the three dominant shells were selected from the simulation results and used as references for phase shift and amplitude calculations. As described above, two Ni-P shells at 0.2266 and 0.2456 nm and one Ni-Ni shell at 0.2678 nm were employed for the calculations. Further details about the three-shell analysis will be described in Chapter 3. These give reasonable parameters for all samples (Table 2.3). For example, fitting for the bulk Ni_2P gives 2 P neighbors at 0.2253 nm and 1.75 P neighbors at 0.2401 nm and 3.99 Ni neighbors at 0.2644 nm. Based on the Ni_2P structure, there is a P neighbor at 0.2369 nm which is close to the second shell. Thus, the decrease in both

coordination number and bond length is reasonable because the EXAFS spectrum is an average over the different bonds. In contrast to bulk Ni_2P, for the supported Ni_2P samples the coordination number of the second shell, Ni-P at 0.2456 nm, increases as dispersion increases, even though the Ni-P bond length decreases. Interestingly, the bond length for the Ni-Ni shell increases with the coordination number as the dispersion increases. It is thus likely that the more dispersed Ni_2P catalyst contains more P atoms, and that the interstitial P atoms lengthen the distance between Ni atoms and weaken the Ni-Ni bond. This is also consistent with the elemental analysis. The Ni_2P/MCM-41 containing highly dispersed Ni_2P particles underwent less loss in P, even after the high temperature reduction. This suggests that the smaller particles have a stronger interaction between the Ni and P atoms.

For the used samples, a preliminary analysis showed that a good fit was not obtained with the three-shell method, particularly for the second shell, Ni(II)-P, which is indicative of deformation of the second shell. The Ni-Ni shell was also deformed and became shorter in bond length. This allowed us to employ a Ni-S shell instead of a second Ni(II)-P shell, and the 2 Ni-Ni shell at 0.2613 nm instead of the use of the third shell (Ni(I)-Ni(II)). The curve-fittings were thus carried out for three dominant shells (2 Ni-P at 0.2266 nm, 6 Ni-S at 0.2369 and 2 Ni-Ni at 0.2613 nm) of which phase shifts and amplitude functions were calculated with FEFF 8.0 code [9] from Ni_2P [11] and NiS [10]. Again, the reducing factor (S_o^2), was fixed as 0.90, during the fitting. This gave consistent and physically realistic values for bond distances (R) and coordination numbers (CN) for all the samples (Table 2.4). The essential result is the presence of a Ni-S bond in the used samples likely due to a phosphor sulfide phase on the samples of the Ni_2P particles. This gives rise to shorter Ni-Ni distances and lower coordination numbers than in the fresh samples.

2.4.2. Catalytic Behavior of Supported Ni_2P Catalysts in the HDS of 4,6-DMDBT

The reaction network of 4,6-dimethyldibenzothiophene (4,6-DMDBT) is similar to that of dibenzothiophene, involving two parallel sequences that lead to desulfurized products [14]. One of the parallel pathways is denoted the direct desulfurization pathway (DDS) and in the case of 4,6-DMDBT results in the formation of 3,3-dimethylbyphenyl (3,3-DMBP). The other parallel pathway is referred to as the hydrogenation pathway (HYD) and involves the pre-hydrogenation of 4,6-DMDBT to 4,6-tetrahydro or hexahydro-DMDBT, which are subsequently desulfurized to methylcyclohexyltoluene (MCHT) and dimethylbicyclohexane (DMBCH) [15,16,17]. The two pathways may be distinguished from studies of selectivity extrapolated to low conversions [14]. However, in this work the relative contributions of these pathways were simply approximated by the relative amounts of the final DMBP and DMBCH products. It is realized that these species are interconverted by dehydrogenation/hydrogenation reactions, but it was the main objective of this work to concentrate more on the effect of sulfur, nitrogen, and aromatic compounds on the HDS rate, than on determining the mechanistic pathways, which has already been addressed [14]. With some important distinctions, to be discussed below, the product distributions obtained in the HDS of 4,6-DMDBT on the supported Ni_2P catalysts and Ni-Mo-S/Al_2O_3 catalysts were similar (Figs. 2.7-10). For all catalysts the major products were 3,3-dimethylbiphenyl (3,3-DMBP), methylcyclohexyltoluene (MCHT), and dimethylbicyclohexyl (DMBCH). Only traces of 4,6-tetrahydro- and 4,6-hexahydrodibenzothiophenes were found.

2.4.2.1. Influence of Temperature

Studies were carried out at two different temperatures (573, 613 K) at the same pressure (3.1 MPa, 450 psig). For the base case of the silica-supported catalysts at 573 K without added S, N or aromatics (Fig. 2.7 A) the conversion was high (97-99 %) and the selectivity favored the HYD pathway (95 %) over the DDS pathway (5 %). At the same conditions (Fig. 2.10 A) the Ni_2P/MCM-41 catalyst showed similar high conversion (99 %) and selectivities, while the Ni-Mo-S/Al_2O_3 catalyst displayed much lower conversion (61 %) and lower preference for the HYD pathway (70 %) over the DDS pathway (30 %). This is similar to the finding for Ni_2P/SiO_2 and Ni-Mo-S/Al_2O_3 in a batch reactor at lower conversion [14]. The high selectivities for the HYD pathway in the present studies are probably due to thermodynamics, which predicts an equilibrium concentration of 4,6-DMDBT and 4,6-tetrahydro-DMDBT at 20 % and 80 %, respectively, at 613 K and 3.1 MPa [18]. The effect of aromatic compounds (tetralin) at relatively large concentration (1 %) was minimal over the Ni_2P/SiO_2-L and Ni_2P/SiO_2-H catalysts (Fig. 2.7 B). The introduction of a N-compound (0.02 % N as quinoline) in the feed led to a decrease in HDS conversion by 20 % for the Ni_2P/SiO_2-L and by 16 % for the Ni_2P/SiO_2-H (Fig. 2.7 D). The Ni_2P/MCM-41 catalyst, however, maintained its activity even after the introduction of quinoline (Fig. 2.10 B). The Ni-Mo-S/Al_2O_3 catalyst had shown a low HDS conversion of 61 % in the absence of N (Fig. 2.10 A), and this was further lowered by the addition of quinoline to 42 % (Fig. 2.10 B), indicating that HDS is strongly inhibited by quinoline at low temperature on the sulfide catalyst. This suggests that at low temperatures Ni_2P catalysts show much better activity and resistance to quinoline than the commercial Ni-Mo-S/Al_2O_3 sample.

The catalytic activity was also tested for these samples at a high temperature, 613 K (340 ^oC). Ni_2P/SiO_2-L showed high HDS conversion at around 99% with the HYD

selectivity being slightly lowered by 10% to 76 %, compared to that at lower temperature (Fig. 2.8 A) and showed high resistance to quinoline and tetralin (Fig. 2.8 B) before the introduction of DMDS. The addition of DMDS (0.3 % S) lowered HDS conversion to 92 % and reduced selectivity to the HYD pathway to 65 % (Fig. 2.8 C). The samples with better dispersion, Ni_2P/SiO_2-H and Ni_2P/MCM-41 (Fig. 2.8 C and 2.10 C), underwent almost no inhibition with 0.02 % N and 0.3 %S in the feed. The lack of inhibition by quinoline for the highly dispersed Ni_2P samples could be due to the need for a large "landing site" for the heteroatomic compound. For the sulfide the increase of temperature from 573 K to 613 K resulted in a substantial increase in conversion from 42 % to 72 % and a moderate increase in selectivity to the HYD pathway from 65 % to 76 % (Fig. 2.10 C).

2.4.2.2. Influence of S-compound

At the low temperature of 573 K addition of DMDS resulted in only a small amount of inhibition of the HDS conversion and little change in the product selectivities for Ni_2P/SiO_2-L and Ni_2P/SiO_2-H (Figs. 2.7 B-E), and Ni_2P/MCM-41 (Fig. 2.10 A). At the high temperature of 613 K addition of DMDS had a small inhibitory effect for conversion on Ni_2P/SiO_2-L, also reducing its selectivity for the HYD route, but had little effect on conversion or selectivity for Ni_2P/SiO_2-H (Fig. 2.8 C). For Ni_2P/MCM-41 sulfur had little apparent effect on conversion and selectivity at low levels (0.3 % S) (Figs, 2.10 A-C), but at higher levels (0.6 % S) resulted in a decrease in selectivity to the HYD route. For the Ni-Mo-S/Al_2O_3 catalyst, sulfur was beneficial for conversion (Fig. 2.10 D) and favored slightly the HYD route. The change in selectivity for the Ni_2P catalysts at high sulfur levels (Figs.

2.8 C, 2.10 D) were in the direction of the selectivity found for the Ni-Mo-S/Al_2O_3 catalyst (Fig. 2.10 D), indicating sulfidation of the surface consistent with the EXAFS results. However, the activity of the phosphides remained higher than that of the sulfide, indicating that its surface properties were distinct.

2.4.3. Relation of Catalytic Behavior to the Nature of Ni_2P Catalyst

The catalytic activity for the supported Ni_2P catalyst samples in HDS of 4,6-DMDBT followed the order, Ni_2P/SiO_2-L < Ni_2P/SiO_2-H < Ni_2P/MCM-41 under 0.65 % S, 0.02 % N, and 1% tetralin at 340 ^oC, which was well correlated with the amount of CO uptake. In a previous study extra P (Ni/P=1/2) in the preparation of Ni_2P on the low surface SiO_2 (~90 m^2 g^{-1}) support gave rise to a better dispersion and also gave a beneficial effect on the catalytic activity as well as the stability [4]. Use of a high surface area siliceous support (MCM-41) has resulted in even higher dispersion, as evident from the amount of CO uptake (Table 2.1) and the EXAFS line shape analysis, and better catalytic performance.

The Ni_2P/SiO_2-H and Ni_2P/MCM-41 showed much better resistance to the inhibition of S and N-compounds with maintenance of higher HDS conversion compared to Ni_2P/SiO_2-L (Figs. 2.9 and 10). The EXAFS analysis confirms that the Ni-Ni bond length is widened with dispersion and this feature comes with an increase in Ni-P coordination and a decrease in Ni-P bond length. Thus the higher resistance to the sulfidation can be explained by the stronger interaction between Ni and P species for the highly dispersed Ni_2P catalysts. It is known that metallic Ni species, having closer Ni-Ni bond lengths, can be easily sulfided [19]. Thus this suggests that lack of P in the Ni_2P phase results in the Ni-Ni bond length to be shorter, leading to sulfidation under the HDS reaction at high temperature and high

pressure. For an example a Ni_2P/K-USY that was obtained with stoichiometric P content (Ni/P=0.5) gave rise to a decrease in Ni-Ni bond length and underwent deactivation due to a severe sulfidation [20]. Similar results were reported for the Ni_2P/SiO_2–L catalysts in the HDS of dibenzothiophene [4]. These results thus suggest that the HDS activity and the resistance to S and N-compound highly depend on the dispersion of the Ni_2P phase.

2.5. Conclusions

Nickel phosphide (Ni_2P) catalysts supported on silica and MCM-41 showed high HDS activity for 4,6-DMDBT compared to a commercial Ni-Mo-S/Al_2O_3 catalyst at 573 K (300 ^oC) and 613 K (340 ^oC) and 3.1 MPa based on equal sites (70 μmol) loaded in the reactor. The desulfurization was dominated by the hydrogenation pathway over the Ni_2P catalysts and showed less inhibition by S and N-compounds compared to the sulfide catalysts. Selectivity and performance was higher on the more dispersed catalysts in the order Ni_2P/MCM-41 > Ni_2P/SiO_2-H > Ni_2P/SiO_2-L and this is attributed to the increase in the number of and quality of active sites. Smaller Ni_2P particles have better resistance to S and N compounds due to the stronger interaction between Ni and P in the dispersed Ni_2P phase. EXAFS line shape analysis indicates the formation of a phospho sulfide phase which is favored for the catalysts with shorter Ni-Ni bond length particularly under high S in feed and at relatively high temperature. The phase is responsible for the high activity of the nickel phosphide catalysts.

References

1. W. R. A. M. Robinson, J. N. M. van Gastel, T. I. Korányi, S. Eijsbouts, J. A. R. van Veen, V. H., and J. de Beer, J. Catal. 161 (1996) 539.
2 . S. T. Oyama, J. Catal. 216 (2003) 343.
3 . D. C. Phillips, S. J. Sawhill, R. Self, and M. E. Bussell, J. Catal. 207 (2002) 266.
4. S. T. Oyama, X. Wang, .Y.-K. Lee Bando, and F. G. Requejo, J. Catal. 210 (2002) 207.
5. X. Wang, P. Clark and S. T. Oyama, J. Catal. 208 (2002) 321.
6. S. T. Oyama, X. Wang, Y.-K. Lee, and W.-J. Chun, J. Catal. 221 (2004) 263.
7. C.-F. Cheng, D. H. Park, and J. Klinowski, J.Chem. Soc., Faraday Trans., 93(1) (1997) 193
8. P. T. Tanev, and L. T. Vlaev, J. Colloid Interface Sci., 160, 110 (1993).
9. A. L. Ankudinov, B. Ravel, J. J. Rehr, and S. D. Congradson, Phys. Rev. B 58 (1998) 7565.
10. WebATOMS version 1.7, "http://millenia.cars.aps.anl.gov/cgi-bin/atoms/atoms.cgi," 15, August, 2002
11. S. Rundqvist, Acta Chem. Scand. 16 (1962) 992.
12. A. Infantes-Molina, J. Mérida-Robles, P. Braos-García, E. Rodríguez-Castellón, E. Finocchio, G. Busca, P. Maireles-Torres, and A. Jiménez-López, J. Catal. 225 (2004) 479.
13. E. A. Stern, Phys. Rev. B 48 (1993) 9825.
14. J. H. Kim, C. Song, Y.-K. Lee, and S. T. Oyama, Energy and Fuels, in print.
15. D. D. Whitehurst, T. Isoda, and I. Mochida, Adv. Catal. 42 (1998) 345.

16. K. Segawa, and S. Satoh, Stud. Surf. Sci. Catal. 127 (1999) 129.

17. M. Egorova,and R. Prins, J. Catal. 224 (2004) 278.

18. K. Sakanishi, T. Nagamatsu, I. Mochida, and D. D. Whitehurst, J. Mol. Catal. A 155 (2000) 101.

19. A. Aguinaga, M. Montes, P. Malet, M. J. Capitán, I. Carrizosa, and J. A. Odriozola, Appl. Catal. A, 110 (1994) 197.

20. Y.-K. Lee and S. T. Oyama, in preparation.

Chapter 3

The Nature of a SiO_2-Supported Ni_2P Catalyst for Hydrotreating: EXAFS and FTIR studies

3.1. Introduction

The previous chapter presented the successful preparation of a highly dispersed Ni_2P catalyst, Ni_2P/SiO_2-H, which exhibited very high and stable hydrotreating activity. More knowledge of the surface and catalytic properties of this supported phosphide catalysts will be useful for the further enhancement of the activity and stability of phosphides for treating heavier feeds.

In this chapter attention is placed on investigating the structural and chemisorption properties of the Ni_2P/SiO_2-H catalyst. Use is made of X-ray absorption fine structure (XAFS) spectroscopy to study the atomic arrangement in the finely dispersed phosphide phase and FTIR analysis to study the chemisorption of CO and pyridine on is surfaces. Activity tests for the HDS of 4,6-DMDBT, HDN of quinoline, and hydrogenation of tetralin are compared on the Ni_2P/SiO_2-H catalyst and a commercial Ni-Mo-S/Al_2O_3 catalyst.

3.2. Experimental

3.2.1. Catalyst and Reference samples

The supported Ni_2P catalyst was prepared as reported before with excess phosphorus (Ni/P=1/2) and a loading of 1.156 mmol Ni/g support (12.2 wt % Ni_2P/SiO_2) using a commercial SiO_2 support (Cabot, Cab-O-Sil) of high surface area (EH-5, 350 $m^2 g^{-1}$). The synthesis of the catalyst involved two steps and was described in the previous chapter. Briefly, in the first step, a supported nickel phosphate precursor was prepared by incipient wetness impregnation of a solution of nickel nitrate and ammonium phosphate, followed by calcination at 673 K. In the second step, the supported metal phosphate was reduced to a phosphide by temperature-programmed reduction (TPR).

Reference NiO/SiO_2-H and P_2O_5/SiO_2-H samples were prepared by impregnation of SiO_2 (Cabot, Cab-O-Sil, EH-5, 350 $m^2 g^{-1}$) with $Ni(NO_3)_2$ (1.16 mmol Ni/g support, 6.4 wt% P) and $(NH_4)_2HPO_4$ (2.3 mmol Ni/g support, 6.6 wt% P), respectively, followed by calcination at 673 K for 3 h. Again, the designation H refers to high surface area. The calcined NiO/SiO_2 sample was then reduced at 673 K for 2 h to form a Ni/SiO_2 sample or was sulfided in a 10% H_2S/H_2 carrier at 673 K for 2 h to form a sulfided NiS/SiO_2 sample. A bulk Ni_2P (Cerac, 99.5 %) reference was used for comparison to experimental EXAFS results. The sulfide catalyst was the same commercial Ni-Mo-S/Al_2O_3 sample (Criterion 424) containing approximately 15 wt% MoO_3, 3 wt% NiO and phosphorus promoter (2-4 wt%) [1].

3.2.2. Characterization of Samples

X-ray diffraction (XRD) patterns, CO chemisorption, and chemical composition of the samples were obtained as before.

X-ray absorption (XAS) spectra at the Ni K edge (8.333 keV) of reference and catalyst samples were also measured as reported in the previous chapter. In order to fit the experimental EXAFS spectra for the fresh and spent samples, the theoretical EXAFS equation for Ni_2P was used to calculate phase shifts and amplitude functions of Ni_2P, using FEFF 8.0 code [2]. Fitting was then carried out for the fresh samples using the three dominant shells (2 Ni-P at 0.2266 nm, 4 Ni-P at 0.2457 and 4 Ni-Ni at 0.2678 nm), using a reducing factor (S_o^2), fixed as 0.90, a value obtained by fitting the Ni-Ni contribution in Ni foil. The quality of the fit was evaluated by the residual factor (R-factor) which is defined by

$$Residual\ factor(R-factor,\%) = \left(\frac{\sum_{i=1}^{N} \left| y_{\exp}(i) - y_{theo}(i) \right|}{\sum_{i=1}^{N} y_{\exp}(i)} \right) \times 100$$

where y_{exp} and y_{theo} are experimental and theoretical data points, respectively.

Transmission infrared spectra of pressed wafers ($\sim$ 15 mg) of Ni_2P/SiO_2 and Ni-Mo-S/Al_2O_3 catalysts were collected in situ in an IR reactor cell placed in a Fourier-transform infrared (FTIR) spectrometer (Bio-Rad Model FTS 3000MX) at a resolution of 2 cm^{-1} and 64 scans/spectrum. The IR cell was equipped with KBr windows, connections for inlet and outlet flows, and thermocouples connected to a temperature controller to monitor and control the temperature. Prior to dosing CO and pyridine, the Ni/SiO_2 and Ni_2P/SiO_2 samples were reduced in H_2 at 723 K for 2 h and the NiS/SiO_2 and Ni-Mo-S/Al_2O_3 samples were sulfided in a 10% H_2S/H_2 stream at 673 K for 2 h at a flow rate of 100 μmol s^{-1} (150 cm^3/min). For the CO IR measurements the samples after pretreatment were cooled to room temperature in a He flow and were exposed to 1 % CO/He until saturation was

achieved. The samples were then purged in He carrier for 300 s to remove gaseous and weakly adsorbed CO species. The spectra were obtained in the absorbance mode and are shown after subtraction of the background spectrum obtained on the samples before the adsorption to make the adsorbate peaks more clear. For pyridine adsorption, the samples were dosed at 373 K with a molar concentration of pyridine of 0.40 % in a He or H_2 carrier at a flow rate of 100 μmol s^{-1} (150 cm^3/min) until saturation was achieved. The samples were then purged in He for 300 s at 373 K to remove the gaseous and weakly adsorbed pyridine. The spectra are shown after subtraction of the background spectrum obtained at the various temperatures without pyridine. Measurements were made at 373, 423, 473, 523 and 573 K with temperature raised in steps using a heating rate of 0.17 K s^{-1} (10 K/min) and using a hold time of 180 s at each temperature.

3.2.3. Activity Test for HDS

Catalytic activities for the HDS of 4,6-DMDBT, the HDN of quinoline, and the hydrogenation of tetralin were carried out as described before at 3.1 MPa (450 psig) at 573 K (300 ^oC) in the same three-phase upflow fixed-bed reactor. Further details about reaction conditions are described in Chapter 2.

3.3. Results

3.3.1. Structural Features of Ni_2P Catalyst

Figure 3.1 shows the powder XRD patterns of the fresh and spent Ni_2P/SiO_2-H catalyst, and a bulk Ni_2P reference. The XRD patterns confirm that a Ni_2P phase is formed

on the SiO_2-H support, and that the phase is retained during the reaction. The physical properties of the Ni_2P/SiO_2-H catalyst are reported in Table 3.1.

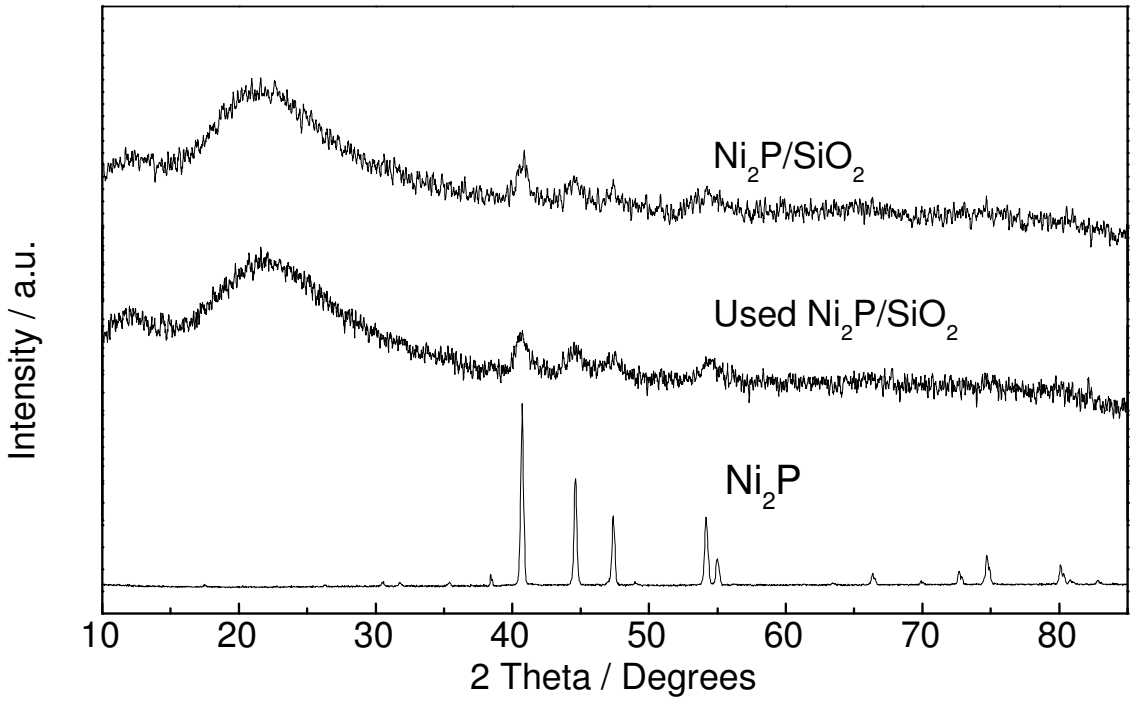

Figure 3.1. XRD patterns of fresh and spent Ni_2P samples.

Table 3.1 Physical properties of Ni_2P catalyst

	CO uptake / μmol g^{-1}	BET area / m^2 g^{-1}	Ni / P molar ratio
Ni_2P/SiO_2-H	33	240	1 / 0.963

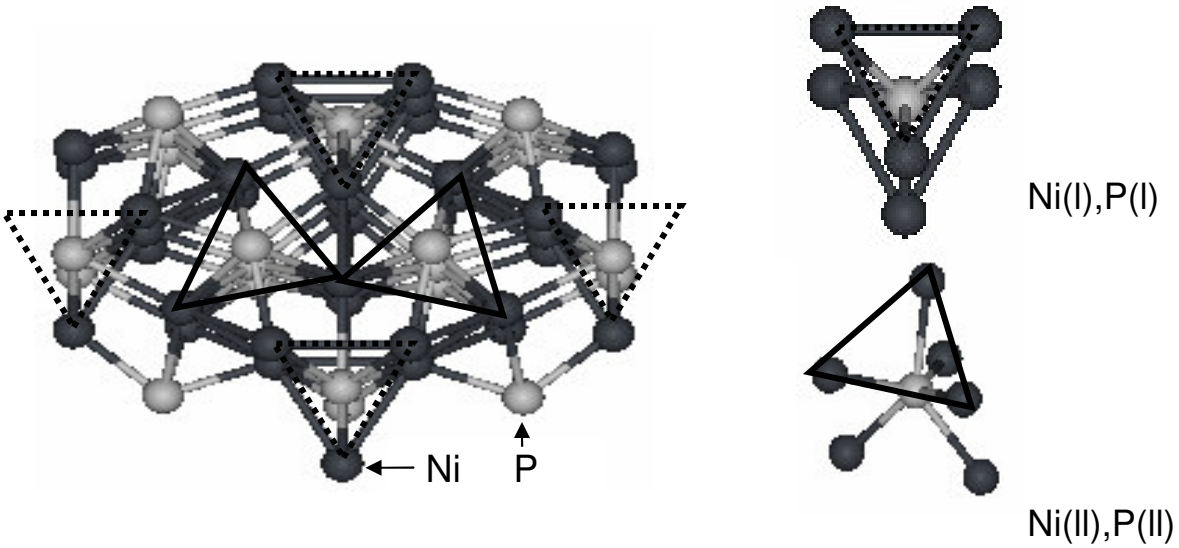

Figure 3.2. Local structure of Ni_2P with two types of trigonal prisms.

Figure 3.2 shows the hexagonal structure of Ni_2P. The Ni_2P unit cell has two types of Ni and P sites (denoted as Ni(I), Ni(II) and P(I), P(II)), which form two different trigonal prisms in Ni_2P consisting of various Ni-P and Ni-Ni subshells. Bond distance and coordination number for the subshells in each trigonal prism are listed in Table 3.3. EXAFS simulations were then carried out taking each Ni site as the absorber in a 0.5 nm cluster in order to obtain phase shifts and effective scattering amplitudes from fitted data of the bulk Ni_2P reference and the Ni_2P/SiO_2-H sample.

Figure 3.3 shows the Ni K-edge EXAFS spectrum after background subtraction, its Fourier transform and the filtered back transform of a Ni foil reference. The first peak in the Fourier transform is centered at 0.2148 nm. The curve-fitting phase shifts and effective scattering amplitudes were calculated from the Ni structure as before using a Feff 8.20 code and with the position of the atom obtained from ATOMS [3]. Table 3.2 reports the curve fitting results by the EXAFS spectra of the Ni foil, which gave a reduction factor, S_o^2 of 0.9 for the absorber Ni atom, with a coordination number of 11.73 and bond distance of 0.2481 nm.

Figure 3.4 shows a comparison between simulated and experimental EXAFS spectra for Ni_2P with the left panels showing the EXAFS oscillation and the right panels showing the Fourier transforms. Figure 3.4 A) shows the simulation for the absorber Ni(I), which gives two distinct peaks centered at 0.175 and 0.240 nm corresponding to Ni-P and Ni-Ni contributions, respectively. Figure 3.4 B) shows the simulation for the absorber Ni(II), which gives one broad peak centered at 0.225 nm, resulting essentially from two overlapping peaks due to Ni-P and Ni-Ni neighbors. Figure 3.4 C) shows the results for the Ni_2P/SiO_2-H catalyst with the FT spectra showing two peaks at 1.74 and 2.27 nm. Figure

3.4 D) shows simulation results for the bulk reference Ni_2P sample with the FT showing peaks at 1.75 and 2.25 nm.

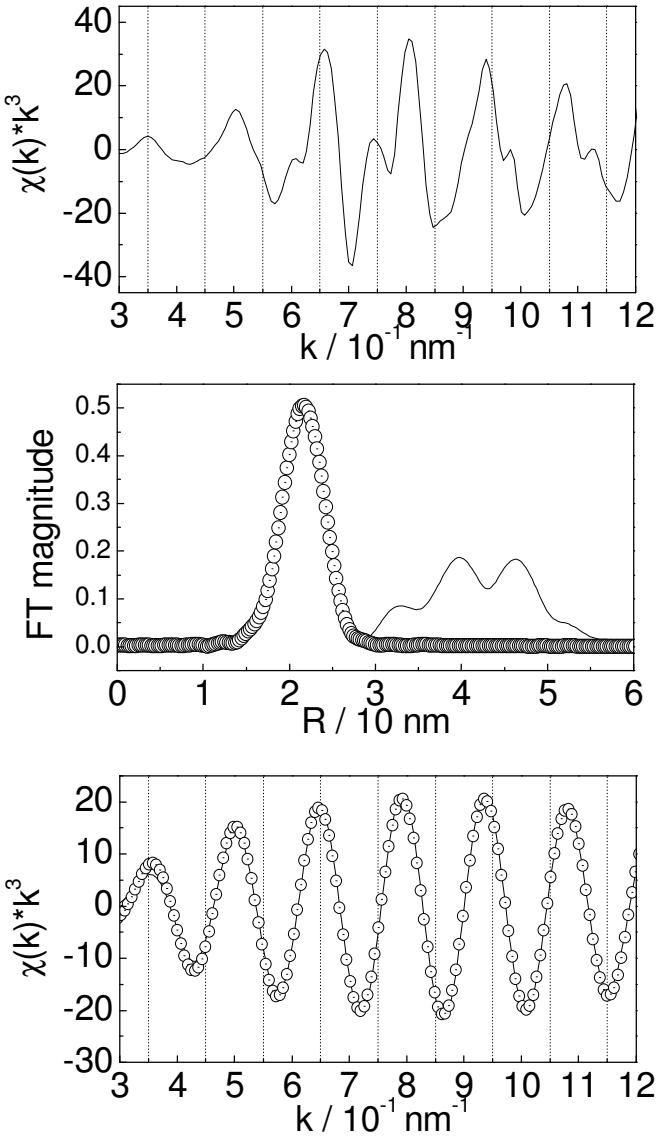

Figure 3.3. Ni K-edge EXAFS spectra, Fourier transforms and Fourier filtered EXAFS spectra of reference Ni foil.

Table 3.2 Curve-fitting result of Ni K-edge EXAFS spectra for Ni foil

Sample	Ni-Ni				R(%) / S_o^2
	CN	R / nm	σ^2 / 10^{-5} nm^2	ΔE / eV	
Feff reference	12	0.2489	-	-	-
Ni foil	11.73	0.2481	5.46	-0.627	0.89 / 0.9

ΔR filtered = 0.1426 - 0.2702 nm, $S_o^2 = 0.9$

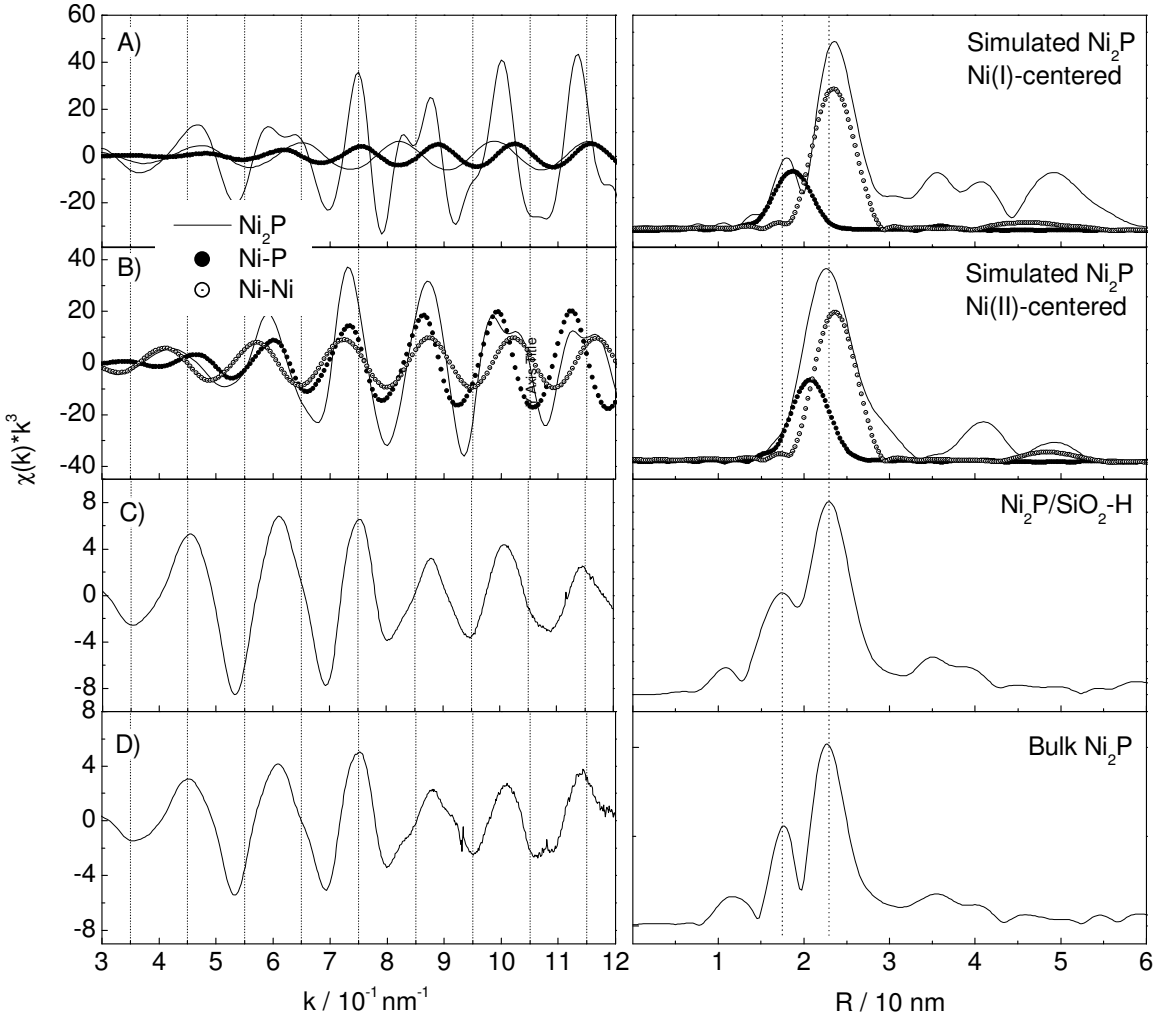

Figure 3.4. Comparison of Ni K-edge EXAFS spectra for the simulated Ni_2P, bulk Ni_2P and Ni_2P/SiO_2-H sample.

Table 3.3 Curve-fitting results of the Ni K-edge EXAFS spectra for the bulk Ni_2P sample

Parameter		Ni-P				Ni-Ni			R (%)
		Ni(I)-P(II)	Ni(I)-P(I)	Ni(II)-P(I)	Ni(II)-P(II)	Ni-Ni(I,II)	Ni-Ni(I)	Ni-Ni(I,II)	
Ni_2P reference coordination number / CN		2	2	1	4	2	2	4	
Ni_2P reference bond length / R		0.2209	0.22662	0.23688	0.24567	0.2605	0.26131	0.26783	
Fit 1	CN		1.43					4.22	2.68
	R / nm		0.222					0.2618	
	σ^2 / 10^{-5} nm^2		7.835					8.0466	
	ΔE / eV		-8.424					-2.192	
Fit 2	CN		2.11	1.471			4.014		0.69
	R / nm		0.2237	0.2392			0.2646		
	σ^2 / 10^{-5} nm^2		0.879	6.91			1.599		
	ΔE / eV		1.25	1.411			0.543		
Fit 3	CN		2.01		1.750			3.99	0.48
	R / nm		0.2253		0.2401			0.2644	
	σ^2 / 10^{-5} nm^2		3.00		0.499			6.00	
	ΔE / eV		0.420		0.423			1.798	
Fit 4	CN		2.1	1.512				4.01	1.51
	R / nm		0.2248	0.2400				0.2649	
	σ^2 / 10^{-5} nm^2		4.76	1.606				6.01	
	ΔE / eV		1.177	1.099				1.941	

ΔR filtered = 0.1427 - 0.27598 nm, $S_o^2 = 0.9$

Table 3.4 Comparison of curve-fitting results of the Ni K-edge EXAFS spectra for the bulk Ni_2P reference and the Ni_2P/SiO_2-H catalyst

Samples	Ni-P								Ni-Ni (I, II)				R(%)
	Ni-P (I)				Ni-P (II)								
Reference parameter	CN	R / nm	σ^2 / 10^{-5} nm^2	ΔE / eV	CN	R / nm	σ^2 / 10^{-5} nm^2	ΔE / eV	CN	R / nm	σ^2 / 10^{-5} nm^2	ΔE / eV	
	2	0.22662			1	0.23688			4	0.26783			
Ni_2P (bulk)	2.0	0.2253	3.00	0.420	1.750	0.2401	0.499	0.423	3.99	0.2644	6.00	1.798	0.48
Ni_2P/ SiO_2-H	1.98	0.2225	6.420	-4.260	3.191	0.2383	8.460	-4.261	3.05	0.2625	8.159	-1.156	1.048

ΔR filtered = 0.1427 - 0.27598 nm, $S_o^2 = 0.9$

3.3.2. Surface Properties of the Ni_2P Catalyst

Figure 3.5 shows room temperature FTIR spectra of adsorbed CO in He flow on Ni/SiO_2-H, sulfided NiS/SiO_2-H, Ni-Mo-S/Al_2O_3 and Ni_2P/SiO_2-H samples. Figure 3.5 A) shows the IR spectrum prior to the introduction of CO for a Ni/SiO_2-H sample, showing no peak. Figure 3.5 B) shows the IR spectrum of adsorbed CO on the Ni/SiO_2-H sample, which gives two broads bands centered at around 2046 cm^{-1} and 1955 cm^{-1}. Figure 3.5 C and D) show the results for sulfided NiS/SiO_2-H and Ni-Mo-S/Al_2O_3 samples, which give only traces of physisorbed CO species observed at 2173 cm^{-1} and 2117 cm^{-1}. Figure 3.5 E) shows the IR spectrum with CO saturation for the Ni-Mo-S/Al_2O_3 sample, which gives the peaks for the physisorbed CO species observed at 2173 cm^{-1} and 2117 cm^{-1}. Figure 3.5 F) shows the IR spectrum prior to the introduction of CO for a Ni_2P/SiO_2-H sample, again showing no peak. Figure 3.5 G) shows the IR spectrum of adsorbed CO on the Ni_2P/SiO_2-H sample, which gives a distinctive IR band at 2086 cm^{-1}. Figure 3.5 H) shows the result for the sulfided Ni_2P/SiO_2-H sample (treated in a flow of 10 % H_2S/H_2 at 673 K for 2 h.), which retained the IR band at 2086 cm^{-1}, with the intensity being slightly lowered.

Figure 3.6 shows FTIR spectra in the high and low wavenumber regions of adsorbed pyridine in a He carrier for NiS/SiO_2-H and Ni-Mo-S/Al_2O_3 samples after pretreatment in a flow of 10 % H_2S/H_2 at 673 K for 2 h. The spectra were obtained after adsorption at 373 K (100 ^oC) and successive heating to various temperatures in a flow of He. For the sulfided Ni/SiO_2-H sample positive peaks centered at 3091 (Fig. 3.6 A), 1595, and 1446 cm^{-1} (Fig. 3.6 C) were observed, which decreased in intensity as temperature was increased. For the Ni-Mo-S/Al_2O_3 peaks centered at 1607, 1489 and 1447 cm^{-1} (Fig. 3.6 D) were observed,

with no distinctive features found in the higher frequency region (Fig. 3.6 D). Again, the intensity of the peaks decreased upon heating.

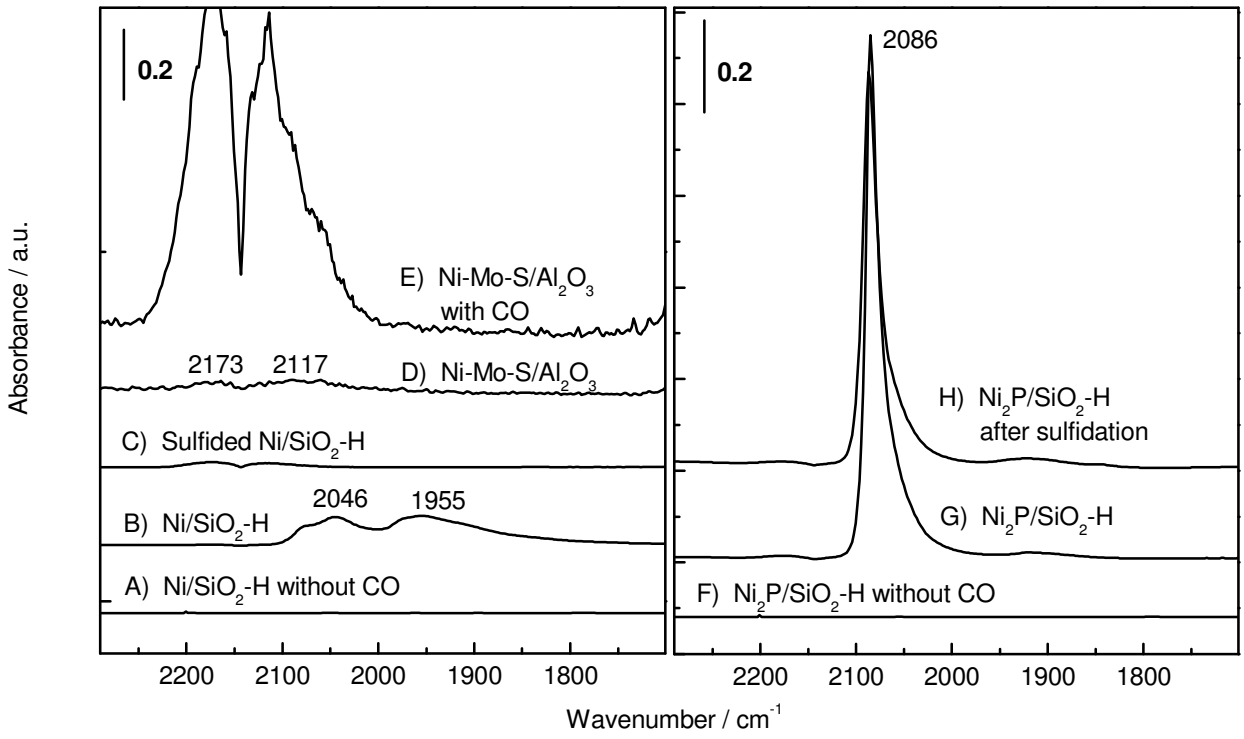

Figure 3.5. FTIR spectra of adsorbed CO on Ni/SiO_2-H, sulfided NiS/SiO_2-H, Ni-Mo-S/Al_2O_3 and Ni_2P/SiO_2-H samples.

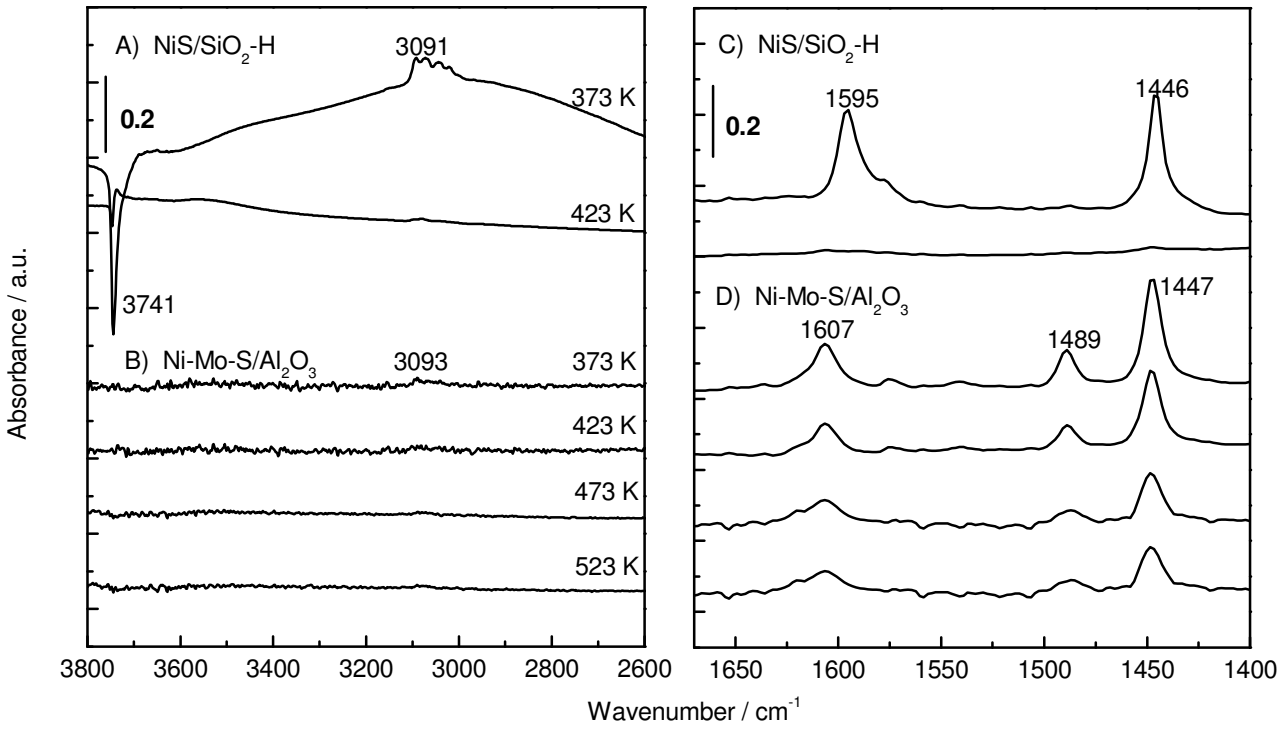

Figure 3.6. FTIR spectra of adsorbed pyridine on Ni/SiO_2-H, sulfided Ni/SiO_2-H and Ni-Mo-S/Al_2O_3

Figure 3.7 shows FTIR spectra in the high and low wavenumber regions of adsorbed pyridine in a He carrier for the Ni_2P/SiO_2-H catalyst. Again, the spectra were obtained after adsorption at 373 K (100 ^oC) and successive heating to various temperatures in a flow of He. Positive peaks centered at 3146 and 3078 cm^{-1}(Fig. 3.7 A) and 1637, 1606, 1597, 1575, 1543, 1490, and 1446 cm^{-1} (Fig. 3.7 B) were observed. Negative peaks at 3741 and 3665 cm^{-1} (Fig. 3.7 A) were also present. An increase in the temperature led to a decrease in the intensity of the peaks.

Figure 3.8 shows FTIR spectra of adsorbed pyridine in a He carrier for the PO_x/SiO_2-H sample. Once again adsorption was carried out at 373 K (100 ^oC), with subsequent sample heating. Positive peaks centered at 3140, 3089, and 3037 cm^{-1}(Fig. 3.8 A) and 1639, 1622, 1546, 1490, and 1452 cm^{-1} (Fig. 3.8 B) were observed. Negative peaks at 3740 and 3660 cm^{-1} (Fig. 3.8 A) were also visible. An increase of the temperature led to a decrease in the intensity of the peaks, with the peaks at 3660, 1546, and 1490 cm^{-1} being retained up to 573 K.

Figure 3.9 compares the FTIR spectra of pyridine adsorbed on the Ni_2P/SiO_2-H (Fig. 3.9 A) and Ni-Mo-S/Al_2O_3 (Fig. 3.9 C) samples under He flow at 573 K (300 ^oC). The behavior of the adsorbed species is also examined on these catalysts at 573 K (300 ^oC) upon switching the carrier flow from He to H_2 (Fig. 3.9 B and 9 D). For the Ni_2P/SiO_2-H sample the main spectral features appear at 1604, 1485, and 1446 cm^{-1} in He but these are shifted to 1597, 1575, 1472, and 1444 cm^{-1} with the introduction of H_2. For the Ni-Mo-S/Al_2O_3 sample the main spectral features appear at 1604, 1485, and 1446 cm^{-1} in He. Unlike for the Ni_2P/SiO_2-H sample, switching the carrier from He to H_2 led to little change in the IR peaks.

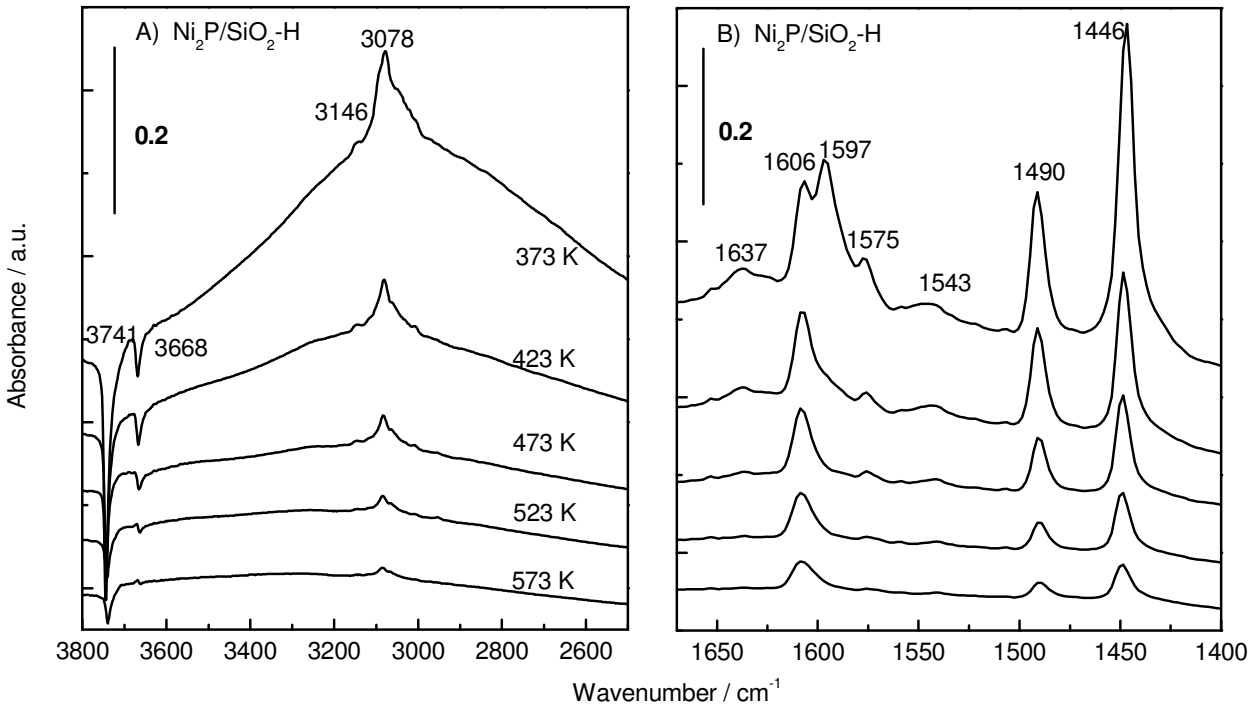

Figure 3.7. FTIR spectra of adsorbed pyridine on Ni_2P/SiO_2-H.

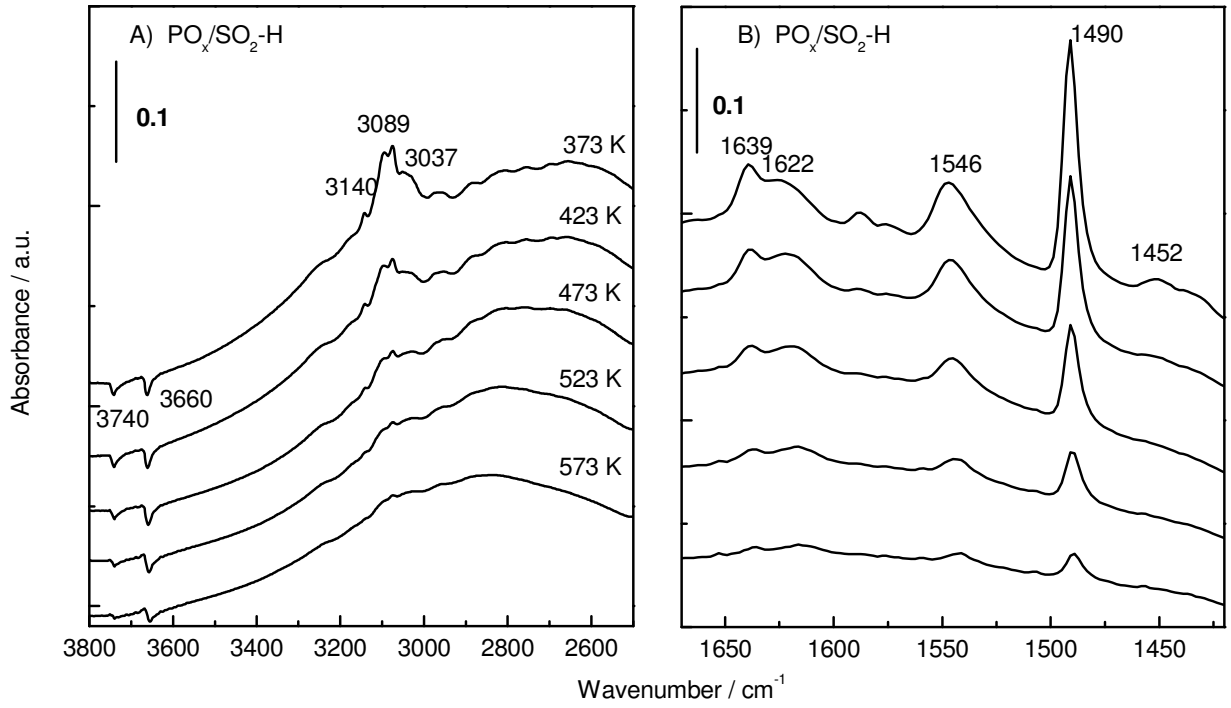

Figure 3.8. FTIR spectra of adsorbed pyridine on P_2O_5/SiO_2-H.

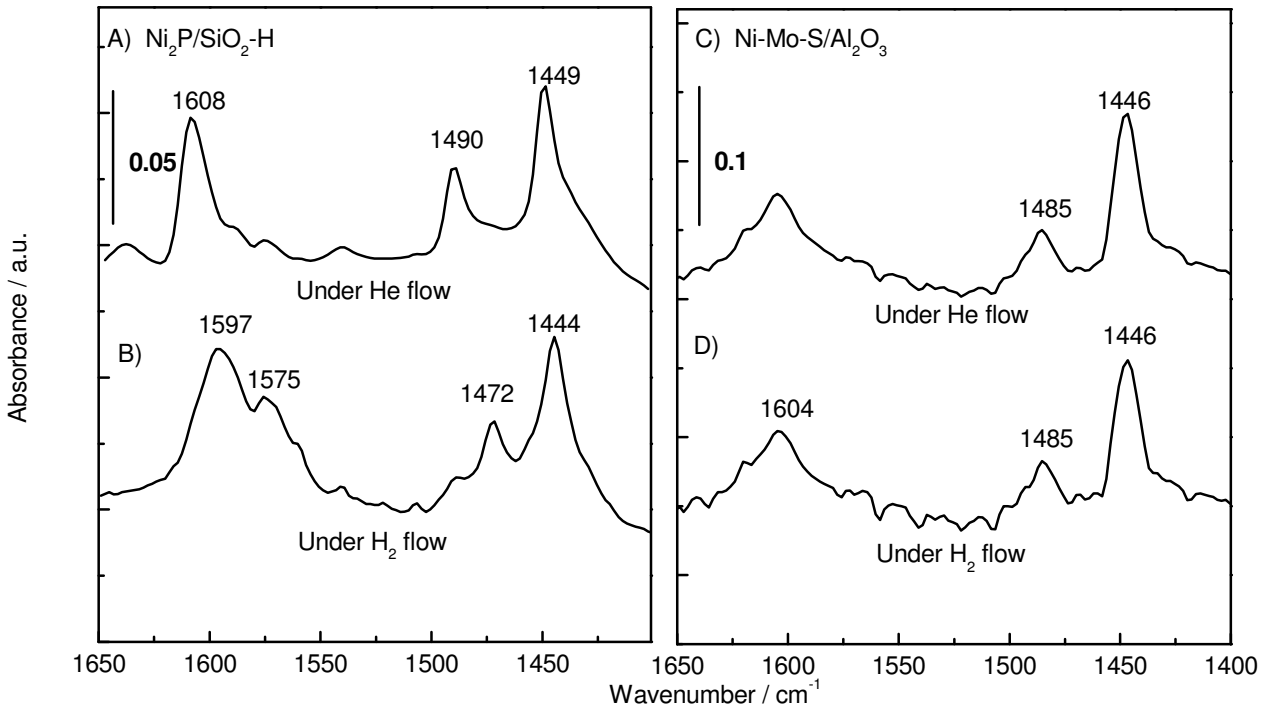

Figure 3.9. In situ FTIR spectra of the hydrogenation of the pyridine at 573 K on Ni_2P/SiO_2-H and Ni-Mo-S/Al_2O_3 samples.

3.3.3. Catalytic Activity in the HDS of 4,6-DMDBT

Figure 3.10 shows the HDS conversion of 4,6-DMDBT and the selectivities toward the HYD and DDS products for the Ni_2P/SiO_2-H and $NiMoS/Al_2O_3$ catalysts at 613 K (300 ^oC) and 3.1 MPa at two levels (0 and 0.02 %) of N content (as quinoline). Initially, the feed contained 4,6-DMDBT (0.05 % S), DMDS (0.3 % S) and tetralin (1 %) dissolved in tridecane. For the Ni_2P/SiO_2-H catalyst the HDS conversion was high at 97 % with the HYD selectivity being 95 %, while for the $NiMoS/Al_2O_3$ catalyst the HDS conversion was low at around 60 % with the HYD selectivity being 70 %. The addition of N (0.02 % N as quinoline) led to a decrease in the HDS conversion from 97 to 85 % for the Ni_2P/SiO_2-H and from 60 to 41 % for the Ni-Mo-S/Al_2O_3 catalyst. This was accompanied by a decrease in the HYD selectivity from 95 % to 94 % for the Ni_2P/SiO_2-H catalysts and from 70 to 64 % for the Ni-Mo-S/Al_2O_3 catalyst. The conversion of tetralin and its product selectivities are also displayed in Figure 3.10. For the Ni_2P/SiO_2-H catalyst the tetralin conversion and HYD selectivity were respectively around 39 % and 89 %, and addition of N led to a slight decrease in conversion from 39 % to 37 % with the HYD selectivity being lowered from 90 to 86 %. For the Ni-Mo-S/Al_2O_3 catalyst the tetralin conversion and HYD selectivity were respectively around 27 % and 76 % and addition of N led to a decrease in the conversion from 27 to 20 % with the HYD selectivity being lowered from 76 to 63 %.

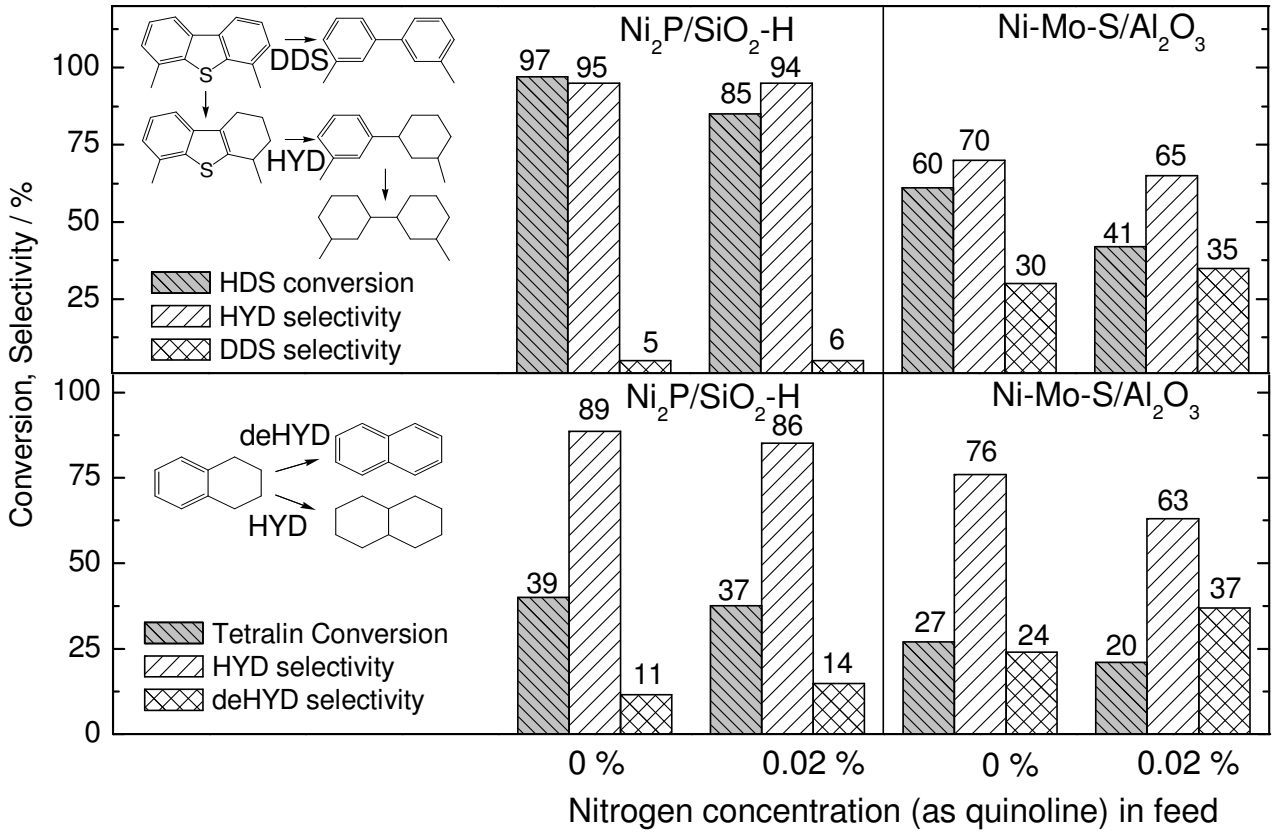

Figure 3.10. Activities in the HDS of 4,6-DMDBT and hydrogenation of tetralin for the Ni_2P/SiO_2-H and Ni-Mo-S/Al_2O_3 at 613 K.

3.4. Discussion

3.4.1. Structural Properties of the Ni_2P/SiO_2-H

The X-ray diffraction patterns of the fresh and spent Ni_2P/SiO_2-H samples indicate that the main bulk phase on the catalyst is Ni_2P (Fig. 3.1). The sample was prepared by temperature-programmed reduction in flowing hydrogen, which led to a loss of phosphorus during reduction and gave a lower phosphorus amount (Ni/P ratio =1/0.963) than the initial value (1/2). The surface area of the fresh Ni_2P/SiO_2-H catalyst (240 $m^2 g^{-1}$) was lower than that of the support (350 $m^2 g^{-1}$), likely due to the pore blocking caused by phosphide particles (Table 3.1). Chemisorption quantities of CO for the fresh sample (33 μmol g^{-1}) were moderate and were retained during reaction [37].

The X-ray diffraction patterns of the catalysts (Fig. 3.1) have low signal to noise and do not yield detailed structural information. EXAFS analysis was thus employed to characterize the highly dispersed Ni_2P phase on the support. Comparison is made with bulk Ni (Fig. 3.3) and Ni_2P (Fig. 3.4) reference samples. As also shown in Chapter 2, the Fourier transform EXAFS spectrum for the Ni_2P/SiO_2-H catalyst show two overlapping peaks in the region 0.15-0.30 nm (Fig. 3.4 C) corresponding roughly to Ni-P and Ni-Ni bonds. For a quantitative analysis Ni K-edge EXAFS simulation for the Ni_2P was conducted with Feff 8.20 code [2] using structural parameters obtained from the literature [4] to obtain the phase shifts and backscattering amplitude functions needed for the fits. Two separate EXAFS simulations were carried out taking the Ni(I) and Ni(II) atoms (Fig. 3.2) to be absorbers in 0.5 nm Ni_2P clusters. The value of the reduction factor ($S_o^2 = 0.9$) for the absorber Ni atom was obtained from the curve fitting of the Ni K-edge EXAFS spectrum for a Ni foil

reference (Fig. 3.3) and was fixed for further curve fittings on bulk and Ni_2P catalyst samples. As can be seen (Fig. 3.4), the simulated Fourier transform for the Ni_2P with Ni(I) as the absorber exhibits the dominant features of the 4 phosphorus neighbors (2 at 0.2209 nm and 2 at 0.2266 nm) and the 8 nickel neighbors (2 at 0.2605 nm, 2 at 0.2613 nm, and 4 at 0.2678 nm), respectively. This allows us to understand the details of the experimental spectrum, which confirms that the first peak centered at 0.181 nm is due to a Ni-P bond and the second peak centered at 0.234 nm is mainly due to a Ni-Ni bond. The simulated Fourier transform for the Ni_2P with Ni(II) as the absorber gave rise to a broad peak centered at 0.2249 nm, in which two dominant features can be observed, the 5 phosphorus neighbors (1 atom at 0.2368 and 4 atoms at 0.2456) and 6 nickel neighbors (2 at 0.2605 nm and 4 at 0.2678 nm), respectively. The broad feature of the peak thus comprises both Ni-P and Ni-Ni contributions.

The contributions from the two nickel absorbers were used to fit the experimental EXAFS spectrum for the bulk Ni_2P. Since the number of independent fitting parameters is limited by 12 as given by the formula [5], $N_{ind} = 2 \cdot \Delta k \cdot \Delta R / \pi + 2$, a three-shell analysis is permissible. Various combinations of subshells, in two and three-shell method, were applied to obtain the best fit. For the two-shell method one type of Ni-P and Ni-Ni shell was employed. In the first shell of Ni-P, two P(I) neighbors at 0.2266 nm were used. In the second shell of Ni-Ni, 4 Ni(I,II) neighbors at 0.26783 nm were used. For the three-shell method two types of Ni-P shells and one type of Ni-Ni shell were employed. In the first shell of Ni-P, two P(I) neighbors at 0.2266 nm were used. In the second shell of Ni-P, either one P(II) neighbor at 0.23688 nm or 4 P(II) neighbors at 0.24567 nm were used and

compared. In the third shell of Ni-Ni, either 2 Ni(I) neighbors at 0.26131 nm or 4 Ni(I,II) neighbors at 0.26783 nm were used and also compared.

Table 3.3 summarizes the structural parameters of the Ni_2P reference sample [2] and compares the curve fitting results of the two (Fit 1) and three-shell methods (Fits 2-4). In both cases, various combinations of subshells were used to obtain the best fit. The three-shell method showed a better R-factor with more reasonable parameters than the two-shell method. For bulk Ni_2P the coordination numbers of the first shell of a Ni(I)-P and the third shell of a Ni-Ni (I,II) are in good agreement with those of the Ni_2P reference, with the bond lengths being slightly lowered in both cases. The coordination number of the second shell of Ni(II)-P was close to 1 and the bond length was between the values of the two different types of P neighbors. It is noted that different combinations of fitting shells in the three-shell method give only little change in parameters, characteristic of the averaging nature of EXAFS. For Fit 3 in Table 3.3 in the first shell of Ni-P, the lower bond length (0.2253 nm) is due to the 2 P next-neighbors at 0.2209 nm. In the second shell of Ni-P a lower coordination number (1.750) and bond length (0.2401 nm) are due to the presence of the 1 P next-neighbor at 0.23688 nm. In the third shell of Ni-Ni, a lower bond length (0.2644 nm) is due to the 2 Ni next-neighbors at 0.26131 nm. Even though various combinations of the fitting reference shells were employed, the resulting parameters displayed only small differences. These results imply that the three-shell analysis is effective to estimate the structural parameters.

The three-shell method was also applied for the Ni_2P/SiO_2 sample (Table 3.4). Table 3.4 summarizes the curve-fitting results of the EXAFS spectra for the bulk Ni_2P sample and the freshly prepared Ni_2P sample. For Ni_2P/SiO_2-H in the first shell Ni(I)-P coordination

number remains constant at around 2.0 with the bond distance being lowered. In the second shell, the Ni(II)-P coordination number was found to be much high at 3.191 with the bond distance being lowered compared to that of the bulk Ni_2P (0.2383 vs. 0.2401 nm). In the third shell a decrease in the Ni-Ni (I, II), coordination number and bond length can be observed. In general supported transition metal catalysts show decreased coordination numbers and bond lengths compared to bulk samples, indicating more highly exposed and contracted feature of the dispersed particles [6]. Similar results were observed for the bond length in the Ni_2P/SiO_2-H sample which was lowered in all the shells compared to those of the bulk Ni_2P. The fitting results for the coordination numbers show an increase for the second shell of Ni-P(II) and a decrease in a third shell of Ni-Ni. These results are likely due to the presence of extra P on the surface of the Ni_2P particles. A study of the effect of Ni/P ratio in the preparation of supported Ni_2P catalysts has shown that higher P is required to obtain highly active and stable catalysts [7]. The introduction of extra P in the preparation is important and was also carried out in this work. Elemental analysis confirms that there is extra P with a Ni/P ratio of 1/0.963 (Table 3.1). Comparison to the stoichiometric Ni/P ratio of 1/0.5 indicates that there is 48 % P excess, although a portion of this probably resides on the support. The increase of the coordination number in the second shell of Ni-P implies that the extra P affects the Ni-Ni coordination. Similar features were found in Mo_2N, in which it was suggested that the extra N could be interstitially located in Mo_2N and could deform the Mo-Mo coordination [8]. The study of the dispersion effect of Ni_2P catalysts supported on a large surface area support (Si-MCM-41) as described in Chapter 2 has shown that high dispersion in Ni_2P results in stronger interactions between Ni and P resulting in a higher coordination number in the second shell of Ni-P and a higher P/Ni molar ratio after

the reduction [37]. It was also suggested that the extra P could reduce the Ni-Ni coordination, as found here.

3.4.2. Surface Properties of the Ni_2P/SiO_2-H

Studies of CO adsorption are useful for characterizing the bonding properties of transition metal species [9-12]. Typically, the IR bands for M^{n+}-CO surface complexes are observed in the wavenumber region 2220-2000 cm^{-1}. For linearly adsorbed CO species on Ni cations four main vibrational regions are found depending on the oxidation state of the Ni. Carbonyl complexes assigned to Ni^{3+}-CO and Ni^{2+}-CO give rise to respective IR bands at around 2155 and 2136 cm^{-1}, which are detected only at low temperature and are easily removed by evacuation at room temperature [10]. The high frequency of vibration and the low stability of the complexes indicates that CO is bonded mainly by electrostatic interactions and/or σ bonds to the Ni ion. Carbonyl complexes assigned to Ni^{+}-CO and Ni^{0}-CO give rise to IR bands at around 2130 and 2065 cm^{-1}, respectively, which are relatively stable and persist after evacuation at room temperature [11, 12]. The low frequency of the vibration and the high stability suggests the presence of π back-bonding due to the higher d-electron density of the Ni species with a lower oxidation state.

For the Ni/SiO_2-H sample IR bands (Fig. 3.5) were observed at relatively low frequency, 2046 and 1955 cm^{-1}, and were assigned to linearly adsorbed and bridging CO species, respectively [9]. After treatment in 10 % H_2S/H_2 at 673 K for 2 h, the IR bands disappeared, indicating that the sulfided Ni metal was not able to chemisorb CO. Similarly to the sulfided NiS/SiO_2-H, the sulfided Ni-Mo-S/Al_2O_3 showed very weak IR peaks (at

2173 cm^{-1} and 2117 cm^{-1}) corresponding to the physisorbed CO species, which is consistent with previous studies [13,14,15]. Only at a very low temperature (140 K) IR bands appeared with low intensity [9], indicating a low electron density on the adsorbing metal sites. In contrast to these samples the Ni_2P/SiO_2-H gave a distinctive and stable IR band at 2086 cm^{-1}. Even after sulfidation the peak reappeared at the same frequency with only the intensity being slightly diminished. This frequency fell in the region between that of Ni^+-CO and Ni^0-CO, indicating the presence of π back-bonding in a low oxidation state. Also, the IR band for bridging CO species was not observed, which is understandable as the bond distance given by EXAFS between Ni-Ni in Ni_2P is not close enough to form bridging CO groups compared to that in Ni metal. Similar results are found for noble metals in a low oxidation state such as Pt and Pd which are well known as hydrogenation catalysts, and display stable IR bands at low frequency (~ 2010 cm^{-1}) at room temperature [9,16,17]. The noble metals are, however, severely deactivated in a sulfur environment with a loss of the active sites [17].

The FTIR studies of pyridine adsorption as a function of temperature on the catalysts and reference samples was carried out to characterize the surface acidic properties. Pyridine is a good probe molecule as it can coordinatively bond to Lewis acid sites or can be protonated on Brønsted acid sites, with the pyridine ring vibrations being modified in a characteristic manner [16]. For example, the CC(N) vibration mode ν_{19b} of the pyridine ring gives rise to wavenumbers at 1439, 1450, or 1545 cm^{-1} depending on whether the molecule is physisorbed, adsorbed on Lewis acid sites, or on Brønsted acid sites [18]. For reduced Ni/SiO_2-H the adsorption of pyridine gives rise to IR bands at 3741, 3091, 1595 and 1446 cm^{-1} at 373 K (Fig. 3.6). The positive peaks at 3091, 1595 and 1446 cm^{-1} correspond to the

vibration modes, ν_7 (CH), ν_{8a} (CC(N)), and ν_{19b} (CC(N)) of the pyridine ring. The negative peak at 3741 cm^{-1} corresponds to an O-H stretching vibration mode on SiO_2 [19]. Since a background spectrum is subtracted from all spectra, the decrease in the intensities of the negative peaks indicates recovery in the O-H concentration with temperature. Initially, the O-H bond on Si-OH is strongly perturbed by its interaction with pyridine, but as the pyridine desorbs the OH concentration rises again. The O-H feature returns to normal (zero intensity) upon heating to 423 K, indicating that the pyridine is only weakly adsorbed on the Ni/SiO_2-H. For sulfided Ni-Mo-S/Al_2O_3 the pyridine adsorption gives rise to IR bands at 1607, 1489 and 1447 cm^{-1} at 373 K and no distinctive peak is found in the higher frequency region (3800-2500 cm^{-1}). The peaks at 1489 and 1447 cm^{-1} correspond to the CC(N) vibration mode ν_{19b} of the pyridine ring and are indicative of the presence of Lewis acid sites due to Al sites on the Al_2O_3 support [20]. These peaks gradually disappear upon heating to 523 K, indicating that pyridine is held with moderate strength on these sites on the Al_2O_3 support.

For reduced Ni_2P/SiO_2-H the adsorption of pyridine gives rise to IR bands at 3741, 3668, 3078, 1606, 1597, 1575, 1543, 1490 and 1446 cm^{-1} at 373 K (Fig. 3.7). The negative peaks at 3741 and 3668 cm^{-1} correspond to hydroxyl vibrations on SiO-H and PO-H, respectively [19]. The broad band at 3078 cm^{-1} corresponds to C-H vibrations in pyridine. The peaks at 1543, 1490 and 1446 cm^{-1} correspond to pyridinium ring vibration modes ν_{19b} of CC(N) on Brønsted acid sites, ν_{19a} of CC(N) on Brønsted and Lewis acid sites, and ν_{19b} of CC(N) on Lewis acid sites [20]. The small peak at 1543 cm^{-1} is assigned to adsorption on Brønsted acid sites, which unlike the case of the Ni-Mo-S/Al_2O_3, is probably due to the PO-H site, as also indicated by a drop in intensity of the band at 3668 cm^{-1}. The assignment of

the PO-H group on the Ni_2P/SiO_2-L and Ni-Mo-S/Al_2O_3 catalysts has already been addressed in a previous study [21], in which an FTIR analysis of 2-methylpiperidine adsorption indicated that a PO-H group on the Ni_2P phase could readily protonate 2-methylpiperidine and form 2-methylpiperidium ion as also found for the case of Ni-Mo-S/Al_2O_3. The results here suggest that the acidity of the PO-H group on the Ni_2P/SiO_2-H is slightly higher than that on the Ni-Mo-S/Al_2O_3. For PO_x/SiO_2-H pyridine adsorption gives rise to IR bands at 3740, 3660, 3089, 1639, 1622, 1546, 1490 and 1452 cm^{-1} at 373 K (Fig. 3.8). It is noted that the peak at 1546 cm^{-1} assigned to adsorption on a Brønsted acid site is much stronger than the peak at 1452 cm^{-1} due to adsorption on a Lewis site, indicating that the Brønsted acidity (due to PO-H groups) is dominant over the Lewis acidity on PO_x/SiO_2-H. Also, the small intensity of the peak at 3740 cm^{-1} indicates that SiO-H groups are scarce on the surface. This implies that the PO_x is located on or close to the SiO-H site, as also discussed in a previous study [21]. The peak assigned to the PO-H groups on PO_x/SiO_2-H is observed at a lower frequency than that on Ni_2P/SiO_2-H (3660 cm^{-1} vs. 3668 cm^{-1}) and persists even after heating to 573 K, indicating a stronger acidity for the PO_x/SiO_2-H than the Ni_2P/SiO_2-H.

In situ FTIR measurements in a flow of hydrogen were carried out to examine the hydrogenation ability of the Ni_2P and Ni-Mo-S/Al_2O_3 catalysts at 573 K (300 ^oC) (Fig. 3.9). Pyridine was adsorbed on freshly pretreated catalysts at 373 K (100 ^oC) and after heating to 573 K in helium the flow was switched to hydrogen. The FTIR spectra showed that after 180 s adsorbed pyridine on the Ni_2P/SiO_2-H was converted to piperidine, while on Ni-Mo-S/Al_2O_3 there was little change in the spectrum. It is thus concluded that the Ni_2P/SiO_2-H surface has two distinctive sites which are very close to each other and are active for

protonation and hydrogenation. The Ni-Mo-S/Al_2O_3 has considerably less hydrogenation ability.

3.4.3. Catalytic Activities of the Ni_2P/SiO_2-H

Recently, more stringent environmental regulations in reducing sulfur in transport fuels have drawn much attention on deep sulfur removal from crude oil. Consequently, the focus for much HDS research has moved to the most refractory sulfur compounds [24,26,27]. In the case of diesel fuels these are typically the so-called sterically hindered dibenzothiophenes, i.e., DBT's with alkyl substituents in the 4- or 4,6-positions [22,23]. The 4,6-dimethyldibenzothiophene (4,6-DMDBT) is typically some ten times less reactive than DBT itself [24,25,26]. Considering that more than 99 % of the refractory sulfur compounds will have to be desulfurized to reduce the sulfur content of the current 500 ppm S to the new standards of 15 ppm S for the United States and Europe, it is essential to desulfurize alkyl substituted-DBT's effectively in order to achieve deep HDS.

Two reaction pathways for the HDS of alkyl substituted DBTs have been proposed. The direct desulfurization pathway (DDS route) leads to 3,3-dimethylbyphenyl (3,3-DMBP), whereas the pre-hydrogenation pathway (HYD route) forms 4,6-tetrahydro- and hexahydro-DMDBT as intermediates, which are desulfurized to methylcyclohexyltoluene (MCHT) and dimethylbicyclohexane (DMBCH) [27,28,29,30]. Standard hydrodenitrogenation and hydrodesulfurization (HDN/HDS) catalysts consist of MoS_2-type phases supported on γ-Al_2O_3 promoted by Co or Ni. The conventional Co–Mo-S/Al_2O_3 catalysts desulfurize primarily via the direct desulfurization route while Ni–Mo-S/Al_2O_3 catalysts, which exhibit a higher hydrogenation activity, desulfurize via the hydrogenation route. The Ni–Mo-

S/Al_2O_3 catalysts, however, exhibit lower HDS activity than the Co-Mo-S/Al_2O_3 catalysts, particularly in the presence of high concentration of aromatics and nitrogen compounds, due to the inhibition caused by those compounds [31]. For this reason gas oil refining currently operates mostly with Co-Mo-S/Al_2O_3 catalysts at moderate temperatures (340-360^oC) and pressures (3.0-5.0 MPa). Nonetheless, these conditions are unable to achieve the low sulfur specification of gas oil of less than 15 ppm S [31]. Increasing the temperature to achieve higher HDS rates causes degradation of the produced oil due to unwanted side reactions. Thus, the development of more effective HDS catalysts is greatly needed.

Studies were carried out with two different feeds at 573 K (300 ^oC) and 3.1 MPa. Initially, a feed containing 0.35 % S (0.3 % S as DMDS and 0.05 % S as 4,6-DMDBT) and 1 % tetralin in a tridecane solvent was used. For Ni_2P/SiO_2-H the HDS reaction proceeded via the HYD pathway (~95%) with high conversion (~97 %). Introduction of a N-compound (quinoline) slightly lowered the HDS conversion by 8.6 % with little change in HYD selectivity. The catalytic activity for tetralin shows that the HYD pathway is also dominant over the deHYD pathway (88 % vs. 12 %) and again, the activity was little affected by the N-compound. Similar catalytic behavior was observed for the Ni-Mo-S/Al_2O_3 but with a much lower HDS conversion particularly in the presence of the N-compound. Also, the Ni-Mo-S/Al_2O_3 showed lower hydrogenation activity for tetralin than the Ni_2P/SiO_2-H and the N-compound had a large effect on both the conversion and the HYD selectivity. These results indicate that the HYD pathways in the reactions for both 4,6-DMDBT and tetralin are more affected by the N-compound for the Ni-Mo-S/Al_2O_3 than the Ni_2P/SiO_2-H. For the Ni-Mo-S/Al_2O_3 catalyst the inhibition behavior of heterocyclic compounds has already been addressed and is well documented [32, 27,29]. The

heterocyclic compounds are known to competitively adsorb on the active sites for hydrogenation particularly at lower temperatures (< 613 K) where the adsorption is thermodynamically more favorable. It is thus understandable that the competitive adsorption by the N-compound on the hydrogenation site of the Ni-Mo-S/Al_2O_3 catalyst leads to a decrease in the conversion and the HYD selectivity for both 4,6-DMDBT and tetralin. For the Ni_2P/SiO_2-H catalyst the catalytic activity was less affected by the N-compounds than the Ni-Mo-S/Al_2O_3 catalyst although the HYD pathways are dominant for both 4,6-DMDBT and tetralin. It is also interesting to note that there is little change in the product selectivity in the HYD pathways with decrease in conversion, which indicates that both hydrogenation and hydrolysis occurs at the same active site on the Ni_2P catalyst.

3.4.4. Bifunctional Behavior of the Ni_2P/SiO_2-H

The Ni_2P/SiO_2-H catalyst shows unique acidic properties with a moderate strength intermediate between that of PO_x/SiO_2-H (higher) and Ni-Mo-S/Al_2O_3 (lower), which enables pyridine and piperidine [21] to be prototonated. Also, the Ni_2P/SiO_2-H catalyst shows a high hydrogenation behavior which is probably due to its electronic properties which retain a metallic nature, despite Ni_2P being a compound. The FTIR studies of CO adsorption reveal that there are sufficient electrons on the Ni site to allow π-back bonding. It is known that π-back bonding is effective for molecular activation, as electrons fill antibonding orbitals. This enhances hydrogenation activity, as observed in metallic Ni, Pt and Pd catalysts [33]. However, these metals are readily sulfided with loss of metallic character. A study of the electronic properties of SiO_2-H supported Ni_2P, MoP, and MoS_2 catalysts using density functional calculations [34] has shown that the electron density

around the metal followed the order, MoS_2/SiO_2-H < MoP/SiO_2-H < Ni_2P/SiO_2-H, which correlated well with the thiophene HDS activities of the catalysts. It was suggested that the higher electron density on the metal cation could enhance HDS activity by facilitating the dissociation of H_2 and the adsorption of thiophene [35,34]. The presence of P in Ni_2P prevents the compound from being bulk sulfided and allows it to retain metallic properties for hydrogenation.

These results thus suggest that the supported Ni_2P catalyst has bifunctional properties, being able to carry out hydrogenation and protonation on metallic Ni and acidic PO-H sites, respectively. The catalytic bifunctional behavior is commonly found in highly dispersed noble metals supported on acidic materials like zeolites, which exhibit higher hydrogenation/dehydrogenation activity than those on non-acidic support [16,17]. The noble metals are, however, very sensitive to sulfur which binds strongly with the metals and causes deactivation. The sulfur resistance of a bimetallic Pt-Pd catalyst has been shown to be due to a strong interaction between Pt and Pd [36]. In contrast to the noble metals, the supported Ni_2P catalysts exhibit high resistance to S and N-compounds particularly in hydrotreating [37]. A study of the effect of dispersion in Ni_2P catalysts supported on a large surface area support (Si-MCM-41) has shown that highly dispersed Ni_2P is particularly active for HDS and resistant to S and N-compounds. It was suggested that a stronger interaction between Ni and P in the dispersed Ni_2P phase could enhance the sulfur resistance [37]. Also, the resistance to N-compounds is probably related to the acidic properties of the Ni_2P, which provides sites for the formation of the protonated N-compounds as intermediate species in the HDN [21]. These results therefore imply that the remarkable activities of the supported Ni_2P catalyst have their origin in the proximity of the Ni and P species which is

responsible for the creation of proximal sites of high activity in hydrogenation and the activation of N-and S-compounds.

3.5. Conclusions

A nickel phosphide catalyst supported on a high surface area SiO_2 of 350 $m^2 g^{-1}$, (Ni_2P/SiO_2-H) was prepared by a temperature programmed reduction method. The structural properties were characterized by powder X-ray diffraction (XRD) and extended X-ray absorption fine structure (EXAFS) which showed that the hexagonal Ni_2P phase was formed on the support and was stable during the reaction. The catalytic activities for HDS of 4,6-DMDBT and tetralin were tested on the Ni_2P/SiO_2-H and Ni-Mo-S/Al_2O_3 catalyst samples at 573 K and 3.1 MPa. The results showed that without N-compounds in the feed the Ni_2P/SiO_2-H exhibited much higher activities than the Ni-Mo-S/Al_2O_3 in HDS with respective conversions of 96 % vs. 61 %. The addition of a quinoline led to a small decrease in HDS conversion to 84 % for the Ni_2P/SiO_2-H catalyst, but a large drop to 42 % for the Ni-Mo-S/Al_2O_3 catalyst. Thus, the Ni_2P catalyst is tolerant of highly inhibitory N-compounds. For Ni_2P/SiO_2-H the HYD pathway in the desulfurization 4,6-DMDBT was dominant and was less inhibited by nitrogen than the Ni-Mo-S/Al_2O_3. A high hydrogenation activity was also obtained for the reaction of tetralin. The surface properties of the catalysts were examined by FTIR measurements of adsorbed CO and pyridine. These showed that the Ni_2P catalyst has high electron density and is able to form π-back-bonded CO species on Ni sites and that Ni_2P has moderate acidity in the form of PO-H sites which are able to protonate N-compounds such as pyridine and piperidine. These results therefore suggest

that the bifunctional properties of the supported Ni_2P catalyst probably contributed to the higher activity in hydrogenation and their high activity in the reaction of N- and S-compounds.

References

1. A. Marafi, S. Fukase, M. Al-Marri, and A. Stanislaus, Energy Fuels, 17 (2003) 661.
2. A. L. Ankudinov, B. Ravel, J. J. Rehr, and S. D. Congradson, Phys. Rev. B 58 (1998) 7565.
3. WebATOMS version 1.7, "http://millenia.cars.aps.anl.gov/cgi-bin/atoms/atoms.cgi," 15, August, 2002.
4. S. Rundqvist, Acta Chem. Scand., 16 (1962) 992.
5. E. A. Stern, Phys. Rev. B 48 (1993) 9825.
6. D. C. Koningsberger, R. Prins (Eds.), X-ray Absorption: Principles and techniques of EXAFS, SEXAFS and XANES, Wiley, New York, 1989.
7. X. Wang, P. Clark, and S. T. Oyama, J. Catal. 208 (2002) 321.
8. Z. Liu, M. Meng, Y. Fu, M. Jiang, T. Hu, Y. Xie and T. Liu, Materials Letters, 54 (2002) 364.
9. K. I. Hadjiivanov and G. N. Vayssilov, Adv. Catal. 47 (2002) 307.
10. E. E. Platero, D. Scarano, G. Spoto, and A. Zecchina, Faraday Discuss. Chem. Soc. 80 (1985) 183.
11. J. B. Peri, J. Catal. 86 (1984) 84.
12. J. B. Peri, Discuss Faraday Soc. 41 (1966) 121.
13. B. Müller, A. D. van Langeveld, J.A. Moulijn, and H. Knözinger, J. Phys. Chem. 97 (1993) 9028.
14. M. Angulo, F. Maugé, J. C. Duchet, and J. C. Lavalley, Bull. Soc. Chim. Belg. 96 (1987) 925.

15. B. M. Vogelaar, P. Steiner, A. D. van Langeveld, S. Eijsbouts, and J. A. Moulijn, Appl. Catal. A. 251 (2003) 85.
16. L. Hu, G. Xia, L. Qu, M. Li, C. Li, Q. Xin, and D. Li, J. Catal. 202 (2001) 220.
17. B. H. Cooper and B. B. L. Donnis, Appl. Catal. A 137 (1996) 203.
18. M. R. Basila, T. R. Kantner, and K. H. Rhee, J. Phys. Chem. 68 (1964) 3197.
19. A. P. Legrand, H. Hommel, and A. Tuel, Adv. Col. Interface Sci., 33 (1990) 91.
20. J. Ward, in: J. A. Rabo (Ed.), Zeolite Chemistry and Catalysis, in: ACS Monograph, Vol. 171, Am. Chem. Society, Washington, DC,1976.
21. S. T. Oyama and Y.-K. Lee, J. Phys. Chem. B, in print.
22. D.R. Kilanowski, T. Teeuwen, V.H.J. de Beer, B.C. Gates, G.C.A. Schuit, and H. Kwart, J. Catal. 55 (1978) 129.
23. T. Kabe, A. Ishihara, and H. Tajima, Ind. Eng. Chem. Res. 31 (1992) 1577.
24. B. C. Gates and H. Topsøe, Polyhedron 16 (1997) 3213.
25. M. Houalla, D.H. Broderick, A.V. Sapre, N. K. Nag, V. H. J. de Beer, B. C. Gates, and H. Kwart, J. Catal. 21 (1980) 523.
26. X. Ma, K. Sakanishi and I. Mochida, Ind. Eng. Chem. Res. 33 (1994) 218.
27. D. D. Whitehurst, T. Isoda, and I. Mochida, Adv. Catal. 42 (1998) 345.
28. K. Segawa and S. Satoh, Stud. Surf. Sci. Catal. 127 (1999) 129.
29. M. Egorova and R. Prins, J. Catal. 224 (2004) 278.
30. J. H. Kim, C. Song, Y.-K. Lee, and S. T. Oyama, Energy and Fuels, in print.
31. K. G. Knudsen, B. H. Cooper, and H. Topsøe, Appl.Catal.A Gen, 189 (1999) 205.
32. H. Topsoe, B. S. Clausen, and F. E. Massoth, in "Catalyisis Science and Technology" (J. R. Anderson and M. Boudard, eds.), Vol. 11. Springer-Verlag, New York, 1996.

33. J. E. Huheey, E. A. Keiter, and R. L. Keiter, Inorganic Chemistry: Principles of Structure and Reactivity, fourth ed., HarperCollins College Publishers, 1993.

34. J. A. José A. Rodriguez, J.-Y. Kim, J. C. Hanson, S. J. Sawhill, and M. E. Bussell, J. Phys. Chem. B, 107 (2003) 6276.

35. J. A. Rodriguez, J. Phys. Chem. B, 101 (1997) 7524.

36. R. M. Navarro, B. Pawelec, J. M. Trejo, R. Mariscal, and J. L. G. Fierro, J. Catal. 189 (2000) 184.

37. Y.-K. Lee and S. T. Oyama, in preparation.

Chapter 4

A Novel Nickel Phosphide (Ni_2P) Catalyst Supported on KUSY Zeolite for the Hydrodesulfurization of 4,6-DMDBT

4.1. Introduction

There has been heightened interest in new supports for HDS catalysts in recent years due to the need to improve catalytic activity, and the availability of new materials of high surface area with new properties. The alteration of catalytic activity by the support may arise as a result of changes in dispersion and morphology of the active component and possible metal support interactions. Catalysts based on USY zeolites are widely used in the petroleum refining industry, particularly in gas oil cracking, where the acidity, selectivity and activity is controlled by the number of aluminum acid sites in the unit cell. USY zeolites containing sulfides of transition metals (Mo, W, Ni or Co) have been found to have high activity in hydrodesulfurization reactions, but to suffer from rapid deactivation due to coke deposition induced by the acid sites present in the zeolite [1,2,3,4]. An important problem in the application of zeolite-supported transition metal sulfides as HDS catalysts is the difficulty of maintaining the metal phase highly dispersed inside the zeolite. Indeed, in many studies it has been demonstrated that after calcination and/or sulfidation only a small part of the metal remains inside the zeolite cages and a large part of the active phase is located outside the zeolite particles.

Metal phosphides are a novel catalyst group for deep hydrotreating and have received much attention due to their high activity for hydrodesulfurization (HDS) and hydrodenitrogenation (HDN) of petroleum feedstocks [5-8]. In contrast to sulfides, which adopt planar morphologies, phosphides are not layered compounds and form spherical particles which can be well dispersed on supports. It has been shown that MoP formed fine isotropic particles on a SiO_2 support (200 m^2g^{-1}) and that it had four times higher activity in the HDS of thiophene than MoS_2/Al_2O_3 [7], at 643 K under atmospheric pressure. Also, the results presented in Chapter 2 on Ni_2P supported on a high surface area MCM-41 support revealed that Ni_2P particles were well dispersed and showed high and stable activity in the HDS of 4,6-DMDBT.

This chapter is focused on highly dispersed Ni_2P catalysts supported on USY, and investigates the effect of the support acidity on the catalytic performance by varying the K-ion exchange levels. It also includes the use of X-ray absorption fine structure (XAFS) spectroscopy to determine the structure of the finely dispersed phosphide phases. Particular attention is placed on examining the effect of nitrogen and sulfur levels on the catalytic behavior, as these compounds are reported to inhibit HDS.

4.2. Experimental

4.2.1. Synthesis of Supported Ni_2P Catalysts

A commercial HUSY zeolite (Si/Al = 40, Zeolyst, CBV 780) support was used as received. Potassium ion-exchange of the HUSY was carried out under vigorous stirring for 12 h in a diluted aqueous solution (0.5 M) of potassium nitrate, (KNO_3, 99%) at 343 K. The

zeolite was then filtered and washed with deionized water at room temperature, dried at 385 K overnight, and finally was calcined in static air at 650 K for 4 h. The potassium content was adjusted by repeating the ion-exchange process to obtain three levels of exchange which were designated: HUSY (no cation-exchange), KHUSY (one exchange), and KUSY (three exchanges).

A series of supported Ni_2P catalysts with varying amounts of total Ni_2P loading were prepared by incipient wetness impregnation of aqueous metal phosphate precursors, followed by temperature programmed reduction (TPR) in flowing hydrogen. In these samples the initial Ni/P ratio in the precursors was fixed at 1/2. Another series of supported Ni_2P catalysts were prepared in the similar manner but with varying amounts of P in the precursors to give initial Ni/P ratios in the range of 1/0.5~1/3. The amount of Ni loading was maintained by 1.156 mmol per g of support in all cases. The reagents employed were again nickel nitrate, $Ni(NO_3)_2 \cdot 6H_2O$ (Aesar, 99%) and ammonium phosphate, $(NH_4)_2HPO_4$ (Aldrich, 99%) and the quantities of reagents used are summarized in Table 4.1. The samples with different Ni_2P loadings are described by their relative Ni_2P loading level, with a loading level of 1.0 corresponding to 12 wt % Ni_2P (1.156 mmol Ni_2P per g of support). In the same manner the samples with different Ni/P ratios are described by the initial molar ratio of Ni/P in the impregnation solutions. The moist paste obtained after impregnation was calcined in air at 673 K for 6 h. The resulting precursor phosphates were reduced to phosphides in quartz U-tube reactors (1 cm o.d.) using hydrogen at a flow rate of 650 μmol s^{-1} per g of starting material (e.g., 300 cm^3(NTP) min^{-1} H_2 flow for a 0.300 g sample) for all syntheses. In the TPR procedure, which was used to identify the reduction characteristics of the material, 0.20 g of material was loaded in a quartz glass u-tube reactor and the effluent

was monitored by a mass spectrometer (Ametek/Dycor MA100). For catalyst preparation larger batches using up to 5.50 g of supported nickel phosphate were used. The Ni_2P /KUSY required a final temperature of 853 K. After reduction, the phosphides were cooled to room temperature under 65 μmol s^{-1} helium and typically were passivated progressively by flowing 78 μmol s^{-1} of 0.1 % O_2/He overnight, followed by 13 μ mol s^{-1} of 0.5 % O_2/He for 2 h, and then allowing ambient air to diffuse into the reactor tube for 24 h before collecting the samples.

The same commercial Ni-Mo-S/Al_2O_3 sample (Criterion 424) used previously was employed to compare the catalytic activities with the phosphide catalysts.

4.2.2. Characterization of Samples

X-ray diffraction (XRD) patterns, CO chemisorption at room temperature (300 K), specific surface area, and chemical composition were measured as described in Chapter 2. The calculation of the pore size distribution (PSD) was performed using the Barrett-Joyner-Halenda (BJH) formula [9].

Pyridine temperature-programmed desorption (TPD) experiments were performed to determine the acid properties of the catalysts. Before TPD measurements, 100 mg of the passivated sample was pretreated in helium for 2 h at 673 K, and was then cooled to 373 K and exposed to the pyridine of a molar concentration of 0.44 % in a He carrier at a flow rate of 100 μmol s^{-1} (150 cm^3/min) until saturation with pyridine was reached. During the adsorption the effluent from the reactor was sampled into a mass spectrometer (Ametek/Dycor MA100) to monitor species. The m/z = 52 signal was monitored because it was the most intense signal in the pyridine mass spectrum. After the reactor was purged in a

He stream, the temperature was raised at a linear rate of 1.7×10^{-1} K s^{-1} (10 K min^{-1}) to 1123 K. Again, the species desorbed was monitored by the mass spectrometer during the heating. Transmission electron microscopy (TEM) was carried out on a Philips CM 30 T electron microscope operated at 100 kV with a LaB_6 filament as the source. Samples were mounted on a copper-supported carbon polymer grid by placing a few droplets of a suspension of ground sample in ethanol on the grid, followed by drying at ambient conditions.

X-ray absorption (XAS) spectra at the Ni K edge (8.333 keV) of reference and catalyst samples were also measured in the same manner as described in Chapter 2.

4.2.3. Activity Test for HDS

Hydrotreating was carried out at 3.1 MPa (450 psig) at two different temperatures, 573 K (300 ^{o}C) and 613 K (340 ^{o}C) in the same three-phase upflow fixed-bed reactor. Further details about reaction conditions are described in Chapter 2. Quantities of catalysts loaded in the reactor corresponded to the same amount of CO or atomic oxygen uptake (70 μmol), and were 2.50 -1.70 g for the Ni_2P/KUSY catalysts of different Ni_2P loadings and 0.83 g for the Ni-Mo-S/Al_2O_3 catalyst, with corresponding liquid hourly space velocities (LHSV) of 0.71-1.10, and 4.0 h^{-1}. For the hydroprocessing reaction the passivated phosphide catalysts were pretreated for 2 h at 623 K in 100 μmol s^{-1} (150 cm^3(NTP) min^{-1}) of H_2, and the sulfide catalyst was pretreated at 578 K for 2 h under 100 μmol s^{-1} of 10 % H_2S/H_2 at a pressure slightly above 1 atm. The experiments were long (~ 200 h) and, for each change in composition or temperature, the reaction system was allowed to run for 40-50 h to establish steady-state.

4.3. Results

Figure 4.1 shows the TPR profiles of the calcined oxidic precursors of the 0.5 Ni_2P/KUSY, 1.0 Ni_2P/KUSY, 1.5 Ni_2P/KUSY, and 2.0 Ni_2P/KUSY samples. A distinctive reduction peak at around 853 K is observed with the peak maximum shifting to slightly higher temperature with increase in Ni_2P loading. Table 4.1 summarizes the quantities of the precursors used in the preparation of the catalyst samples.

Figure 4.2 shows the powder XRD patterns of the fresh Ni_2P catalyst samples and a bulk Ni_2P reference. For the samples with lower loading levels of 0.5 and 1.0 Ni_2P no peaks for a Ni_2P phase were detected, but these became visible at higher loading levels of 1.5 and 2.0 Ni_2P.

Table 4.2 summarizes the physical properties of the Ni_2P catalyst samples. For the fresh samples the amount of CO uptake initially increased for the sample with loading levels of 0.5 and 1.0, but then decreased for the higher loading level samples. For the used samples the amount of CO uptake was reduced compared to the fresh samples, with the greatest decrease observed for the samples with lowest (0.5) and highest (2.0) loading levels. The specific surface areas of the samples decreased uniformly with loading level, with the used samples showing a small reduction compared to the fresh samples. A reduction in both micropore and mesopores volumes were observed in all cases.

Figure 4.3 shows the N_2 adsorption and desorption isotherms of the KUSY and 1.0 Ni_2P/KUSY samples, which are typical of the rest of the samples. For the KUSY sample the hysteresis loop is mainly flat, indicating inkbottle type pores, with a small enhancement in the upward curvature of the hysteresis loop also observed in the nitrogen relative pressure

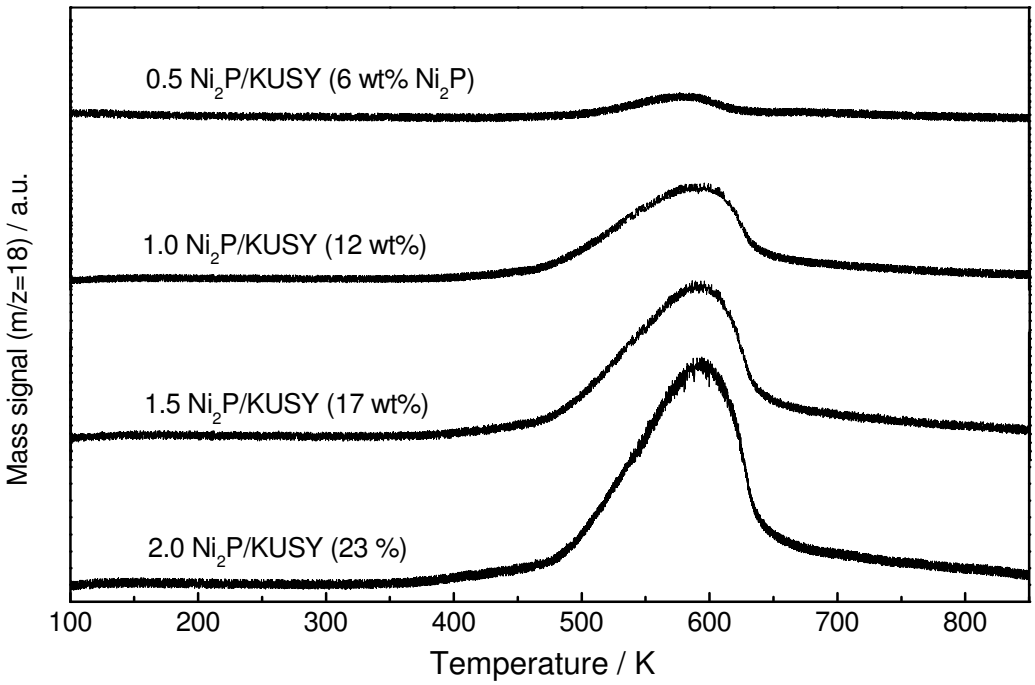

Figure 4.1. TPR profiles of synthesis of Ni_2P/KUSY samples.

Table 4.1 Quantities used in the preparation of the samples

Sample	Materials					
	Zeolite support / g	$Ni(NO_3)_2 \cdot 6H_2O$ / mol	Ni / wt %	$(NH_4)_2HPO_4$ / mol	P / wt %	Ni_2P / wt %
Loading levels						
0.5	20	0.0115	3.16	0.0230	3.33	6.49
1.0	20	0.0230	5.93	0.0462	6.29	12.22
1.5	20	0.0345	8.38	0.0690	8.85	17.23
2.0	20	0.0460	10.57	0.0920	11.16	22.73
Initial Ni/P ratios						
1/0.5	20	0.0230	6.22	0.0115	1.64	7.86
1/1	20	0.0230	6.12	0.0230	3.23	9.35
1/3	20	0.0230	5.75	0.0690	9.11	14.86

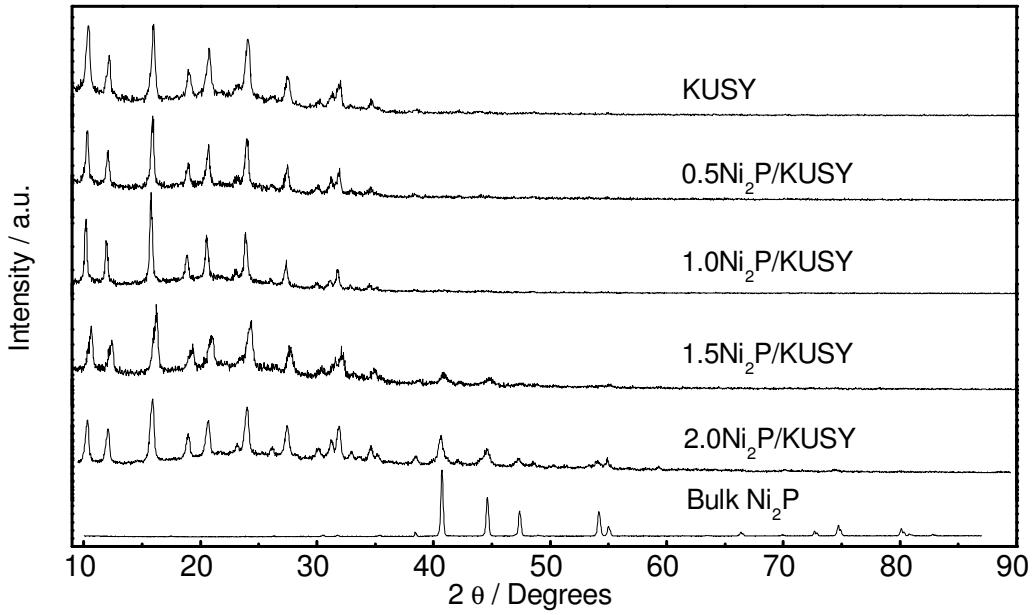

Figure 4.2. Powder XRD patterns of the fresh Ni_2P catalyst samples and bulk Ni_2P reference.

Table 4.2 Physical properties of KUSY- supported Ni_2P samples

Sample	Condition	CO uptake / μmol g^{-1}	BET area / m^2 g^{-1}	Pore volume / cm^3 g^{-1}		
				V_{micro} [a]	V_{meso} [b]	V_{total}
HUSY	-	-	790	0.235	0.352	0.587
KUSY	-	-	784	0.231	0.350	0.581
0.5 Ni_2P/KUSY	Fresh	38	678	0.225	0.273	0.498
	Used	15	613	0.209	0.261	0.470
1.0 Ni_2P/KUSY	Fresh	42	562	0.189	0.241	0.430
	Used	39	531	0.168	0.235	0.403
1.5 Ni_2P/KUSY	Fresh	35	482	0.169	0.231	0.400
	Used	29	434	0.151	0.221	0.372
2.0 Ni_2P/KUSY	Fresh	29	412	0.140	0.170	0.310
	Used	9	389	0.119	0.139	0.258

[a] Micropore volume from t-plot. [b] V_{total}- V_{micro}.

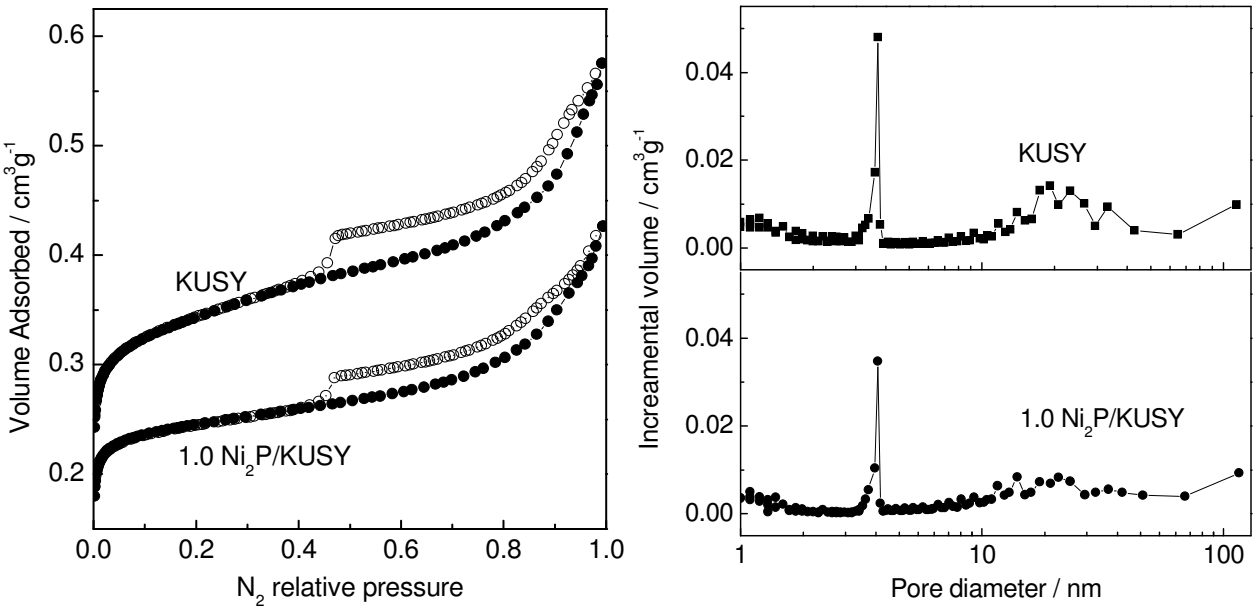

Figure 4.3. N_2 adsorption and desorption isotherms of KUSY and 1.0 Ni_2P/KUSY.

Table 4.3 Elemental analysis results for the fresh and used Ni_2P samples with different loadings

Sample	Condition	Molar ratio		
		P / Ni	S / Ni	S / P
Bulk Ni_2P (Cerac)		0.49	-	-
0.5 Ni_2P/KUSY	Fresh	1.371	-	-
0.5 Ni_2P/KUSY	Used*	0.954	0.218	0.228
1.0 Ni_2P/KUSY	Fresh	1.124	-	-
1.0 Ni_2P/KUSY	Used*	0.917	0.160	0.174
1.5 Ni_2P/KUSY	Fresh	1.062	-	-
1.5 Ni_2P/KUSY	Used*	0.876	0.144	0.164
2.0 Ni_2P/KUSY	Fresh	0.984	-	-
2.0 Ni_2P/KUSY	Used*	0.798	0.119	0.149

*0.65 % S in feed

range of 0.8-0.95, indicating cylindrical type pores. Introduction of Ni_2P onto the KUSY lowered the overall N_2 adsorption volume, with the overall shape of the hysteresis loop remaining unchanged. Figure 4.3 also shows the pore size distributions for the KUSY and 1.0 Ni_2P/KUSY samples as calculated from the desorption branch using the BJH method. The peak at a diameter of 3.5 nm is an artifact of the BJH method for mesoporous materials with pore size less that 4 nm [10]. A wide range of mesopores of size 4-40 nm is observed.

Table 4.3 summarizes the molar ratios of P/Ni, S/Ni, and S/P in the samples before and after reaction, as determined by ICP-AES. Although the samples were prepared with an initial Ni/P ratio of 1/2, the freshly prepared samples were found to contain lower phosphorus amounts than the initial value, with Ni/P ratios ranging from 1/1.371 to 1/0.984. After reaction, the samples underwent further loss in P to give Ni/P ratios, ranging from 1/0.954 to 1/0.798. It was found that more P was retained for the samples with higher dispersion and that also sulfur was found to be associated with the catalysts after reaction. This was also found for the SiO_2 supported samples.

Figure 4.4 shows TEM micrographs of the Ni_2P/KUSY catalysts with different Ni_2P loading levels. The 0.5 Ni_2P /KUSY sample appeared to have very small particles of size smaller than 3 nm. The 1.0 Ni_2P /KUSY sample had primarily particles of size from 3 to 5 nm with a few particles of size around 1 nm. The 2.0 Ni_2P/KUSY sample had relatively large particles of sizes over 10 nm.

Figure 4.5 shows the Ni K-edge EXAFS spectra and Fourier transforms of the freshly prepared samples with different loading levels and those of a bulk reference Ni_2P sample. For the bulk Ni_2P sample the Fourier transform gave two distinctive peaks, a smaller one at 0.171 nm and a larger one at 0.228 nm. For the supported Ni_2P samples there were also two

main peaks located at almost the same positions as those of the bulk Ni_2P reference, but with the larger peak weakened and broadened as the loading level of the Ni_2P decreased. Table 4.3 summarizes the crystallographic Ni_2P standard data from the literature [11] and the curve-fitting results of the EXAFS spectra for the freshly prepared Ni_2P samples and the bulk Ni_2P reference. For the bulk Ni_2P the coordination numbers of the subshells are in good agreement with those of the standard Ni_2P with the bond lengths being slightly lowered. For the KUSY supported Ni_2P samples in the first shell corresponding to a Ni-P bond the coordination number remains constant at around 2.0, with the bond distance being lowered. In the second shell corresponding to another Ni-P bond, the coordination number appeared much larger than that of the bulk Ni_2P and gradually decreased with an increase in loading levels, while the bond length increased. In the third shell corresponding to a Ni-Ni bond the coordination number increased with loading levels.

Figure 4.6 shows the HDS conversion of 4,6-DMDBT as a function of time on stream for the samples with different loading levels. The activity was based on equal numbers of sites (70 μmol $g^{-1}$of CO or atomic oxygen uptake) loaded in the reactor. Both the 1.0 Ni_2P/KUSY and 1.5 Ni_2P/KUSY catalysts exhibited a high and stable activity of around 95-99 % HDS conversion. Both the 0.5 Ni_2P/KUSY and 2.0 Ni_2P/KUSY catalysts gave lower conversions at around 56 % and 86 %, respectively. For the Ni-Mo-S/Al_2O_3 catalyst the HDS conversion was low at 80 %. Table 4.5 summarizes the product distributions. The HDS conversion followed the order 1.0 Ni_2P/KUSY > 1.5 Ni_2P/KUSY > 2.0 Ni_2P/KUSY > Ni-Mo-S/Al_2O_3 > 0.5 Ni_2P/KUSY. In all cases, the HYD pathway was dominant over the DDS pathway of the HDS of 4,6-DMDBT and the quinoline HDN conversion level was high at 100 %. In the case of tetralin the hydrogenation pathway was

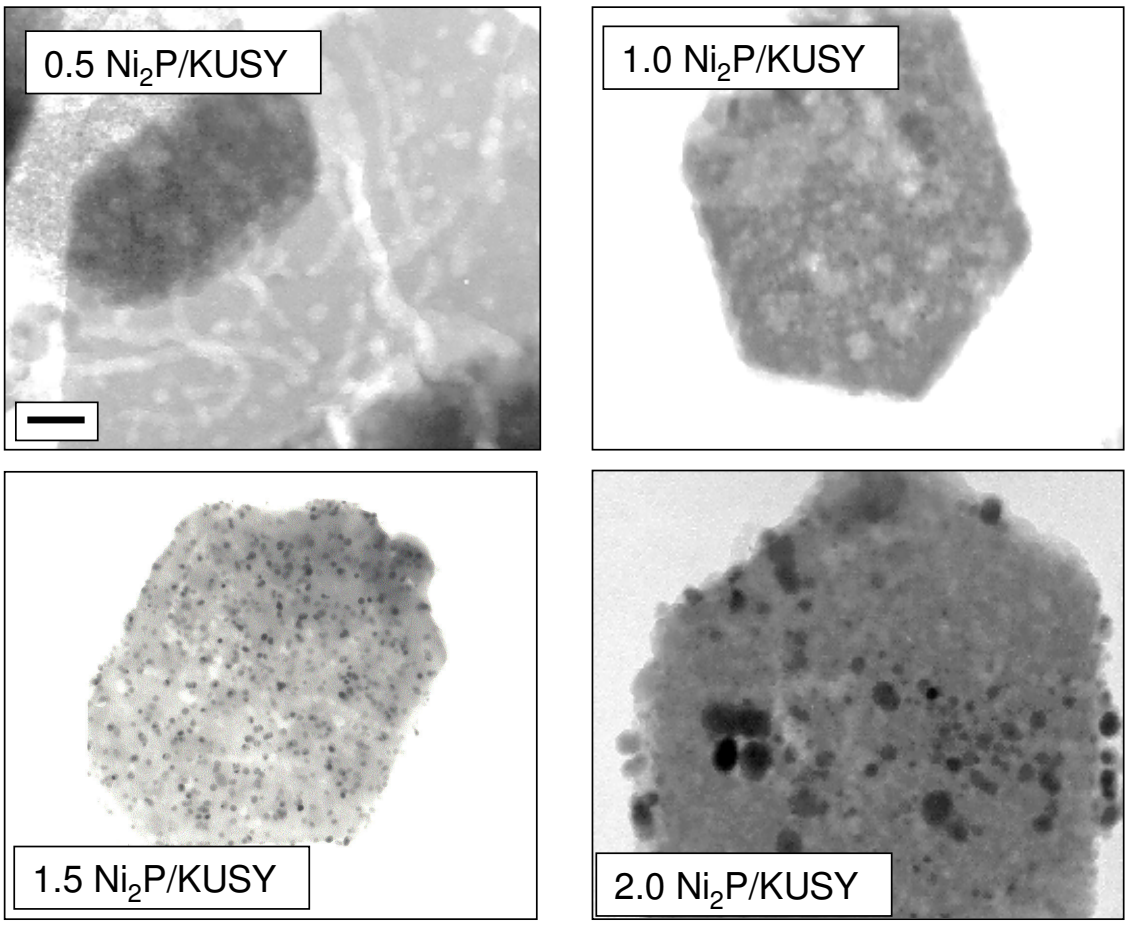

Figure 4.4. TEM micrographs of Ni_2P/KUSY samples with different Ni_2P loadings.

Scale bar = 50 nm.

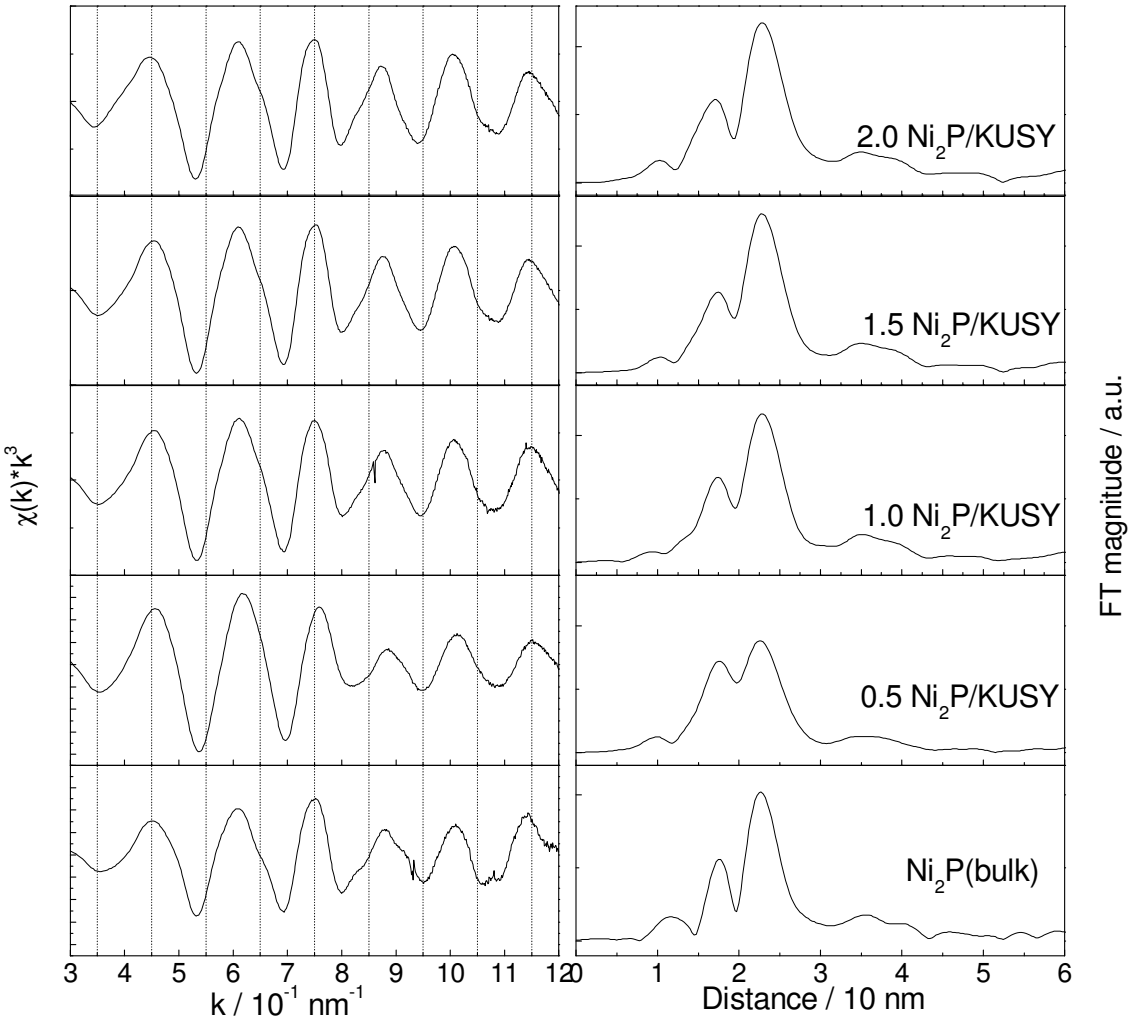

Figure 4.5. Comparison of Ni K-edge EXAFS spectra and Fourier transforms for the fresh samples with different Ni_2P loadings.

Table 4.4 Curve-fitting results for the fresh Ni_2P samples with different loadings

Samples	Ni-P								Ni-Ni (I, II)				R / %
	Ni-P (I)				Ni-P (II)								
	CN	R / nm	σ^2 / 10^{-5} nm^2	ΔE / eV	CN	R / nm	σ^2 / 10^{-5} nm^2	ΔE / eV	CN	R / nm	σ^2 / 10^{-5} nm^2	ΔE / eV	
Feff reference	2	0.22662			1	0.23688			4	0.26783			
Ni_2P (Bulk)	2.0	0.2253	3.00	0.420	1.750	0.2401	0.499	0.423	3.99	0.2644	6.00	1.798	0.48
0.5 Ni_2P / KUSY	2.0	0.2200	3.005	-0.785	4.167	0.23518	5.507	-0.736	3.56	0.26253	9.102	3.102	1.39
1.0 Ni_2P / KUSY	2.0	0.2203	3.8588	-0.017	4.502	0.23617	6.4803	0.055	3.71	0.26424	8.5709	4.002	1.99
1.5 Ni_2P / KUSY	2.0	0.22192	3.9918	-0.057	4.320	0.23938	6.5830	-0.028	3.992	0.26384	7.8016	2.433	1.46
2.0 Ni_2P / KUSY	2.0	0.22223	3.5673	-1.352	3.896	0.24001	4.6422	-1.344	4.131	0.26371	8.38293	2.496	1.13

ΔR filtered 15136 - 0.27605 nm, $S_o^2 = 0.9$

$$Residual\,(R,\%) = \left(\frac{\sum_{i=1}^{N} \left| y_{\exp}(i) - y_{theo}(i) \right|}{\sum_{i=1}^{N} y_{\exp}(i)} \right) \times 100$$

dominant over the dehydrogenation pathway and produced cis/trans-decalin. The only exception was the high loading sample 2.0 Ni_2P/KUSY.

Figure 4.7 shows the Ni K-edge EXAFS spectra and Fourier transforms of the freshly prepared samples with initial Ni/P ratios of 1/0.5, 1/1.0, 1/2.0, and 1/3.0 and of the bulk Ni_2P reference. The low P content sample Ni_2P/KUSY (1/0.5) showed a single broad peak in the Fourier transform but the rest of the samples had two main peaks located in almost the same positions as those of the bulk Ni_2P reference. Higher contents of P led to a widening of the larger peak. Table 4.6 summarizes the curve-fitting results of the EXAFS spectra for the freshly prepared Ni_2P samples with the different initial Ni/P ratios. These were obtained using the procedures described in Chapters 2 and 3. In the first shell, corresponding to a Ni-P distance, higher P led to a decrease in bond length but little change in the coordination number. For the second shell, corresponding to another Ni-P distance, higher P resulted in an increase in the coordination number and bond length. For the third shell, corresponding to a Ni-Ni distance, higher P led to a decrease in coordination number but an increase in bond length.

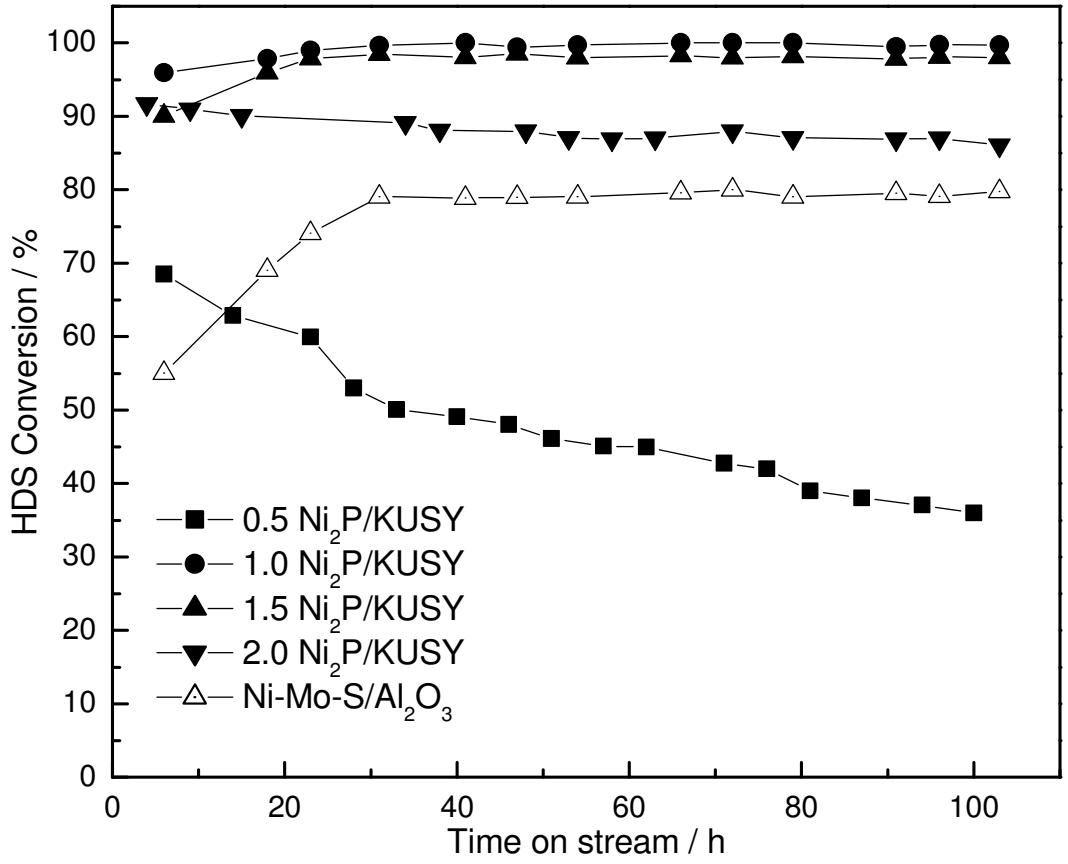

Figure 4.6. HDS conversion of 4,6-DMDBT on the Ni_2P/KUSY catalysts with different loadings as a function of time on stream.

Table 4.5 Product distribution of hydrotreating for the Ni_2P/KUSY catalysts with different loadings

Reactant	Conversion / %						Product	Relative selectivity / %				
	Type	0.5 Ni_2P / KUSY	1.0 Ni_2P / KUSY	1.5 Ni_2P / KUSY	2.0 Ni_2P / KUSY	Ni-Mo-S / Al_2O_3		0.5 Ni_2P / KUSY	1.0 Ni_2P / KUSY	1.5 Ni_2P / KUSY	2.0 Ni_2P / KUSY	Ni-Mo-S / Al_2O_3
4,6-DMDBT	DDS	13	12	23	34	10	DMBP	24	12	24	39	12
	HYD	43	88	75	52	72	DMCHB	61	66	53	40	63
	HDS	56	100	98	86	80	DMBCH	15	22	23	21	25
Quinoline	HDN	100	100	100	100	100	PCH	93	92	90	88	87
							PB	7	9	11	12	14
Tetralin	HYD	4	10	5	3	17	trans-Decalin	53	51	40	27	57
							cis-Decalin	12	27	20	17	18
	De-HYD	2	3	3	4	6	Naphthalene	33	22	41	56	26

DMBP: 3,3'-dimethylbiphenyl, DMCHB: dimethylcyclohexylbenzene, DMBCH: dimethylbicyclohexane, PCH: propylcoclohexane, PB: propylbenzene, 5-THQ: 5,6,7,8-tetrahydro-quinoline, OPA: orthopropylaniline, 1-THQ: 1,2,3,4-tetrahydroquinoline

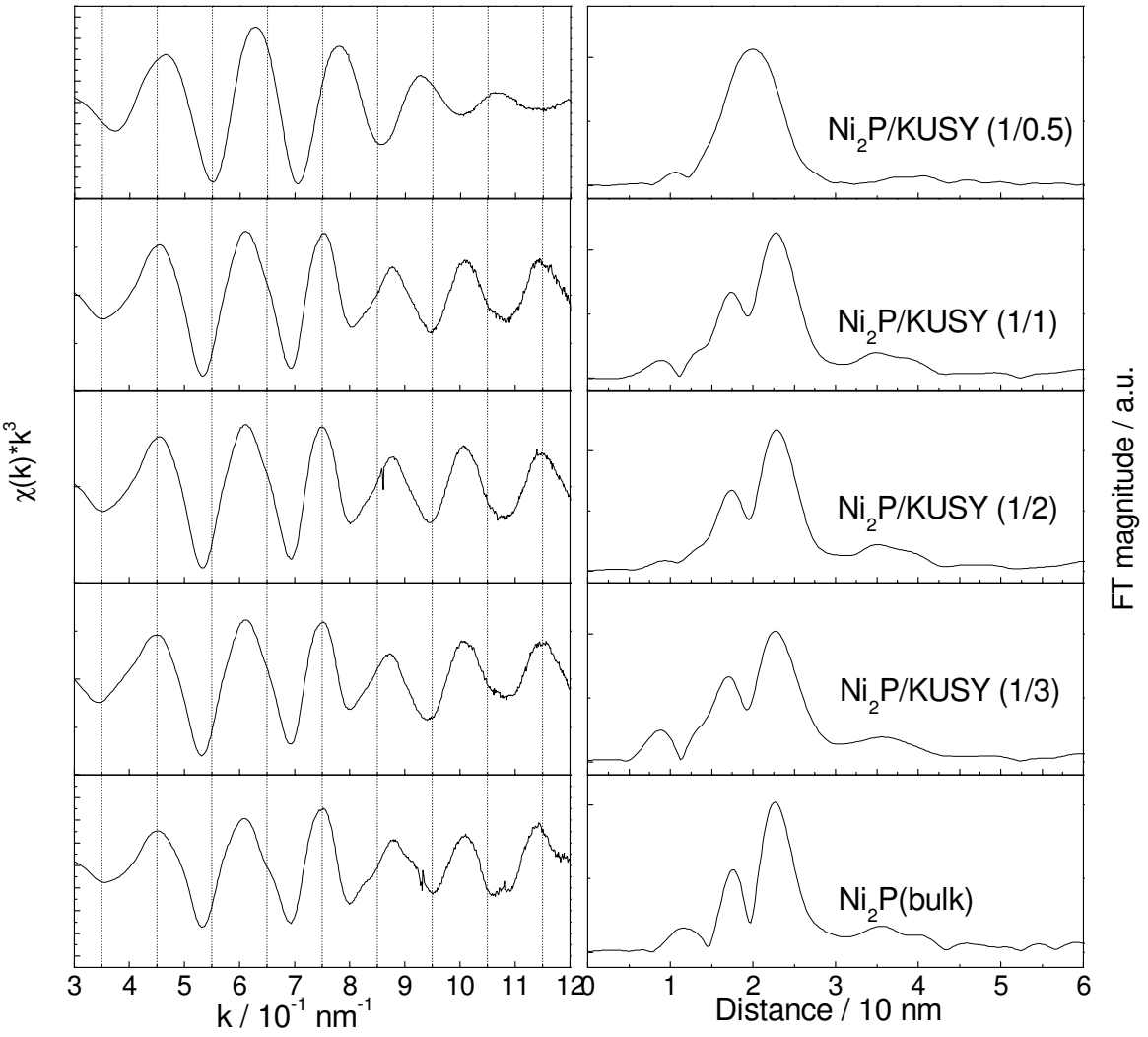

Figure 4.7. Comparison of Ni K-edge EXAFS spectra and Fourier transforms for the fresh samples with different initial Ni/P ratios.

Table 4.6 Curve-fitting results for the fresh Ni_2P samples with different initial Ni/P ratios

Samples	Ni-P								Ni-Ni (I, II)				R / %
	Ni-P (I)				Ni-P (II)								
	CN	R / nm	σ^2 / 10^{-5} nm^2	ΔE / eV	CN	R / nm	σ^2 / 10^{-5} nm^2	ΔE / eV	CN	R / nm	σ^2 / 10^{-5} nm^2	ΔE / eV	
Feff reference	2	0.22662			1	0.23688			4	0.26783			
Ni_2P (Bulk)	2.0	0.2253	3.00	0.420	1.750	0.2401	0.499	0.423	3.99	0.2644	6.00	1.798	0.48
Ni_2P (1/ 0.5) / KUSY	1.9	0.2233	7.936	-3.932	0.727	0.2359	2.4079	-3.1973	6.12	0.2503	12.500	-7.999	1.108
Ni_2P (1/ 1.0) / KUSY	2.0	0.2211	2.676	-1.3248	3.329	0.23621	3.019	-1.3194	3.99	0.26312	7.229	0.9791	0.814
Ni_2P (1/ 2) / KUSY	2.0	0.2203	3.8588	-0.017	4.502	0.23617	6.4803	0.055	3.71	0.26424	8.5709	4.002	1.99
Ni_2P (1/ 3) / KUSY	2.0	0.21923	6.1509	-1.7775	4.754	0.23636	4.2239	-1.792	3.64	0.2654	6.5285	4.2321	1.31

ΔR filtered 15136 - 0.27605 nm, $S_o^2 = 0.9$

$$Residual(R,\%) = \left(\frac{\sum_{i=1}^{N} \left| y_{\exp}(i) - y_{theo}(i) \right|}{\sum_{i=1}^{N} y_{\exp}(i)} \right) \times 100$$

Figure 4.8 shows the HDS conversion of 4,6-DMDBT as a function of time on stream for the samples with different P levels. Again, the activity was compared based on equal number of chemisorption sites (70 μmol $g^{-1}$of CO) loaded in the reactor. The Ni_2P/KUSY (1/0.5) catalyst initially gave high HDS conversion of around 90 % but underwent deactivation. The Ni_2P/KUSY (1/1) and Ni_2P/KUSY (1/2) catalysts exhibited very high and stable HDS conversion of around 95-99 %. The Ni_2P/KUSY (1/3) catalyst showed slightly lower HDS conversion of around 85 % but maintained stability during reaction. Table 4.7 summarizes the product distributions. For the Ni_2P/KUSY (1/0.5) catalyst the direct desulfurization (DDS) pathway for the HDS of 4,6-DMDBT was dominant with a DDS selectivity of 64 % and showed lower activity in the HDN of quinoline (59 % of HDN conversion). It also exhibited almost no activity in the tetralin reaction. Increase in P content led to better HDS activity with an increase in the HYD selectivity in the HDS of 4,6-DMDBT. In the case of tetralin, increase in the P content also led to an increase in the HYD selectivity from 41 % for the Ni_2P/KUSY (1/1) to 77 % for the Ni_2P/KUSY (1/2) and the Ni_2P/KUSY catalyst gave more hydrogenated species decalin than dehydrogenated one naphthalene.

Table 4.8 reports the molar ratios of P/Ni, S/Ni, and S/P of the samples before and after reaction, as determined by ICP-AES. It can be seen that after reaction, more S is retained on the Ni_2P sample with a lower P content.

Table 4.9 reports the K content and the physical properties of the K ion-exchanged USY supports. Around 65 % exchange was obtained with one K solution treatment, and 81 % exchange was achieved with three successive treatments. These samples were used as supports to examine the effect of acidity on the catalytic properties of the materials.

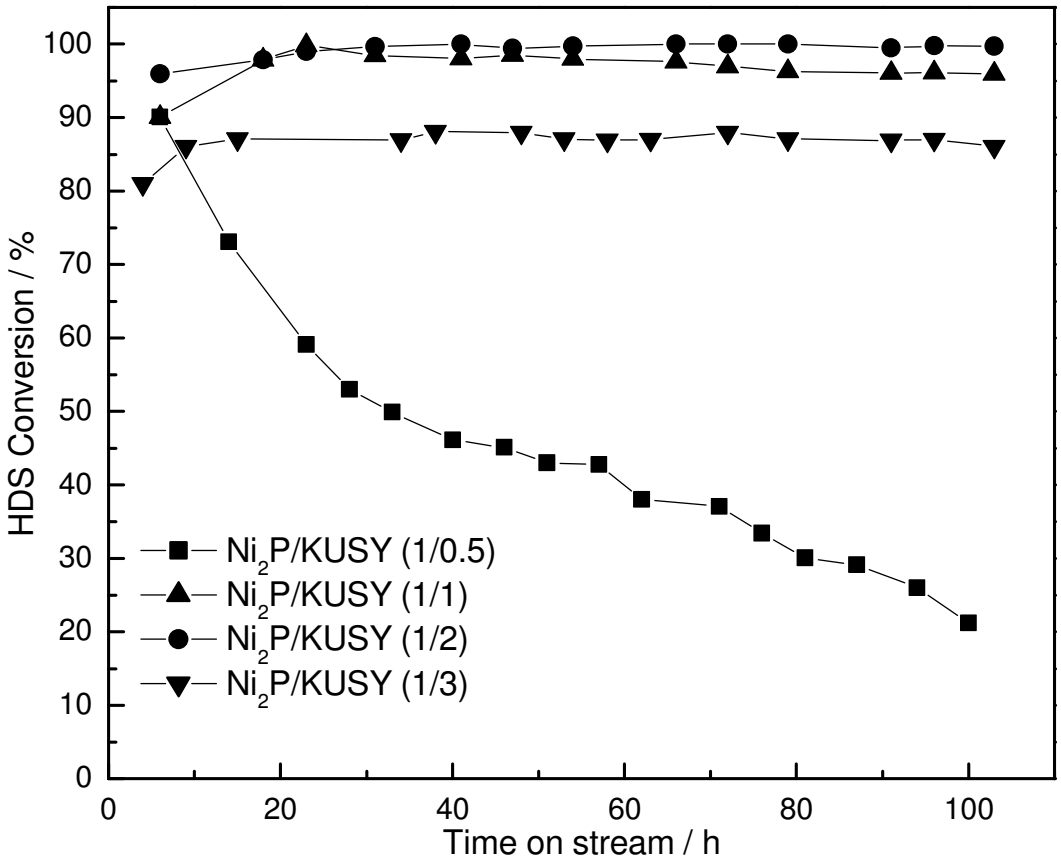

Figure 4.8. HDS conversion of 4,6-DMDBT on the Ni_2P/KUSY catalysts with different initial Ni/P ratios as a function of time on stream.

Table 4.7 Product distribution of hydrotreating for the Ni_2P/KUSY catalysts with different initial Ni/P ratios

Reactant	Conversion / %					Product	Relative selectivity / %			
	Type	Ni_2P (1/0.5) / KUSY	Ni_2P (1/1) / KUSY	Ni_2P(1/2) / KUSY	Ni_2P (1/3) / KUSY		Ni_2P (1/0.5) / KUSY	Ni_2P (1/1) / KUSY	Ni_2P(1/2) / KUSY	Ni_2P (1/3) / KUSY
4,6-DMDBT	DDS	16	40	12	11	DMBP	64	42	12	13
	HYD	9	55	88	75	DMCHB	23	40	66	71
	HDS	25	95	100	86	DMBCH	13	18	22	17
Quinoline	HDN	59	100	100	100	PCH	68	83	92	90
						PB	23	27	8	10
	HYD	5				5-THQ	3			
						OPA	2			
						1-THQ	3			
Tetralin	HYD	-	4	10	8	trans-Decalin	-	27	51	46
		-				cis-Decalin	-	13	27	24
	De-HYD	-	6	3	2	Naphthalene	-	60	22	30

DMBP: 3,3'-dimethylbiphenyl, DMCHB: dimethylcyclohexylbenzene, DMBCH: dimethylbicyclohexane, PCH: propylcoclohexane, PB: propylbenzene, 5-THQ: 5,6,7,8-tetrahydro-quinoline, OPA: orthopropylaniline, 1-THQ: 1,2,3,4-tetrahydroquinoline

Table 4.8 Elemental analysis results for the fresh and used Ni_2P samples with different initial Ni/P ratios

Sample	Condition	Molar ratio		
		P / Ni	S / Ni	S / P
Bulk Ni_2P (Cerac)		0.49	-	-
Ni_2P/KUSY (1/0.5)	Fresh	0.487		
Ni_2P/KUSY (1/0.5)	Used*	0.435	0.334	0.768
Ni_2P/KUSY (1/1.0)	Fresh	0.873	-	
Ni_2P/KUSY (1/1.0	Used*	0.713	0.214	0.300
Ni_2P/KUSY (1/2.0)	Fresh	1.124	-	-
Ni_2P/KUSY (1/2.0	Used*	0.917	0.160	0.174
Ni_2P/KUSY (1/3.0)	Fresh	1.355	-	
Ni_2P/KUSY (1/3.0)	Used*	0.994	0.119	0.119

*0.65 % S in feed

Table 4.9 Properties of the K-ion exchanged USY supports

Number of ion exchange	Sample	Ion exchange* / %	BET area / $m^2\ g^{-1}$	Pore volume / $cm^3\ g^{-1}$		
				V_{micro} [a]	V_{meso} [b]	V_{total}
0	HUSY	-	790	0.235	0.352	0.587
1	KHUSY	65	788	0.230	0.350	0.580
2	KHUSY-2	79	-	-	-	-
3	KUSY	81	784	0.231	0.350	0.581

* Based on an atomic ration of K/Al from the elemental analysis

Figure 4.9 shows the pyridine TPD profiles for the HUSY, KHUSY, and KUSY supports. For HUSY two peaks were observed at a low temperature of 473 K and at a high temperature of 751 K, corresponding to pyridine desorptions from Lewis and Brønsted acid sites, respectively. With increase in the K ion-exchange levels the peak intensity at the high temperature of 751 K was reduced.

Figure 4.10 shows the product gas chromatogram for the HDS of 4,6-DMDBT on 1.0 Ni_2P/HUSY, 1.0 Ni_2P/KHUSY, and a commercial Ni-Mo-S/Al_2O_3 catalysts. For the 1.0 Ni_2P/HUSY a measurable conversion of 5.6 % of the tridecane solvent to cracking products was obtained, but this was considerably reduced for the Ni_2P/KHUSY catalyst and became negligible for the 1.0 Ni_2P/KUSY catalyst, indicating an effective neutralization of the support acidity. The Ni_2P/KHUSY catalyst also exhibited very high and stable HDS activity with a conversion of 99 %.

Figure 4.11 shows the HDS conversion and the product selectivities for the HYD and DDS pathways of 4,6-DMDBT as a function of time on stream. Initially, a feed containing 0.35 % S (0.05 % S as 4,6-DMDBT and 0.3 % S as DMDS), 0.02 % N as quinoline, and 1 % tetralin in a tridecane solvent was introduced. For 1.0 Ni_2P/KHUSY the HDS conversion was high and stable at 97-100 % and the selectivity favored the HYD pathway (95 %) over the DDS pathway (5 %). After 40 h on stream 0.3 % S (as DMDS) was added to the feed (Fig. 4.11 B), and that resulted in a small drop in HYD selectivity to 87 %. After 83 h 0.03% N as quinoline was added (Fig. 4.11 C), and this gave a slight decrease in HDS conversion to 94 % but with no distinctive change in selectivities. A similar reaction sequence was carried out for the Ni-Mo-S/Al_2O_3 catalyst. The HDS conversion was initially 73 % and increased to 80 % upon increase of DMDS by 0.6 % S, but the introduction of the

N-compound led to a decrease in HDS conversion to 69 %.

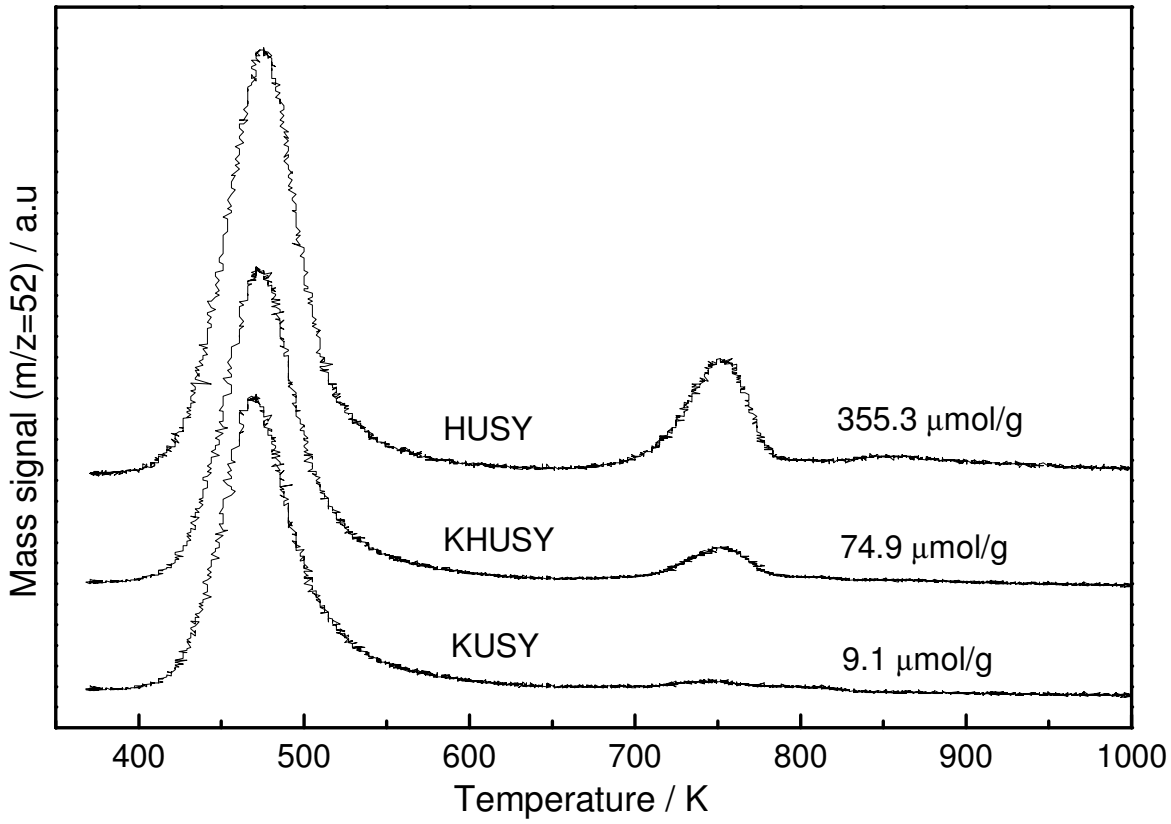

Figure 4.9. Pyridine TPD profiles for HUSY, KHUSY, and KUSY supports.

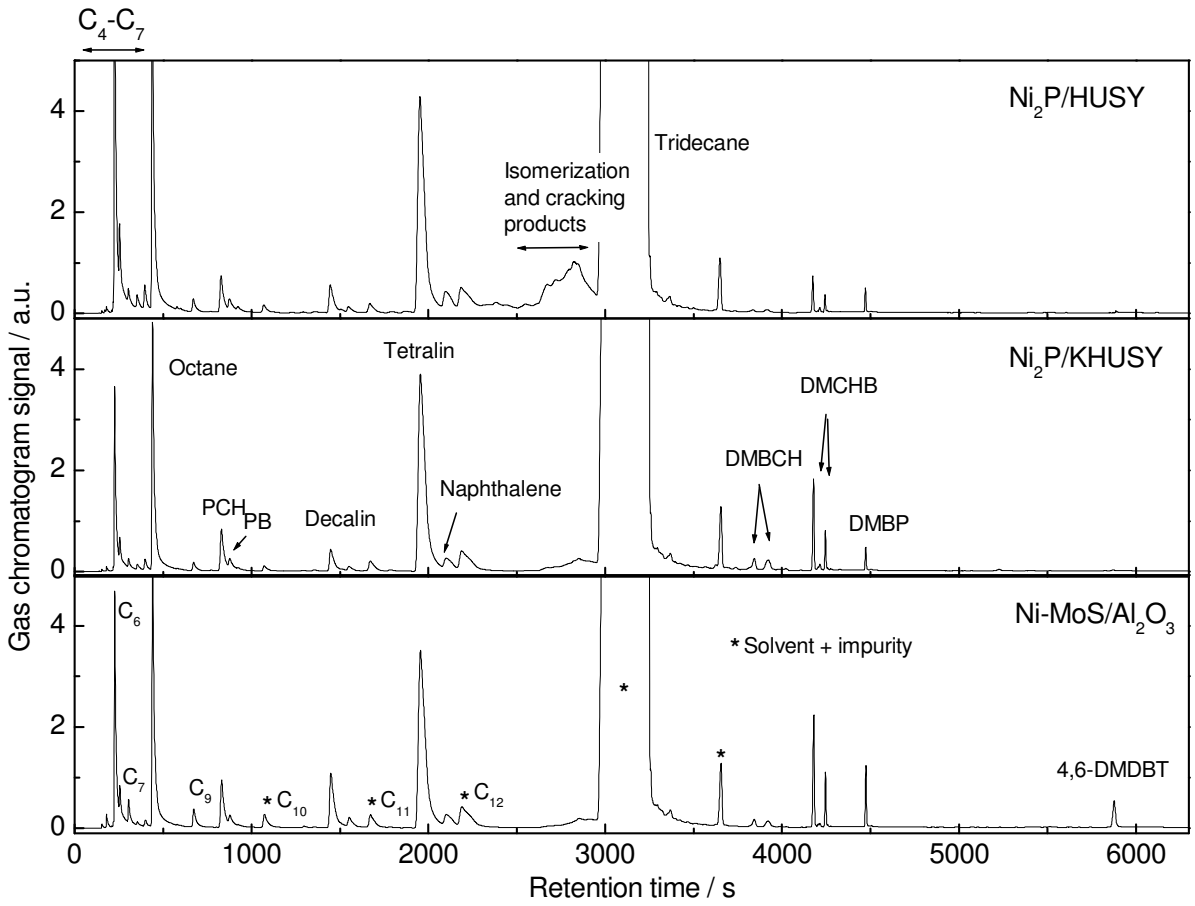

Figure 4.10. Product gas chromatograms for Ni_2P/HUSY, Ni_2P/KHUSY, and Ni-Mo-S/Al_2O_3.

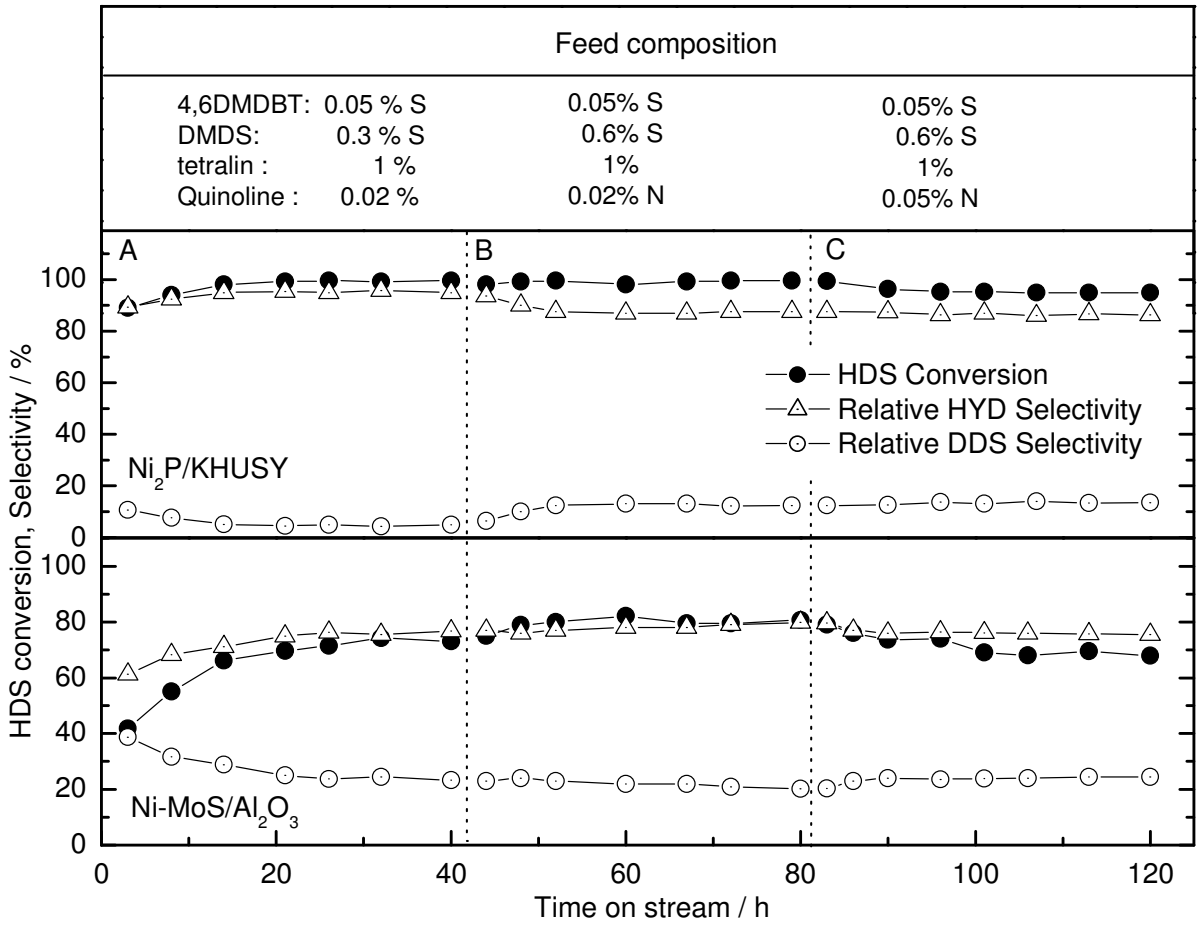

Figure 4.11. HDS conversion and product selectivities on the Ni_2P/KHUSY, and Ni-Mo-S/Al_2O_3 catalysts.

4.4. Discussion

4.4.1. Studies of the Effect of Ni_2P Loading

The KUSY supported Ni_2P catalysts were prepared by the temperature-programmed reduction (TPR) of supported nickel phosphate precursors. The TPR profiles give a distinctive reduction peak at a moderately high temperature of around 873 K with the peak being more broadened for the samples with higher loadings, consistent with a longer diffusion path for the removal of oxygen in the larger particles. These are similar to those obtained with the SiO_2 and MCM-41 supports where the peaks occur at 860 and 875 K.

The samples were first prepared with excess phosphorus using a P/Ni ratio 2/1. Elemental analysis shows that there was a loss of the phosphorus during preparation (Table 4.3) with P/Ni ratios of 0.984-1.371, approaching the stoichiometric value of 0.5 for Ni_2P. This is similar to the silica supported samples. Previous work has shown that phosphorus is removed as PH_3 during the reduction procedure [19]. Elemental analysis revealed that more P remained on the samples with lower loadings (Table 4.3). This suggests that there are stronger interactions between Ni and P in the smaller particles.

The XRD patterns show that the USY support is well crystallized and the TEM micrographs indicate well-developed mesopores in a size range of 10-40 nm created by the hydrothermal treatment used in the preparation of the material. The influence of the thermal treatment on the structure of zeolite Y is well known [12,13,14]. Briefly, the steaming procedure used lowers the amount of framework Al species, enhances the stability of the zeolites and at the same time generates the mesopores within the crystals. The treatment also leads to a redistribution of acidic centers and an enhancement in the acid strength. It is

believed that the strength of the acid sites is related to the number of sites, isolated sites being stronger, and to the hydrogen transfer activity. Studies using 3D-TEM have shown that USY (Zeolyst, CBV780) has mesopores in the size range of 4-40 nm in the form of cavities and cylindrical pores [15]. The mesoporous nature of the materials is very important in the area of the gas oil treatment because it allows access to bulky molecules.

In this work, the Ni_2P/KUSY catalysts were found to consist of spherical particles of Ni_2P homogeneously dispersed within the grains of the support. The size of the particles varied with loading level with sizes in the range of 1-4 nm, 10-15 nm, and over 20 nm for loading levels of 1.0, 1.5, and 2.0, respectively. The particles are likely situated in the mesoporous cavities and at the external surface of the zeolite crystals. The gradual decrease in the microporosity suggests that there are also small particles not visible by TEM situated within the supercages, the size of which is 1.3 nm (Table 4.2). These Ni_2P particles are not numerous enough to totally block the pores, causing only a gradual decrease in pore volume.

The characteristic XRD signals of Ni_2P on the KUSY supports are visible for the samples with higher loadings of 1.5 and 2.0 Ni_2P (Fig. 4.2), although their overall peak intensity is low. The broader, less intense XRD peaks indicate a high dispersion of the phosphide phase, as also indicated by the high CO uptake (Table 4.2). In the case of the 0.5 and 1.0 Ni_2P/KUSY, XRD shows no peaks due to Ni_2P, indicating that crystallite size is below 0.4 nm. In all cases the retention of the USY peaks indicates that the framework structure does not deteriorate seriously during the synthesis steps which include calcination at 673 K followed by reduction at 893 K.

EXAFS analysis is particularly useful for characterizing highly dispersed phases on supports with large surface area. Fourier transform EXAFS spectra for the supported Ni_2P

catalysts show two overlapping peaks in the region 0.15-0.30 nm. The previous studies of EXAFS simulations of supported Ni_2P catalysts in Chapters 2 and 3 have shown that a three-shell analysis using Feff code can be effectively applied for the Ni_2P with structural parameters obtained from the literature [11]. Two Ni-P shells at 0.2266 and 0.2456 nm and one Ni-Ni shell at 0.2678 nm were employed for the calculations. The same analysis gives reasonable parameters for all samples here (Table 4.4). Unlike the case of the bulk Ni_2P, for the supported Ni_2P samples the coordination number in the second shell of Ni-P at 0.23688 nm increased and grew for the small crystallites. This suggests that the Ni_2P crystallites are decorated with phosphorus on the surface in a coordination corresponding to that of the second shell with a Ni-P distance of 0.2456 nm. This is consistent with the elemental analysis results, which indicate a proportionally higher P content for the smaller particles and suggest that in the smaller crystallites the Ni-P interaction is stronger. This is reasonable. Also, the bond length and coordination number for the Ni-Ni shell were found to increase with the dispersion of the Ni_2P. Again this follows from the larger P content in the more dispersed Ni_2P catalysts which lengthens the distance between Ni atoms and weakens the Ni-Ni bond. The study of a highly dispersed Ni_2P catalyst on an MCM-41 support as reported in Chapter 2 showed that highly dispersed Ni_2P particles underwent less loss in P, even after high temperature reduction. This again suggests that the smaller particles have a stronger interaction between the Ni and P atoms.

Studies of catalytic activity in HDS were again carried out with 4,6-dimethyldibenzothiophene (4,6-DMDBT) as a model S compound in this study, because the compound represents the family of the most refractory S-containing molecules in oil distillates [16]. Again, the results are interpreted in terms of the direct sulfur desulfurization

(DDS route) and the hydrogenation (HYD route). It is known that hydrogenation of neighboring phenyl groups reduces the steric hindrance caused by the methyl groups [16,17,18]. With some important distinctions, to be discussed below, the product distributions obtained in the HDS of 4,6-DMDBT on the supported Ni_2P catalysts and Ni-Mo-S/Al_2O_3 catalysts were similar (Figs. 4.6-11). For all catalysts the major products were 3,3-dimethylbiphenyl (3,3-DMBP), methylcyclohexyltoluenes (MCHT), and dimethylbicyclohexyl (DMBCH). Only traces of 4,6-tetrahydro- and 4,6-hexahydrodibenzothiophenes were found.

The catalytic activity was tested for these samples at a relatively high temperature, 613 K (340 ^oC) (Fig. 4.6) and reactivity was found to follow the order 1.0 Ni_2P/KUSY > 1.5 Ni_2P/KUSY > 2.0 Ni_2P/KUSY > Ni-Mo-S/Al_2O_3 > 0.5 Ni_2P/KUSY. The comparison was again made on the basis of equal chemisorption sites loaded in the reactor, with CO used as chemisorption probe for the phosphide and O_2 for the sulfide. The Ni_2P catalysts with loading levels of 1.0 and 1.5 Ni_2P showed high and stable HDS conversion of around 99% and favored the HYD pathway for the HDS of 4,6-DMDBT (Table 4.5). The Ni_2P catalysts with loading level of 0.5 underwent deactivation, very likely due to the lack of the Ni_2P phase as indicated from the EXAFS results (Fig. 4.5). In the absence of sufficient phosphorus the Ni-rich phase probably transforms to a nickel sulfide phase, which is known to have poor activity in HDS [19].

4.4.2. Studies of the Effect of P Content

In previous studies nickel phosphide catalysts have been shown to have unique catalytic behavior in the HDS of dibenzothiophene and the HDN of quinoline [19,20], where

the initial Ni to P ratio and the Ni_2P loading levels were important in determining catalytic activity. It was found that extra phosphorous in the preparation of Ni_2P at levels corresponding to an initial Ni to P ratio of 1/2 (four-fold excess of P over stoichiometric) on the low surface SiO_2 (~90 m^2 g^{-1}) support gave a beneficial effect on the catalytic activity and stability, and also gave rise to a better dispersion of the Ni_2P phase. Here, a similar effect was observed on the KUSY supports. The EXAFS analysis showed that a stoichiometric P content (Ni/P = 1/0.5) in the preparation of Ni_2P gave a P-deficient phase with higher Ni-Ni coordination number and shorter Ni-Ni bond lengths similar to those in metallic nickel (Fig. 4.7 and Table 4.6). Increase in the P content led to an increase in the coordination number in Ni-P bonds particularly for the second shell, and a gradual decrease in the Ni-Ni coordination number with lengthening of the intermetallic bond distance. These results imply that the extra P in the preparation of Ni_2P is located at a distance close to that of a second Ni-P shell probably on the surface of the crystallites.

Reaction tests for the HDS of 4,6-DMDBT (Fig. 4.8) on the catalysts indicate that a sample with an initial Ni/P ratio of 1/0.5 underwent serious deactivation and that the sample with a Ni/P ratio of 1/3 showed a lower activity compared to the samples with a Ni/P ratio of 1/2 and 1/1. Excess phosphorous as in sample with Ni/P ratio of 1/3 probably results in site blockage and a low active site density. The elemental analysis revealed that relatively higher amount of S was associated with the catalyst of an initial Ni/P = 1/2 during the reaction, consistent with exterior sulfidation of the particles.

4.4.3. Studies of the Effect of USY Support Acidity

Compositions based on USY zeolites containing sulfides of transition metals (Mo,

W, Ni or Co) are quite active in hydrodesulfurization reactions, but deactivate rapidly due to coke deposition, probably induced by the acid sites present in the zeolites. The materials also have difficulty in retaining the metal phase highly dispersed inside the zeolite. Indeed, in many studies [1-4] it has been demonstrated that after calcination and/or sulfidation only a small part of the metal remains inside the zeolite cages and a large part of the active phase is located outside the zeolite particles.

Differently from sulfides, phosphides do not have a layered structure and adopt a spherical morphology as evident from the TEM micrographs (Fig. 4.4), and their size range and uniformity indicates that they are situated in the mesopores for loading levels of 1.0 and 1.5. The acidity of the support was adjusted by controlling the potassium ion concentration. Potassium is known as an effective cation to neutralize the strong acid sites of zeolites [21]. As can be seen in Table 4.9, the USY supports retained the porosity after the ion-exchange treatments. The pyridine TPD analysis (Fig. 4.9) demonstrates that potassium ion-exchange effectively poisons acid sites, especially the stronger ones.

The catalytic performance was strongly affected by the potassium content. The Ni_2P/USY sample showed a high HDS conversion of around 95 % but gave rise to 5.6 % cracking of the tridecane solvent (Fig. 4.10). For Ni_2P/KHUSY the HDS conversion was also high and stable at around 99% and the cracking was considerably reduced. This result is consistent with a previous study of the cracking of heptane on a KUSY catalyst [21], in which a K exchange of only 57 % also led to a substantial decrease in cracking from 37.9 % for HUSY and to 0.9 % for K-ion exchanged USY. These results imply that the residual acidic sites on KHUSY are possibly located in the crystal (i.e. supercage) sites where the solvent molecules of tridecane may not be reached.

The catalytic activities of Ni_2P/KHUSY and Ni-Mo-S/Al_2O_3 samples were compared with various feed compositions (Fig. 4.11) to examine the effect of S (as DMDS) and N (as quinoline) compounds on the HDS of 4,6-DMDBT. For Ni-Mo-S/Al_2O_3 the activity was low with HDS conversion of 70-80 % and the addition of the N-compound (0.05 % N) led to a decrease by 14 % in the HDS conversion, with the HYD selectivity being slightly lowered. Like the case of Ni_2P/KUSY catalyst the Ni_2P/KHUSY catalyst showed high and stable activity with HDS conversion of 99 % favoring the hydrogenation pathway with 90 % HYD selectivity, and exhibited resistance toward S and N compounds. The inhibition by N-compounds of the HYD pathway of 4,6-DMDBT over Ni-Mo-S/Al_2O_3 catalyst is well known and can be exacerbated at a low temperature (~ 613 K) because of the adsorption equilibrium [22]. The study of the HDS of 4,6-DMDBT on a Ni-Mo-S/Al_2O_3 catalyst at 613 K and 3.1 MPa also revealed that the HDS conversion was affected significantly by the addition of a N-compound leading to a decrease in HDS conversion by 33 % as reported in Chapter 2.

4.5. Conclusions

A series of Ni_2P catalysts supported on potassium ion exchanged USY zeolites were prepared by temperature programmed reaction with different Ni_2P loading levels and Ni/P ratios.

The different loading of Ni_2P in the catalyst led to changes in the catalyst dispersion, interaction between Ni-P and Ni-Ni bonds of Ni_2P, and its activity. The particle size was increased with loading level with sizes in the ranges of 1-4, 10-15, and over 20 nm for

loading levels of 12, 17, and 22 wt% Ni_2P, respectively. The particles were invisible for the Ni_2P/KUSY sample with a loading level of 0.5 (6 % Ni_2P), which showed low HDS activity due to the lack of Ni_2P phase. Ni_2P/KUSY samples with loading levels of 12 and 17 wt % Ni_2P showed high and stable HDS conversion of 95-99 %, which were related to the high dispersion and stronger Ni-P interaction in the of Ni_2P particles, while the higher loading of 34 wt % Ni_2P on KUSY led to lower activity due to its poor dispersion.

The P content in the catalyst had a significant effect on the catalyst structure and its activity. Use of a stoichiometric amount of P in the preparation of Ni_2P on KUSY (i.e. initial Ni/P ratio = 1/0.5) resulted in a low catalytic activity below 40 % HDS conversion, which was likely due to the formation of a P deficient Ni_2P phase after reduction. Use of an excess P in the preparation of Ni_2P on KUSY (i.e. initial Ni/P ratio = 1/2) led to a high and stable HDS conversion of 99 %, which was likely due to the enhanced dispersion and strong interaction between Ni and P species in the Ni_2P, as indicated by the CO chemisorption results and the EXAFS analysis. The present study also showed that K-ion exchange reduced cracking.

References

1. P. Dufresne, A. Quesada, and S. Mignard, Stud. Surf. Sci. Catal. 53 (1990) 301.
2. J. Leglise, J. M. Manoli, C. Potvin, G. Djega-Mariadassou, and D. Cornet, J. Catal. 152 (1995) 275.
3. R. Cid, J. Neira, J. Godoy, J. M. Palacios, and A. L´ opez Agudo, Appl. Catal. A. 125 (1995) 169.
4. W. J. J. Welters, G. Vorbeck, H. W. Zandbergen, J. W. de Haan, V. H. J. de Beer, and R. A. van Santen, J. Catal. 150 (1994) 155.
5. W. R. A. M. Robinson, J. N. M. van Gastel, T. I. Korányi, S. Eijsbouts, J. A. R. van Veen, V. H., and J. de Beer, J. Catal. 161 (1996) 539.
6. W. Li, B. Dhandapani, and S. T. Oyama, Chem. Lett. (1998) 207.
7 . D. C. Phillips, S. J. Sawhill, R. Self, and M. E. Bussell, J. Catal. 207 (2002) 266.
8. S. T. Oyama, J. Catal. 216 (2003) 343.
9. P. T. Tanev, and L. T. Vlaev, J. Colloid Interface Sci., 160, 110 (1993).
10. A. H. Janssen, A. J. Koster, and K. P. de Jong, J. Phys. Chem. B 106 (2002) 11905.
11. S. Rundqvist, Acta Chem. Scand., 16 (1962) 992.
12. J. M. Thomas, Angew. Chem. 111 (1999) 3800.
13. C. C. Freyhardt, M. Tsapatsis, R. F. Lobo, K. Balkus Jr, and M. E. Davis, Nature, 295 (1996) 295.
14. A. Corma, V. Fornes, S. B. Pergher, Th. L. M. Maesen, and J. G. Buglass, Nature, 396 (1998) 353.
15. A. H. Janssen, A. J. Koster, and K. P. de Jong, Angew. Chem. Int. Ed. 40 (2001) 1102.
16. B. C. Gates and H. Topsøe, Polyhedron 16 (1997) 3213.

17. M. Houalla, D. H. Broderick, A.V. Sapre, N. K. Nag, V. H. J. de Beer, B. C. Gates, and H. Kwart, J. Catal. 21 (1980) 523.

18. X. Ma, K. Sakanishi and I. Mochida, Ind. Eng. Chem. Res. 33 (1994) 218.

19. S. T. Oyama, X. Wang, .Y.-K. Lee Bando, and F. G. Requejo, J. Catal. 210 (2002) 207.

20. S. T. Oyama, X. Wang, Y.-K. Lee, and W.-J. Chun, J. Catal. 221 (2004) 263.

21. R. Kumar, W. C. Cheng, K. Rajagopalan, A.W. Peters, and P. Basu, J. Catal. 143 (1993) 594.

22. M. Egorova and R. Prins, J. Catal. 225 (2004) 417.

Chapter 5

Mechanism of Hydrodenitrogenation on Phosphides and Sulfides

5.1. Introduction

The previous chapters presented results on the preparation of highly dispersed nickel phosphide catalysts, which exhibited high activities in hydrotreating reactions. However, little is known about the mechanism for the hydrodenitrogenation (HDN) on the nickel phosphide catalyst, and this is the topic of this chapter. This subject is of great importance because nitrogen compounds strongly inhibit hydrodesulfurization (HDS) (1), and so their removal is key for obtaining ultra-low sulfur products.

Hydrodenitrogenation (HDN) of compounds in oil fractions is more difficult than hydrodesulfurization, requiring more severe conditions and greater hydrogen consumption (2). In most cases the preferred pathway for the HDN of heterocyclic molecules involves hydrogenation of aromatic rings associated with nitrogen atoms because it is easier to break C(sp^3)-N bonds than C(sp^2)-N bonds. Thus, quinoline undergoes complete hydrogenation of its heterocyclic and benzenic rings before removal of nitrogen (3,4,5), indole is hydrogenated to octahydroindoline (6) and pyridine is hydrogenated to piperidine (7,8,9). For this reason saturated compounds such as piperidine and its derivatives have been the subject of considerable study (10). The work is described in a comprehensive discussion of the mechanism of piperidine HDN by Hadjiloizou, et al. (11), an in-depth review of catalytic denitrogenation by Perot (12), and a more recent, insightful monograph by Prins (13). In

many cases for sulfides (14), carbides (15), and nitrides (16), the C-N bond cleavage proceeds by a β-elimination mechanism catalyzed by a Brønsted acid - Lewis base site (17,18). Although there is some uncertainty about the rate-limiting step (14,15,19), there is agreement that HDN involves a multi-functional mechanism with hydrogenation and C-N bond cleavage carried out on different active sites (20,21,22,23) depending on the structure of the nitrogen containing heterocyclic compound, the reaction conditions, and the type of catalyst.

In this work, the mechanism on Ni_2P/SiO_2-L and Ni-Mo-S/Al_2O_3 was studied using 2-methylpiperidine, which has been shown to be a good probe molecule for HDN (24). Infrared studies at reaction conditions allowed the determination of the structure of the reaction intermediate, a piperidinium species, and the likely mechanism of reaction. The HDN mechanism on Ni_2P/SiO_2-L was also probed using piperidine and several of its derivatives to determine the effect of amine structure on reactivity, and hence, reaction pathway. Piperidine, $C_5H_{10}N$, is a saturated cyclic secondary amine obtained by the hydrogenation of pyridine. The HDN of piperidine involves the cleavage of two C-N bonds and its conversion is representative of the reaction of other cyclic nitrogen compounds. The work is important because there are many pyridine derivatives in petroleum and their HDN pathway involves hydrogenation to piperidine intermediates. It was found that the results could be explained by either a dual mechanism involving an S_N2 pathway for piperidines with little substitution around the N atom and an E2 pathway for sterically hindered piperidines.

5.2. Experimental

5.2.1. Materials

The support used in this study was a fumed silica (Cabosil, L90). The catalyst precursors were nickel nitrate, $Ni(NO_3)_2 \cdot 6H_2O$ (Aesar, 99 %) and ammonium orthophosphate $(NH_4)_2HPO_4$ (Aldrich, 99 %). The chemicals utilized in the study of the mechanism were dibenzothiophene (Aldrich, 99.5 %), quinoline (Aldrich, 99.9 %), benzofuran (Aldrich, 99.9 %), tetralin (Aldrich, 99.5 %), tetradecane (Jansen Chimica, 99 %), piperidine (Aldrich, 99.9 %), 2-methyl piperidine (Aldrich, 99.9 %), 3-methyl piperidine (Aldrich, 99.9 %), 4-methyl piperidine (Aldrich, 99.9 %), 2,6-dimethyl piperidine (Aldrich, 99.9 %), octane (Acros, 99%), dimethyl disulfide (Aldrich, 99 %), and ethylamine (Aldrich, 97 %). The chemicals used as gas chromatography reference samples were 1,4-pentadiene (Aldrich, 99.9 %), pentane (Aldrich, 99.9 %), 1-pentene (Aldrich, 99.9 %), 3-methyl-1,4-pentadiene (Aldrich, 99.9 %), 4-methyl-1-pentene (Aldrich, 99.9 %), 3-methyl-1-pentene (Aldrich, 99.9 %), 2-methyl-1-pentane (Aldrich, 99.9 %), hexane (Aldrich, 99.9 %), 3-methyl-1-pentane (Aldrich, 99.9 %), 2-methyl-1-pentene (Aldrich, 99.9 %), 1-hexene (Aldrich, 99.9 %), trans-2-hexene (Aldrich, 99.9 %), 1,4-hexadiene (Aldrich, 99.9 %), 3-methyl-1,3-pentadiene (Aldrich, 99.9 %), trans-2-heptene (Aldrich, 99.9 %), heptane (Aldrich, 99.9 %), pyridine (Aldrich, 99.9 %), 2-picoline (Aldrich, 99.9 %), 3-picoline (Aldrich, 99.9 %), 4-picoline (Aldrich, 99.9 %), 2,6 –lutidine (Aldrich, 99.9 %),1-aminohexane (Aldrich, 99%), 2-aminohexane (Fluka, 97%), and 2-methylpyridine (2-picoline, Aldrich, 98%). The compound 2-methyl-3,4,5,6-tetrahydropyridine was not available commercially, and was identified because of its close retention time to 2-

methylpyridine, based on the work of Egorova, et al. (24). The gases employed were He (Airco, Grade 5), CO (Linde Research Grade, 99.97 %), 0.5 % O_2/He (Airco, UHP Grade), H_2 (Airco, Grade 5), N_2 (Airco, 99.99 %), 10 % (v/v) H_2S/H_2 (Air Products, 99.999 %) and 30 % N_2/He (Airco, UHP Grade).

5.2.2. Catalyst Samples

The phosphide catalyst used in this study was the same nickel phosphide supported on silica, Ni_2P/SiO_2-L used in Chapter 2, prepared with excess phosphorus (Ni/P=1/2) and a loading of 1.16 mmol Ni / g support (12.2 wt.% Ni_2P/SiO_2-L). The synthesis of the catalyst involved two steps and was described in the previous chapters. Briefly, in the first step, a supported nickel phosphate precursor was prepared by incipient wetness impregnation of a solution of nickel and phosphorus components, followed by calcination. In the second step, the phosphate was reduced to a phosphide by the method of temperature-programmed reduction (TPR). A reference Ni_2P/SiO_2-L with lower initial P content (Ni/P = 1/0.5) was prepared in a similar manner. The same commercial Ni-Mo-S/Al_2O_3 sample (Criterion 424) was used and a reference PO_x/SiO_2-L sample was prepared by impregnation of SiO_2-L with $(NH_4)_2HPO_4$ (6.6 wt% P) followed by calcination at 673 K.

5.2.3. Characterization

The synthesized phosphide material was characterized by CO chemisorption, N_2 physisorption, and x-ray diffraction (XRD) measurements.

Infrared spectra of 2-methylpiperidine adsorbed on the Ni_2P/SiO_2-L, Ni-Mo-S/Al_2O_3 and blank SiO_2-L were collected using a Fourier transform infrared spectrometer (Bio-Rad Model FTS 3000MX) equipped with a heatable transmission cell with water-cooled KBr windows. The samples were pressed into self-supporting wafers with a diameter of 20 mm and a weight of 13 mg. IR spectra were collected in absorbance mode at a resolution of 2 cm^{-1} and 64 scans in the region 4000 – 400 cm^{-1}. Studies of the effect of temperature were performed on these samples to determine the identity and stability of the adsorbed species on the catalyst surface. Background FTIR spectra on SiO_2-L, PO_x/SiO_2-L, and Ni_2P/SiO_2-L were obtained in He at various temperature. In situ FTIR measurements on Ni_2P/SiO_2-L and Ni-Mo-S/Al_2O_3 were made in a gas mixture of H_2S and H_2 at conditions of reaction (sulfur concentration of 3000 ppm) in order to simulate the chemical environment in which the reactivity and mechanism tests were performed. The Ni_2P/SiO_2-L samples were pretreated in a H_2 flow at 723 K for 2 h and the Ni-Mo-S/Al_2O_3 in 10 % H_2S/H_2 for 2 h in the same manner as before the CO chemisorption and reactivity measurements.

For the measurements of 2-methylpiperidine the samples were dosed at 373 K with a molar concentration of the piperidine of 0.51 % in He or H_2 carrier at a flow rate of 100 μmol s^{-1} (150 cm^3/min) until saturation was achieved. The samples were then purged in He carrier for 300 s at 373 K to remove gaseous and weakly adsorbed 2-methylpiperidine. The spectra are shown after substraction of the background spectrum obtained at the various temperatures without 2-methylpiperidine to make the adsorbate peaks more clear. Measurements were made at 373, 423, 473, 523 and 573 K in step programming mode using a heating rate of 0.17 K s^{-1} (10 K/min) and a hold time of 180 s at each temperature.

5.2.4. Reactivity Studies

The reactivity of 2-methylpiperidine was measured at 603 K and 3.1 MPa in a three-phase packed-bed reactor with a feed liquid containing 2000 ppm wt. nitrogen, 3000 ppm wt. sulfur (dimethyl disulfide), 1wt% wt. internal standard (nonane), and balance aliphatics (tetradecane). The detailed description of the testing system is reported elsewhere in Chapter 2. Samples were collected in sealed septum vials every 2 or 3 hours during daytime and were analyzed off-line with a gas chromatograph (Hewlett Packard, 5890A) equipped with a 0.32 mm i.d. x 50 m fused silica capillary column (CPSIL-5CB, Chrompack, Inc.) and a flame ionization detector. Reaction products were identified by matching retention times to standards injected separately. The peak areas were calibrated with the same method described elsewhere (15). Flow rates and quantities of catalysts were varied to obtain a wide range of contact times. Catalyst amounts ranged from 0.01 g to 0.79 g for the Ni_2P/SiO_2-L catalyst and 0.010 to 0.34 g for the Ni-Mo-S/Al_2O_3 catalyst. Prior to reactivity measurements, the catalyst samples were pretreated in exactly the same manner as before the chemisorption measurements. Different liquid flow rates (5-20 cm^3/h) and catalyst amounts (10-200 mg) were used to obtain site-times from 0.15 to 10 μmol h g^{-1}. The site time is a measure of contact time (normalized to chemisorption sites to permit comparison between catalysts), and was obtained from the following formula.

$$\text{Site time} = \left[\frac{\text{liquid flow rate (ml/h)} \cdot \text{apparent density (g/ml)}}{\text{catalyst weight (g)} \cdot \text{chemisorption uptake } (\mu\text{mol/g})} \right]^{-1}$$

where the apparent density of the Ni_2P/SiO_2-L catalyst was (0.34 g/cm^3) and that of the Ni-Mo-S/Al_2O_3 was (0.61 g/cm^3). The same volume (7.0 cm^3) of catalyst sample diluted with glass beads was loaded.

For the measurements of piperidine and its derivatives the system was operated at 3.1 MPa and various temperatures with an inlet liquid flow rate of 5 cm^3/h and a hydrogen flow rate of 100 μmol s^{-1} (150 cm^3 NTP min^{-1}), with 3000 wppm S as dimethyldisulfide and levels of piperidine corresponding to 2000 wppm N. Quantities of catalysts loaded in the reactor corresponded to the same amount of *ex situ* CO or atomic oxygen uptake (70 μmol), and were 2.50 g for the Ni_2P/SiO_2-L catalyst and 0.73 g for the Ni-Mo-S/Al_2O_3 catalyst. The experiments were long (~ 300 h), for each change in temperature, the reaction system was allowed to run for 48 h to establish steady-state. The results of several measurements were averaged. After several changes of operating conditions, the reactivity of the catalyst was tested at a previous condition to verify that no deactivation occurred. Analytical results were obtained by gas chromatography. Although not all products were identified, sufficient standards were available to identify the main component types and to obtain total and HDN conversions.

5.3. Results

5.3.1. Properties of the catalyst

The XRD patterns of the fresh Ni_2P/SiO_2-L and a typical used sample together with the reference patterns of SiO_2-L, bulk Ni_2P, and a powder diffraction file standard (Ni_2P, PDF 3-953), are shown in Figure 5.1.

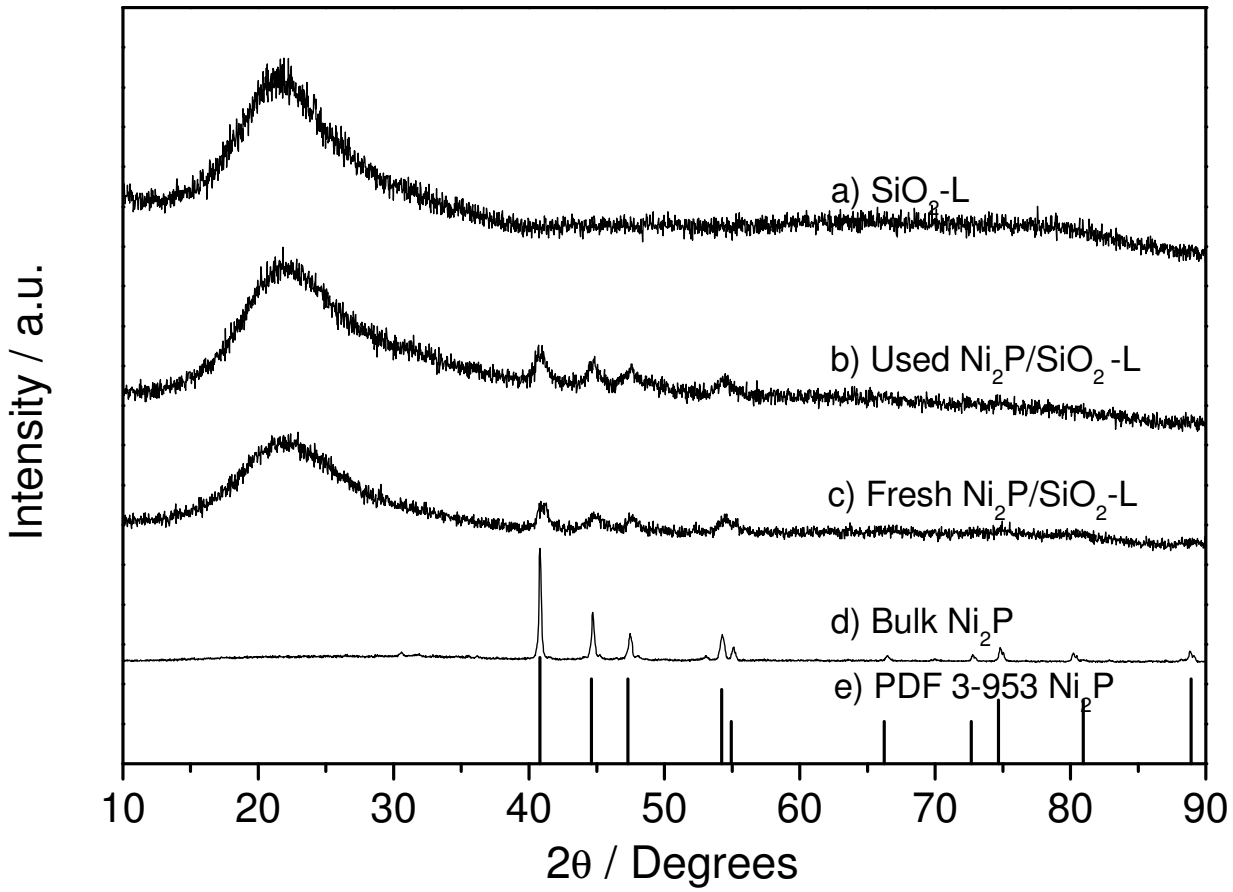

Figure 5.1. XRD patterns of the fresh and used Ni_2P/SiO_2-L.

Table 5.1 Characteristics of the catalysts

Sample	Surface area $m^2\ g^{-1}$	CO or O_2 uptake $\mu mol\ g^{-1}$
Ni_2P/SiO_2-L (fresh)	97	28
Ni_2P/SiO_2-L (used)	89	24
Ni-Mo-S/Al_2O_3	160	95

The figure reveals that the fresh sample consisted of amorphous silica and finely dispersed Ni_2P (25) with a hexagonal structure (Space group: $P_{\bar{6}2m}$, D^2_{3h}, Struckturbericht notation: revised C22) with lattice parameters, a = b = 0.5859 nm, c = 0.3382 nm. Table 5.1 summarizes the surface area and chemisorption values for the fresh and used phosphide catalysts and the fresh sulfide catalysts. There was little change in the phosphide catalysts due to reaction, consistent with the stable behavior observed in the reactivity runs.

5.3.2. Reactivity studies

The results of the 2-methylpiperidine reactivity measurements on the Ni_2P/SiO_2-L catalyst are shown in Figure 5.2. The left panel shows the relative concentrations of the 2-methylpiperidine and the various products as a function of site-time. The right panel shows the selectivity to the various products also as a function of the site-time. The major initial products are 2-aminohexane, 2-methyl-3,4,5,6-tetrahydropyridine, and 2-methylpyridine but their selectivity declines with time, with that of 2-aminohexane diminishing very rapidly. The main final products are 2-hexene and n-hexane, whose selectivity increase with time. The principal isomer obtained was the trans-2-hexene (~80 %). A lesser initial product is 1-amino hexane, which also rises sharply initially, but then declines rapidly in time. The product 1-hexene also appears initially, but its selectivity then dips slightly and then recovers. The selectivity at a site-time of 0.13 μmol h/g for 2-aminohexane was 33% while that for 1-aminohexane was 10%.

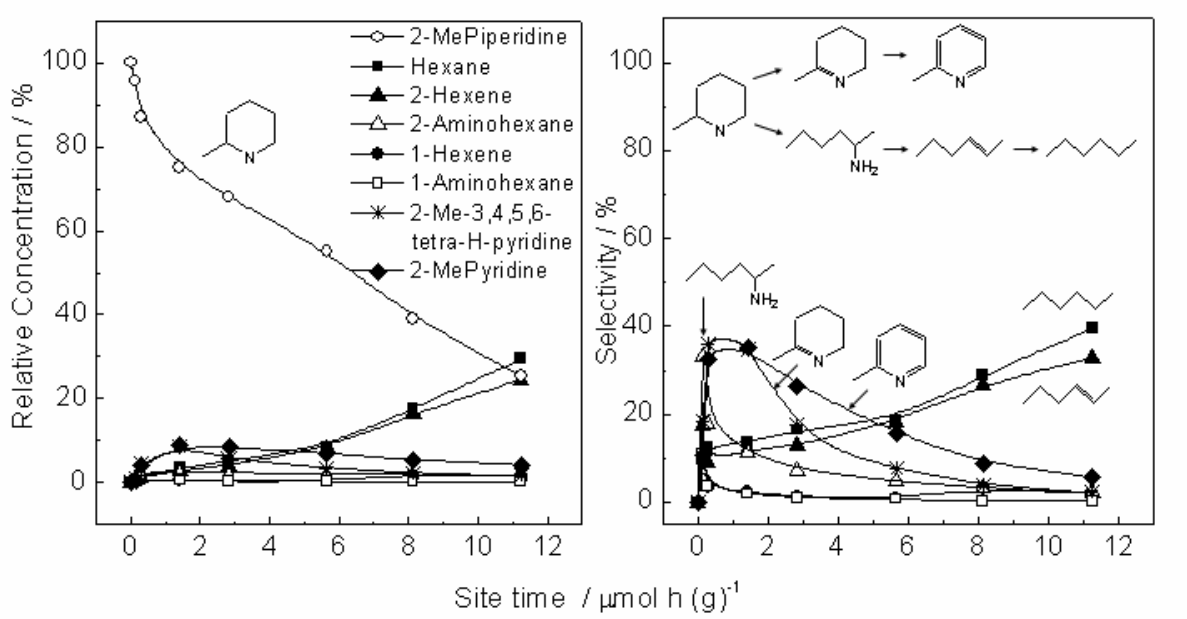

Figure 5.2. Relative concentrations and selectivity to products in the HDN of 2-methylpiperidine on Ni_2P/SiO_2-L.

The results of the 2-methylpiperidine reactivity measurements on the Ni-Mo-S/Al_2O_3 catalyst are shown in Figure 5.3. The left panel again shows the relative concentrations of the 2-methylpiperidine reactant and the various products as a function of site-time. The right panel similarly shows the selectivity to the various products as a function of site-time. Again, the major initial products are 2-aminohexane, 2-methyl-3,4,5,6-tetrahydro-pyridine, and 2-methylpyridine but they decline at increasing site-times, again 2-aminohexane very rapidly. The major product this time is hexane. The product 2-hexene also increases with site-time, but then decreases at longer times. A lesser initial product is 1-aminohexane, whose concentration is highest at the shortest site-time, but then declines rapidly. The product 1-hexene also appears early, but then declines. The selectivity at a site-time of 0.14 µmol h/g for 2-aminohexane was 38% while that for 1-aminohexane was 12%.

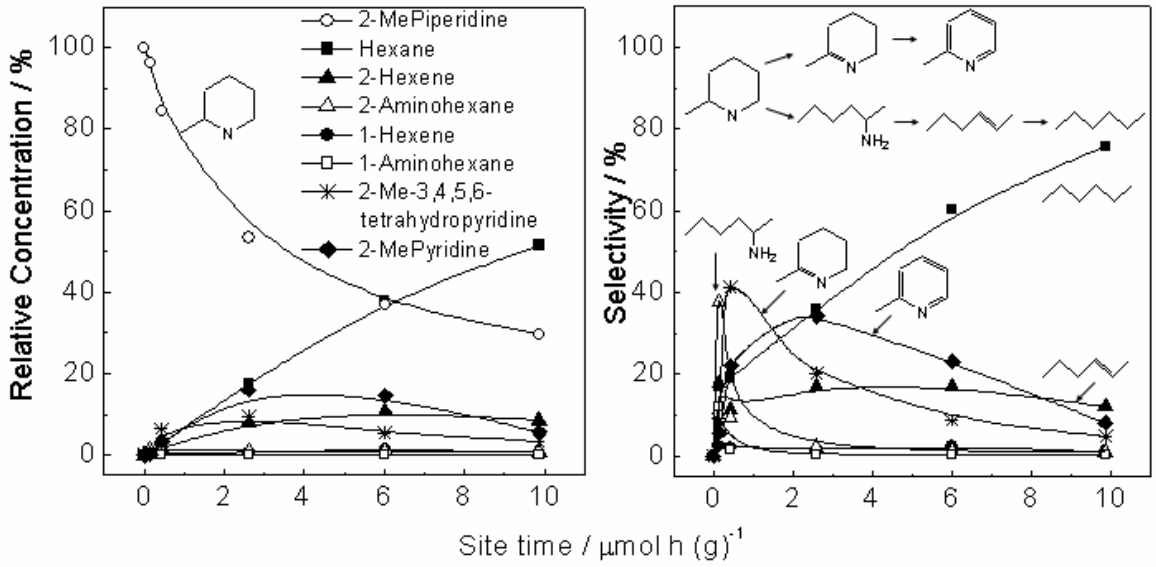

Figure 5.3. Relative concentrations and selectivity to products in the HDN of 2-methylpiperidine on Ni-Mo-S/Al_2O_3.

The results of the studies on Ni_2P/SiO_2-L of piperidine and its derivatives are presented in Figures 5.4 and 5. Figure 5.4 shows the total conversion of the piperidines, which included condensation, aromatization, and HDN reactions as a function of temperature. The figure shows that the conversion sequence followed the order: 4-methylpiperidine ~ piperidine > 2,6-dimethylpiperidine > 3-methylpiperidine > 2-methylpiperidine. Figure 5.5 shows the pure HDN conversion, which followed a similar sequence, except that 3-methylpiperidine had higher conversions than 2,6-dimethylpiperidine.

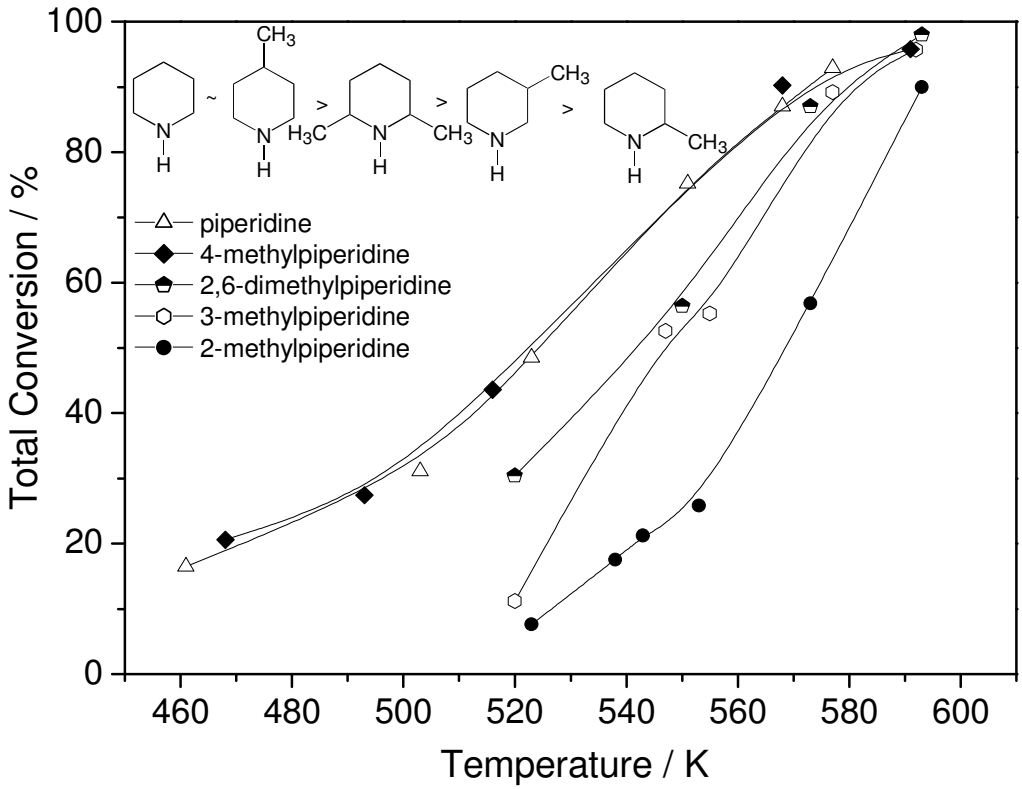

Figure 5.4. Total conversion of piperidines [adapted from ref.26].

The selectivity and product distribution for each molecule are not presented since all the products could not be identified. However, estimates of the type and quantity of the products were made using available references, and reasonable mass balances were obtained (100 ± 5 %). The selectivity to the HDN products increased with temperature, as expected from thermodynamic equilibrium considerations, as condensation products are not favored at higher temperature (15). The selectivity to the main hydrocarbon products also increased with temperature, as expected from the occurrence of sequential hydrogenation reactions.

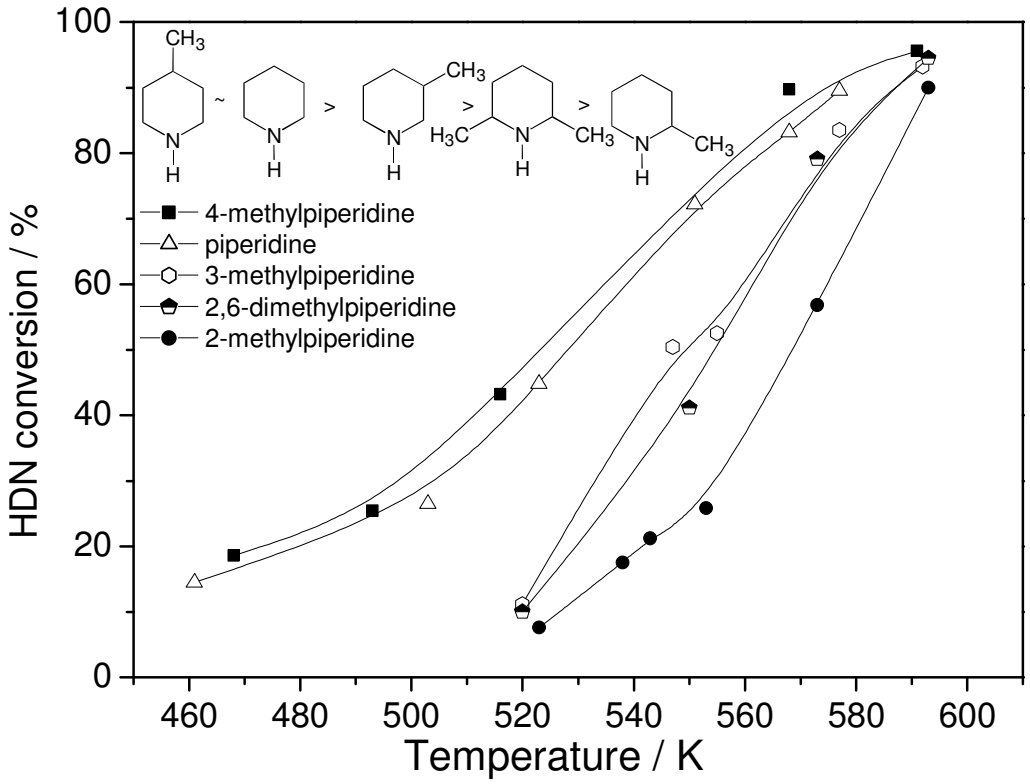

Figure 5.5. HDN conversion of piperidines [adapted from ref.26].

5.3.3. Infrared measurements

Figure 5.6 shows the FTIR spectra of 2-methylpiperidine adsorbed on the blank SiO_2-L support under He flow. The main spectral features at temperatures lower than 423 K were found at 3742, 3298, 2942, 2865, 2804, 2734, 2610, and 1452 cm^{-1}. The IR peak at 3742 cm^{-1} corresponds to a hydroxyl band of SiO_2-L (27) and appears as a negative feature. In this figure, as well as others to be presented, a decrease in intensity of a negative band indicates growth of the peak. Thus, as the temperature is raised from 373 K to 573 K, the

concentration of the hydroxyl band is actually increasing, even though the intensity is decreasing. The opposite applies to positive peaks. As can be seen, the intensity of all features decreases rapidly as the temperature is increased up to 473 K.

Figure 5.7 shows the FTIR spectra of 2-methylpiperidine adsorbed on the Ni_2P/SiO_2-L catalyst under He. The main spectral features appear at 3742, 3670, 3247, 2983, 2949, 2807, 2738, 1016, and 1454 cm^{-1}. The peaks are similar to those obtained on SiO_2-L, but with important differences. There are now two negative peaks at high wavenumber, the band at around 3247 appears as a shoulder on a rising background, the main features between 3000-2600 cm^{-1} are shifted to higher wavenumber, and there is a large new feature at 1016 cm^{-1}.

Figure 5.8 shows the hydroxyl region for 2-methylpiperidine adsorbed on SiO_2-L, two Ni_2P/SiO_2-L catalysts with different P content, and PO_x/SiO_2-L. The major O-H stretching band appears at 3741-3744 cm^{-1} on all samples. A second O-H band appears at 3668 cm^{-1} for the Ni_2P/SiO_2-L samples and at 3660 cm^{-1} for the PO_x/SiO_2-L sample.

Figure 5.9 shows the in situ spectra of 2-methylpiperidine on Ni_2P/SiO_2-L at reaction conditions in a carrier gas of 3000 ppm H_2S/H_2. The spectra are identical to those obtained with a He carrier (Fig. 5.7). Major features are two negative peaks at 3742 and 3670 cm^{-1}, a shoulder at 3247 cm^{-1}, and peaks at 2983, 2949, 2867, 2803, 2732, 1616, and 1456 cm^{-1}.

Figure 5.10 shows the corresponding in situ spectra of 2-methylpiperidine on Ni-Mo-S/Al_2O_3 at reaction conditions, also taken in a carrier gas of 3000 ppm H_2S/H_2. In this case a single negative peak is observed at 3675 cm^{-1}, and peaks similar to those obtained on the Ni_2P/SiO_2-L, but slightly displaced in position. The shoulder appears at 3206 cm^{-1}, and the major peaks at 2978, 2947, 2866, 2800, 2732, 1598, and 1455 cm^{-1}.

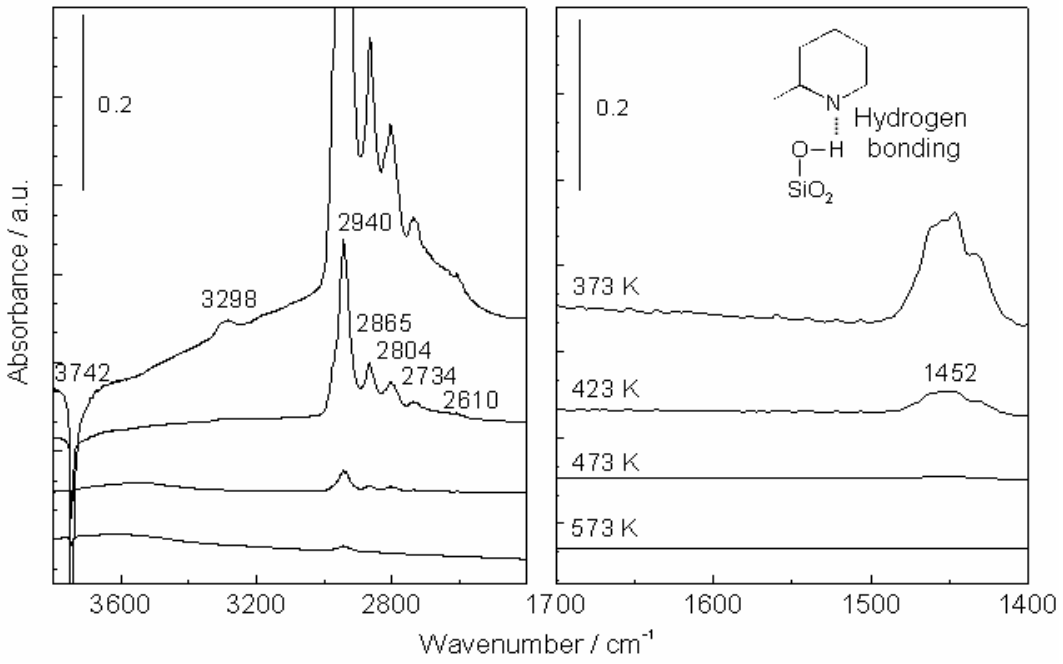

Figure 5.6. FTIR spectra of 2-methylpiperidine adsorbed on SiO_2-L in a He atmosphere as a function of temperature.

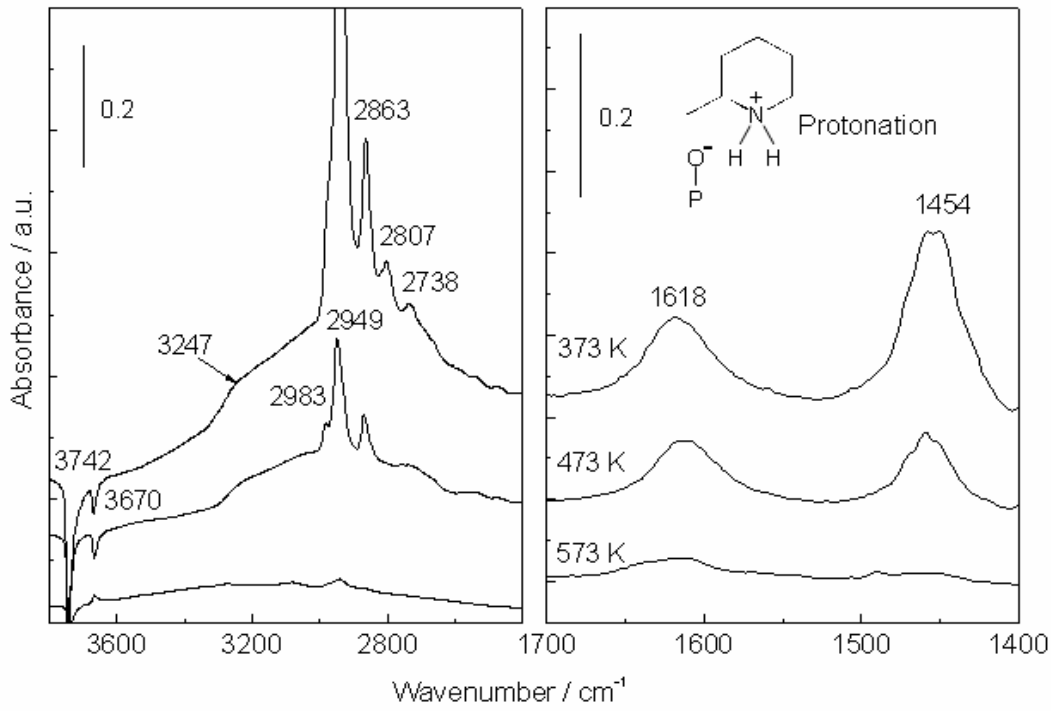

Figure 5.7. FTIR spectra of 2-methylpiperidine adsorbed on Ni_2P/SiO_2-L in a He atmosphere as a function of temperature.

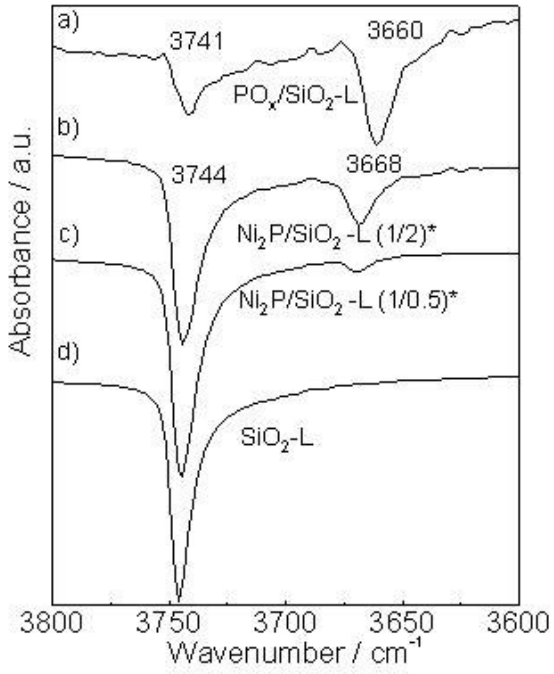

Figure 5.8. FTIR spectra of 2-methylpiperidine adsorbed on a) PO_x/SiO_2-L, b) Ni_2P/SiO_2-L, c) Ni_2P/SiO_2-L and d) SiO_2-L at 373 K in He. *Initial Ni/P ratios in the precursors.

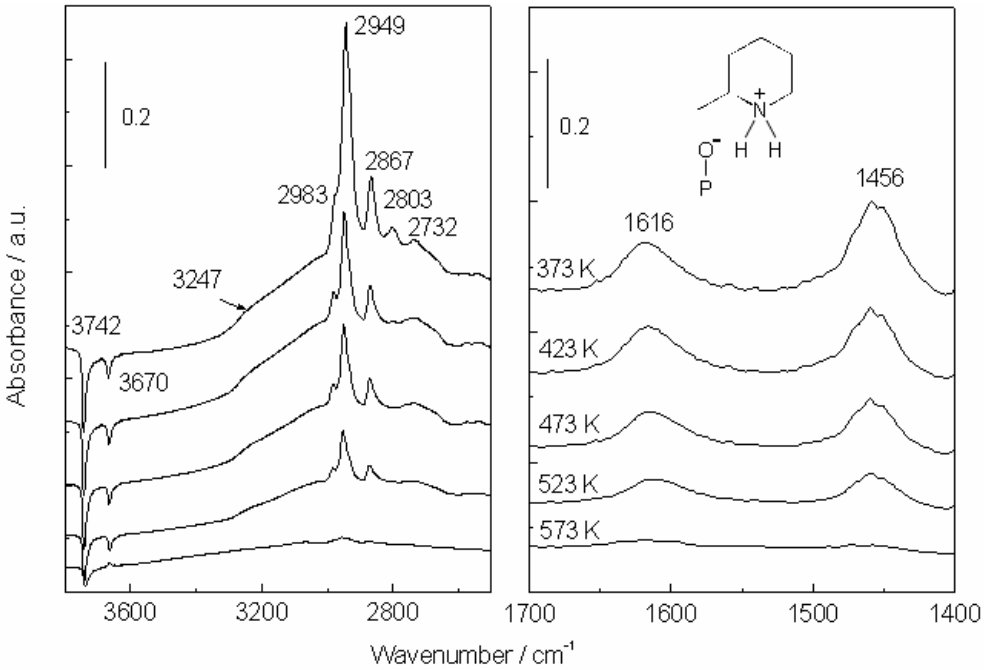

Figure 5.9. FTIR spectra of 2-methylpiperidine adsorbed on Ni_2P/SiO_2-L in a gas mixture of 3000 ppm S (H_2S/H_2) as a function of temperature.

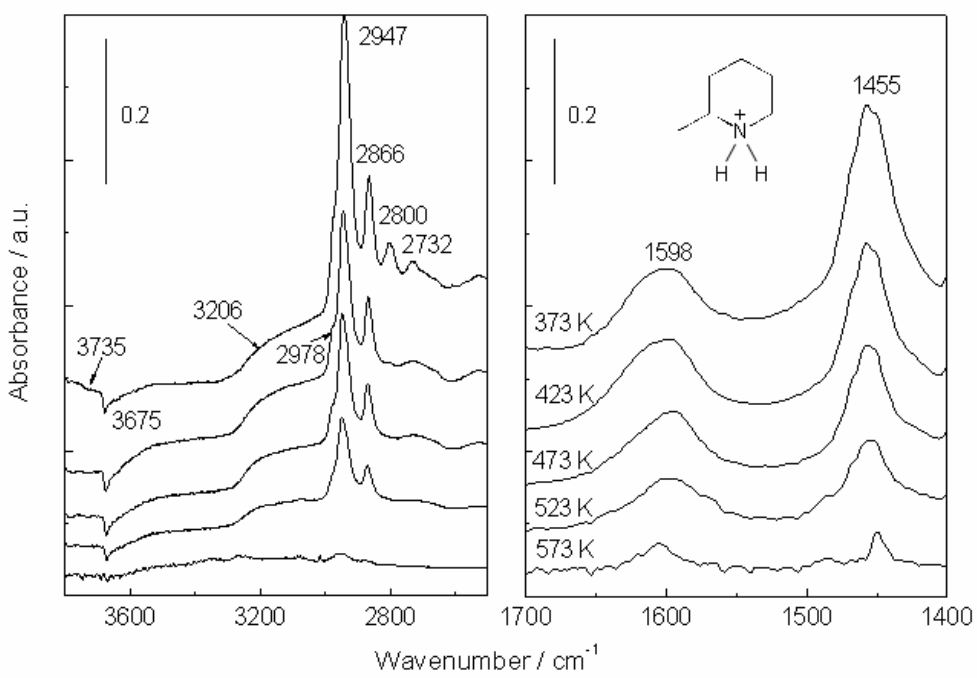

Figure 5.10. FTIR spectra of 2-methylpiperidine adsorbed on Ni-Mo-S/Al_2O_3 in a gas mixture of 3000 ppm S (H_2S/H_2) as a function of temperature.

5.4. Discussion

5.4.1. Review of Reaction Mechanisms for Piperidine Hydrodenitrogenation

HDN is a process which comprises many nitrogen removal reactions and is relatively more difficult than HDS. Generally, the hydrodenitrogenation of heterocyclic nitrogen compounds does not occur directly and is preceeded by the hydrogenation of aromatic nitrogen heterorings, before the hydrogenolysis of C-N bonds (12).

Nelson and Levy (17), Ho (5), Ledoux (28), and Hadjiloizou, et al. (11) describe several mechanisms by which amines can react. In the case of piperidine in the E2 binuclear elimination mechanism the molecule is first protonated to a quarternary ammonium species and subsequently undergoes attack by a base (B^-) on a β-hydrogen atom to form a primary

amine and an olefin functionality (Scheme 5.1). The olefin is subsequently hydrogenated. This mechanism is a generalized form of the Hofmann degradation (exhaustive methylation), which involves pyrolisis of a quarternary ammonium hydroxide to form a tertiary amine and an olefin (29). The elimination occurs with an *anti* configuration between the β-hydrogen atom and the leaving amine group (23).

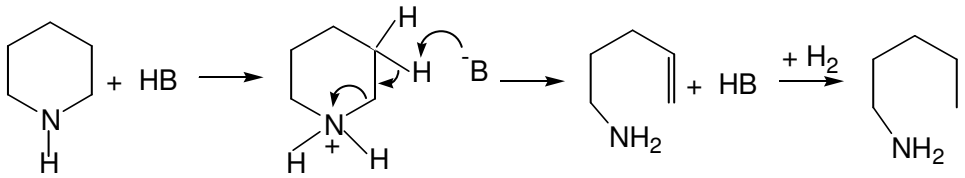

Scheme 5.1. E2 Elimination Mechanism

The direct hydrogenolysis of the C-N bond in alkylamines is unlikely to occur, as the easier C-C bond hydrogenolysis reaction is not observed (13). Also the hydrogenolysis does not explain the positive effect of H_2S that has been reported in a number of HDN studies, notably by the group of Satterfield (3,30,31), but also by others (4,8,10,32). Instead, the primary amine reacts further by either another E2 elimination or, more likely, through a displacement reaction by a sulfhydryl species (Scheme 5.2). The resulting thiol does undergo a facile hydrogenolysis reaction because of the weakness of the C-S bond (13).

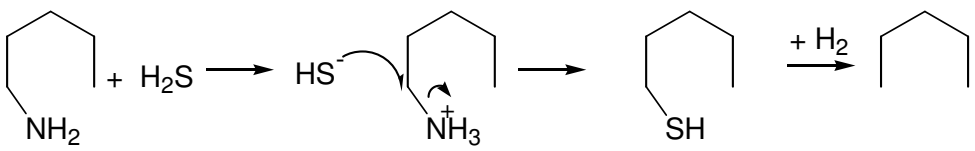

Scheme 5.2. Amine Displacement Mechanism

Piperidine can also react by a substitution mechanism in which attack by a nucleophile occurs on the α-carbon (Scheme 5.3). This is a binuclear nucleophilic substitution (S_N2) and results in a primary amine and incorporation of the nucleophile. The amine and the nucleophile, usually a sulfhydryl species, are subsequently removed as in Scheme 5.2.

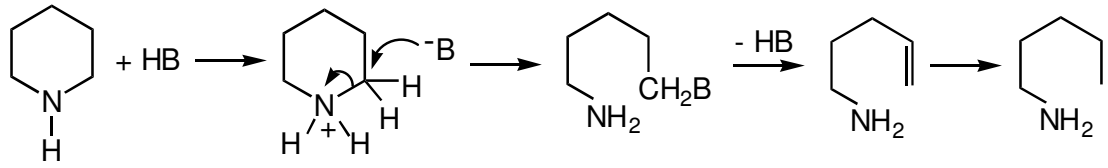

Scheme 5.3. S_N2 Nucleophilic Substitution Mechanism

Other possible pathways for piperidine activation are the mononuclear analogs of Scheme 5.1 and 5.3, namely the E1 and S_N1 reactions (Scheme 5.4). The reactions again start with the protonation of the nitrogen atom, but then the molecule undergoes an internal rearrangement to form a ring-opened carbocation. Loss of a proton produces the E1 product and attack by an external nucleophile (B^-) then produces the S_N1 product. Clearly, formation of the free carbocation intermediate requires a highly substituted α-carbon next to the nitrogen atom.

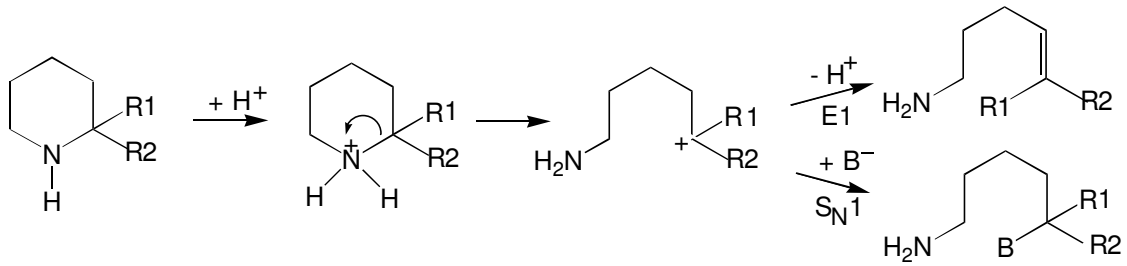

Scheme 5.4. E1 or S_N1 Mechanism

The elimination and substitution mechanisms discussed above require a proton donor, and are of an acid-base type. However, it has been found that pure acidic sites are not able to perform the same kind of HDN chemistry. For example, Fish, et al. (33) reported that a zeolite was inactive for C-N bond cleavage in 1,2,3,4-tetrahydroquinoline and Ledoux and Sedrati (34) found that denitrogenation of piperidine occurred on alumina but only at elevated temperatures (651 K) and resulted in cracking reactions. Similarly Rajagopal, et al. (35) found denitrogenation of piperidine at high temperatures (591 K) on SiO_2-Al_2O_3, but also cracking and condensation products.

An alternative to the elimination and substitution mechanisms was proposed by Laine (36,37,38), who suggested two pathways for piperidine ring opening. The first involved the formation of a cyclic metal alkyl species via a metallaazocyclopropane (aziridinium ring) intermediate (Scheme 5.5). This metal alkyl species can undergo hydrogenation and two reductive eliminations to restore the metal catalyst and produce pentylamine.

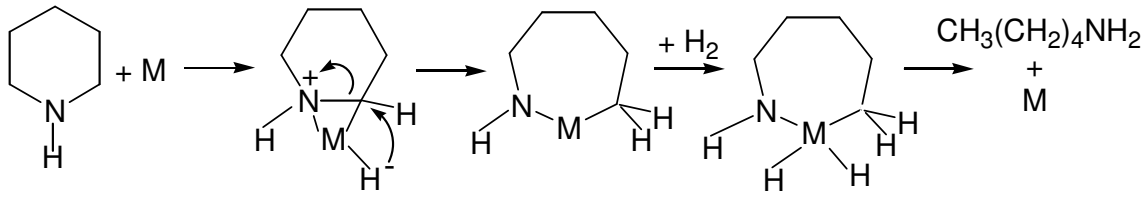

Scheme 5.5. Metallaazocyclopropane Formation Mechanism

The second organometallic pathway involved the formation of a metal carbene species via an iminium complex intermediate (Scheme 5.6). In this scheme and the previous the negative charge is depicted to reside on the hydrogen atom attached to the metal to indicate the hydride nature of the complex.

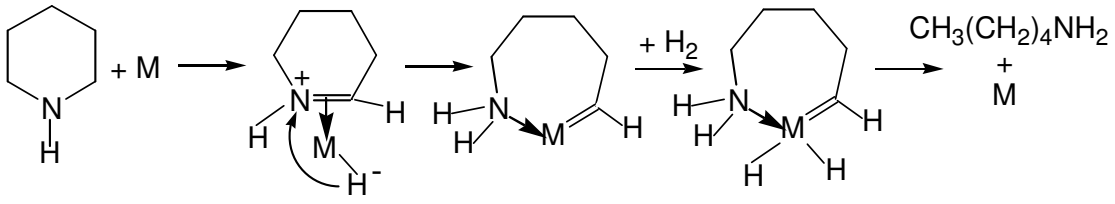

Scheme 5.6. Iminium Ion Complex Formation Mechanism

Mentioned was made earlier of the positive effect of H_2S on the HDN reaction. This was accounted for by Lane through nucleophilic attack on the iminium complex intermediate to form a thiohemiaminal (Scheme 5.7). The ring opened product can readily form the alkane.

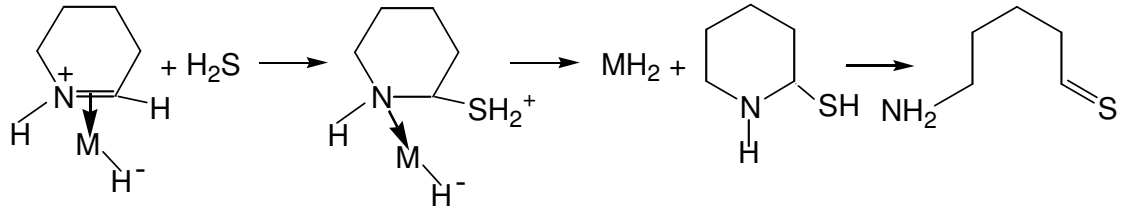

Scheme 5.7. Thiohemiaminal Formation Mechanism

A complication in the study of the mechanism of piperidine HDN is the occurrence of condensation side reactions. For example, Hadjiloizou, et al. (11) found considerable N-containing byproducts using a Co-Mo-S/USY-SiO_2-Al_2O_3 catalyst, although this was partly due to reactions on the highly acidic support. A number of studies report the formation of N-pentylpiperidine (39). Portefaix et al. (40) suggest its formation through an adsorbed activated piperidium complex which undergoes nucleophilic attack by a second piperidine molecule.

The intermediate on the surface that leads to condensation products can also be a Schiff's base complex (Scheme 5.8) (36,41). This can react with a surface olefin intermediate to form 2-*n*-pentylpiperidine.

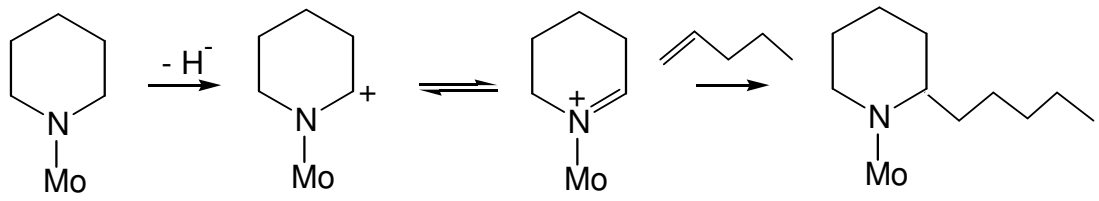

Scheme 5.8. 2-*n*-Pentylpiperidine Formation Mechanism

5.4.2. Mechanism of 2-Methylpiperidine Denitrogenation

The product distributions obtained in the denitrogenation of 2-methylpiperidine on both the Ni_2P/SiO_2-L and Ni-Mo-S/Al_2O_3 catalysts were similar (Figs. 5.2 and 5.3). For both catalysts the major initial product at low site-time was 2-aminohexane and the major ultimate products were 2-hexene and n-hexane. However, in both cases there was also the initial production of 1-aminohexane and 1-hexene. The 1-aminohexene was produced with a selectivity at low site-time of about a third that of the 2-aminohexene on both catalysts. These results can be understood from the reaction network for 2-methylpiperidine reported by Egorova, et al (24).

As can be seen, piperidine can react by either of two pathways. The E2 elimination pathway (Scheme 5.1) results in the formation of a 6-amino-2-hexene, which undergoes hydrogenation to 1-aminohexane. The S_N2 pathway (Scheme 5.3) results in a 5-amino-1-hexene, which undergoes hydrogenation to 2-aminohexane. The aminohexenes are not observed, probably because they remain as surface intermediates and do not desorb prior to

hydrogenation of their double bonds. The finding that the predominant initial product is 2-aminohexane indicates that the S_N2 pathway is the preferred mechanism of HDN on both the Ni_2P/SiO_2-L and Ni-Mo-S/Al_2O_3 catalysts. This is in agreement with the conclusions of Egorova, et al (24) who studied the reaction with an unpromoted Ni-Mo-S/Al_2O_3 at 613 K and 5.0 MPa. The 2-aminohexane subsequently undergoes elimination or substitution and hydrogenation

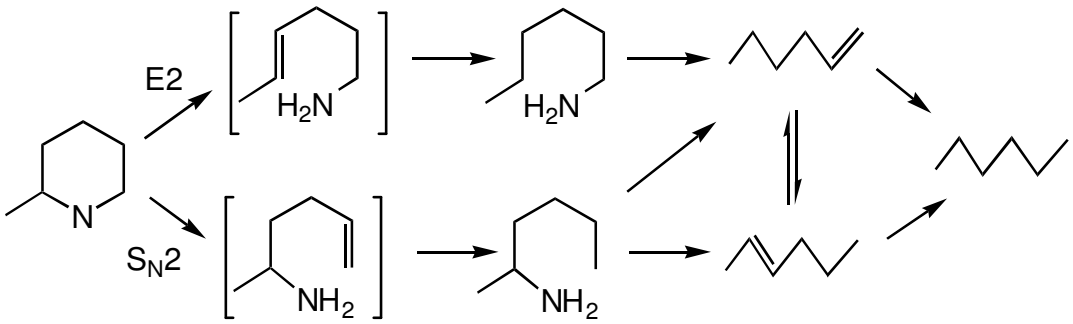

Scheme 5.9. Reaction Network for 2-Methylpiperidine HDN

The olefins that are produced are also intermediate products and their selectivity declines at long site-times in favor of the ultimate product, hexane. The preferred hexane isomer, 2-hexene, is probably produced not only from 2-aminohexane but also from the isomerization of the less-thermodynamically stable 1-hexene. This explains the low selectivity to 1-hexene despite the observation of 1-aminohexane initially in both the Ni_2P/SiO_2-L and Ni-Mo-S/Al_2O_3 catalysts. Overall, for the HDN network both catalysts display very similar behavior, although the sulfide catalyst shows higher hydrogenation activity, with greater production of n-hexane. The results here reproduce the findings of Egorova, et al. (24).

Both the Ni_2P/SiO_2-L and Ni-Mo-S/Al_2O_3 catalysts produce at short site-times substantial amounts of the dehydrogenation products 2-methyl-3,4,5,6-tetrahydropyridine and 2-methylpyridine. The maximum selectivity to the tetrahydropyridine product occurs at a site-time of 0.25 μmol h/g for Ni_2P/SiO_2-L with 36% and at 0.44 μmol h/g for Ni-Mo-S/Al_2O_3 with 41%. The maximum selectivity to the pyridine product occurs at a site-time of 1.42 μmol h/g for Ni_2P/SiO_2-L with 35% and at 2.57 μmol h/g for Ni-Mo-S/Al_2O_3 with 34%. The tetrahydropyridine is probable an intermediate in the route to pyridine, as it appears at lower site-times. These products are probably the result of equilibrium dehydrogenation reactions, and are observed at low site-time when the concentration of the 2-methylpiperidine reactant is high. The relative amounts of the pyridine products produced on the Ni-Mo-S/Al_2O_3 catalyst in this study conducted at 3.0 MPa is higher than those reported by Egorova, et al. (24) carried out at 5.0 MPa because the lower pressure favors dehydrogenation.

5.4.3. Mechanism of Other Piperidine Derivatives

Examination of piperidine derivatives other than 2-methylpiperidine can give insight about the reaction pathway. An attempt was made in this study to do this by comparing the reactivity of the compounds listed in Table 5.2. These compounds have different numbers of α and β hydrogens and could potentially provide further information about the reaction mechanism.

This method was used first by Portefaix, et al. (40), who compared the gas-phase reactivity of several methyl-substituted piperidines. The catalyst employed was a commercial Ni-Mo-S/Al_2O_3 and the reaction conditions were 20 bar and 548 K with 1.3

mol % of the piperidine reactant. It was reported that in the presence of sulfur (1.7 mol %) the rate of formation of HDN products followed the order below (Scheme 5.10):

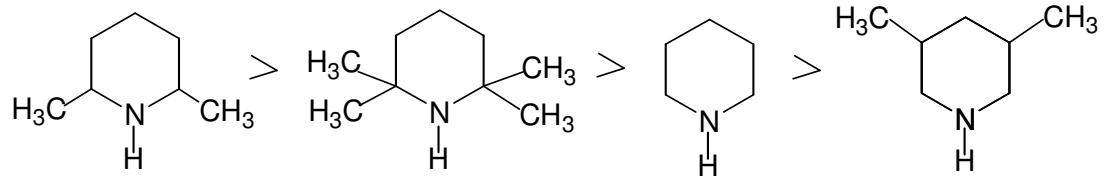

2,6-dimethylpiperidine > 2,2,6,6-tetramethylpiperidine > piperidine > 3,5-dimethylpiperidine

Scheme 5.10. Proposed Reaction Order of Methyl-Substituted Piperidines in Sulfides

In the absence of sulfur the rate of formation of the HDN products was only slightly lower, and the same order was retained. The authors concluded that the reactivity was dominated by the number of β-hydrogen atoms in the reactant amine, and that inductive effects by the electron-donating methyl groups or steric effects were secondary. The authors suggested that HDN proceeded by a nucleophilic attack on a β-hydrogen in an elimination process (Scheme 5.1). The nucleophile could be an S^{2-} or SH^- group on the surface.

Some condensation products were observed, but except for the case of unsubstituted piperidine, these were not identified or quantified. It was qualitatively found that condensation did not correlate with the number of β-hydrogen atoms, and the authors suggested that the reaction could be bimolecular with the amine itself taking the role of the nucleophile.

As discussed earlier, recent results by the group of Prins (24) gave rise to an opposite conclusion. A thorough investigation was carried out of the reaction network of 2-methylpiperidine over a sulfided Ni-Mo/Al_2O_3 catalyst at 613 K and 4.8 MPa H_2 in the presence of 20 kPa H_2S.

Table 5.2 Characteristics of Piperidine Reactants and Reactivity Results at 520 K.

Structures	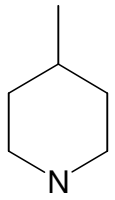	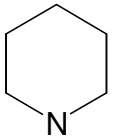	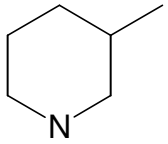	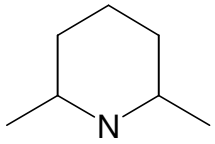	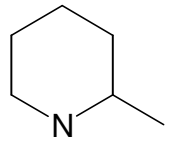
# α-H	4	4	4	2	3
# β-H	4	4	3	10	7
Main Product	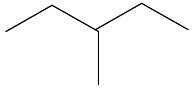	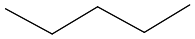	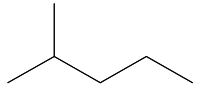	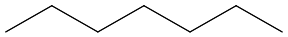	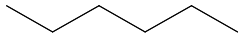
Total conversion	47.9	45.5	11.3	30.6	7.3
HDN conversion	47.0	41.7	11.2	9.9	7.2
Selectivity	98.1	91.6	99.1	32.3	98.6
Mechanism	S_N2-type	S_N2-type	S_N2-type	E2-type	S_N2-type

The main HDN pathway was shown to involve the formation of 2-aminohexane, which proved that the ring opening of 2-methylpiperidine involved the methylene group, not the carbon atom bearing the methyl group. This implied the occurrence of a substitution reaction on the less hindered carbon atom. Repetition of the work by Portefaix, et al. (40) reproduced the reported conversion trend, but analysis of the products revealed that the majority of species were not HDN products, but dehydrogenated and isomerized molecules. Thus, the previous conclusion that the HDN of piperidine derivatives was related to the number of β-H atoms in the molecules was shown to be incorrect.

As discussed in the previous section, our studies on 2-methylpiperidine reproduces the results of Egorova, et al. (24) on a commercial Ni-Mo-S/Al_2O_3, and indicates that the same substitution pathway occurs on Ni_2P/SiO_2-L. The question arises as to whether this holds for the other piperidines. A recent study, also from the group of Prins (42), showed that the substitution reaction was preferred on primary and secondary alkylamines, because the strong C-N bond prevented the direct elimination reaction. Our findings are generally in agreement with this view. The order of reactivity in HDN (Fig. 5.3) follows the sequence: 4-methylpiperidine ~ piperidine > 3-methylpiperidine > 2-methylpiperidine. This sequence follows the order of increasing substitution in the carbons next to the N atom, and is consistent with the occurrence of a nucleophilic attack (Scheme 5.3), which is susceptible to steric hindrance. Although, somewhat distant, the methyl group in 3-methylpiperidine does exert some steric influence and its reactivity is lower than that of piperidine or 4-methylpiperidine. The order does not track with the number of α hydrogens (Table 5.2), so the reaction pathway is unlikely to be a metal-mediated reaction (Schemes 5.5-7). Neither

does the order follow the number of β hydrogens, indicating that an elimination reaction (Scheme 5.1) is not involved.

The only species that does not follow this order is 2,6-dimethylpiperidine (Fig. 5.3). This molecule is more hindered than 2-methylpiperidine, yet has higher HDN reactivity on Ni_2P/SiO_2-L. A possible explanation is that the two methyl groups on the carbons around the nitrogen atom impede the substitution reaction not only because of steric hindrance but also because a nucleophilic attack requires inversion around the carbon atom, and the molecule may be too constricted on the surface center. This molecule, however, has 10 hydrogens in the β position, four of which (in the 3 and 5 positions in the ring) are particularly accessible to produce stable di-substituted olefins. For this reason this molecule alone in the sequence may prefer to react by an elimination pathway. It should be noted here that in this study a mixture of cis- and trans- oriented dimethyl species were used. The pure isomers may lead to different pathways.

The results on 2,6-dimethylpiperidine discussed above are in apparent conflict with the findings of Egorova, et al. (24), who found that the order of HDN reactivity was piperidine > 2-methylpiperidine > 2,6-dimethylpiperidine on Ni-Mo-S/Al_2O_3. The discrepancy can be explained from the use of different reaction conditions in the two studies. Compared to the present work the previous investigation employed higher temperature (613 K vs. 520 K for the Table 5.2 results), pressure (5.0 MPa vs. 3.1 MPa), sulfur levels (21,000 wppm vs. 3000 wppm), and amine concentration (17,000 wppm vs. 2000 wppm). Aside from the temperature, the higher pressure, and higher H_2S and amine concentrations will tend to favor the bimolecular S_N2-type reaction, over the elimination reaction. Thus, the observation of the high rates of the substitution reaction in the work of Egorova, et al. (24).

A summary of the likely reaction pathways for the different piperidine derivatives is provided at the bottom of Table 5.2. The unhindered piperidines react by an S_N2-type substitution mechanism, while the hindered 2,6-dimethylpiperidine prefers an E2-type elimination mechanism. The results of this study provide an interesting conclusion. Studies of the reactivity of a family of homologous compounds, although useful in certain cases, are not an appropriate means of identifying a reaction mechanism, because different members of the family can react in different ways. The detailed product distribution from each compound needs to be examined to help ascertain the reaction pathway.

5.4.4. Nature of the Catalyst and Surface Intermediate

Ni_2P/SiO_2-L has been shown to be a highly active, novel hydroprocessing catalyst (43,44,45). The XRD analysis of the catalyst before and after reaction (Fig. 5.1) indicates that the bulk Ni_2P phase is stable at the hydrotreating conditions. The previous studies using EXAFS showed a slight sulfidation of the sample (44,45), which suggested that the active surface phase during the hydrotreating reactions was probably a complex containing both S and P components. The bulk remains Ni_2P, however.

Understanding the behavior of the adsorbed species is desirable for elucidating information about the reaction mechanism. Fourier transform infrared spectroscopy (FTIR) is particularly useful for characterizing acidic sites on hydroprocessing catalysts as shown in Chapter 3. In this study, FTIR measurements of 2-methylpiperidine adsorption were performed on the Ni_2P/SiO_2-L and commercial Ni-Mo-S/Al_2O_3 to obtain insight on the nature of the adsorbed intermediate and the acidic sites on the surface.

The IR spectrum of 2-methylpiperidine adsorbed on the SiO_2-L support (Fig. 5.6) in a helium stream is similar to that of the gas phase molecule (46). The weak peak at 3298 cm^{-1} is due to the N-H stretching in the piperidine. The peaks in the region 3000-2600 cm^{-1} are due to C-H stretching modes (47). The feature centered at 1452 cm^{-1} actually consists of several overlapping peaks which are due to various C-C and C-N stretches. The SiO_2 O-H stretching mode (~3742 cm^{-1}) shows an increase in intensity after 2-methylpiperidine adsorption at 373 K and heating to 573 K. Being a negative peak, this indicates that the concentration of free hydroxyls rises as the temperature is raised. The intensity of all other features decreases rapidly as the temperature is increased up to 573 K, which indicates a decrease in their concentration. All these results are indicative of desorption of the 2-methylpiperidine as the temperature is raised, with little remaining adsorbed over 473 K. The lack of substantial band shifts from the gas-phase spectrum indicates that the 2-methylpiperidine is adsorbed weakly on SiO_2, probably via hydrogen bonding with the silanol groups. The hydrogen bonding probably perturbs the N-H band, which shows low intensity.

The FTIR spectrum of 2-methylpiperidine adsorbed on the Ni_2P/SiO_2-L catalyst in a helium stream is different from that on the SiO_2-L support. In the hydroxyl region there are two negative peaks at 3742 and 3670 cm^{-1} rather than a single negative peak at 3741-3744 cm^{-1}. In the N-H stretching region at 3249 cm^{-1} a prominent shoulder is displayed on a rising background whereas on the SiO_2-L the band appeared at 3298 cm^{-1}, but only at the lowest temperature. In the C-H stretching region (3000-2700 cm^{-1}) the major features are retained but there are small shifts in the peak positions. In the low wavenumber region there is a new prominent feature at 1618 cm^{-1}, which falls in the region of NH_2 scissor bending

modes. At the lowest wavenumber, in the region of C-C and C-N stretches, again a combination of bands appears centered at 1454 cm^{-1}, but with a different intensity pattern and lesser breath. The major changes observed, especially the appearance of the strong NH_2 scissors mode, are consistent with the formation of a piperidinium ion. The interaction with the Ni_2P/SiO_2-L surface is clearly stronger than that of piperidine with the SiO_2 surface, as the adsorbed species is retained strongly at 473 K and diminish only at 573 K. On the SiO_2-L the adsorbed species is mostly desorbed at 473 K.

The question arises as to the identity of the acid site that forms the piperidium ion. Clearly the silanol groups on the SiO_2, indicated by the band of 3742 cm^{-1}, are not acidic enough for the protonation. The O-H feature at 3670 cm^{-1}, whose concentration increased as that of piperidium ion decreased, was likely to be involved. In order to obtain insight about that feature, measurements were made with PO_x/SiO_2-L as well as with Ni_2P/SiO_2-L samples prepared with different initial Ni/P ratio. The results are shown in Figure 5.8. The PO_x/SiO_2-L sample shows bands at 3741 and 3660 cm^{-1} due to O-H groups associated with the SiO_2 and PO_x components respectively. The band at 3660 cm^{-1} is close to that of the Ni_2P/SiO_2-L catalyst at 3668 cm^{-1}. Moreover in the Ni_2P catalyst prepared with less initial phosphorus the band is decreased. These results suggest that the O-H groups are associated with the phosphorus component in the Ni_2P/SiO_2-L catalyst. The O-H groups are similar to those found on PO_x/SiO_2-L but not the same. A representation is provided in Figure 5.11. The top drawing shows the PO_x/SiO_2-L retained with P-OH groups, while the bottom drawing shows the Ni_2P/SiO_2-L catalyst. There are P-OH groups here also, but associated with the Ni. The oxygen in the hydroxyl groups probably comes from incompletely reduced phosphate species formed during the passivation step of the preparation.

A previous study has shown that the PO-H groups on phosphates are not capable of forming pyridinium ions when using pyridine as a probe molecule (49). The finding that the PO-H group can readily protonate 2-methylpiperidine to form 2-methylpiperidium ions can be explained by the difference in the basicity of the molecules. Piperidine ($pK_a = 11.0$) is more basic than pyridine ($pK_a = 5.2$) because the N lone pair is not involved in aromatic bonding. Also, the methyl group located on the α position of the piperidine acts as an electron donor further increasing the basicity of the molecule.

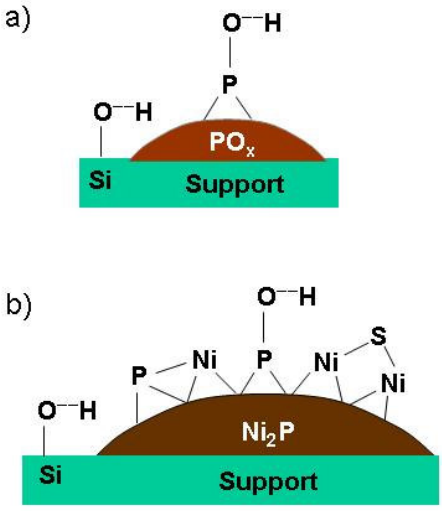

Figure 5.11. Proposed structural models of a) PO_x/SiO_2-L and b) Ni_2P/SiO_2-L.

The decrease in the peak intensity of the terminal SiO_2 O-H stretching modes on the PO_x/SiO_2-L at 3741 cm^{-1} suggests that PO_x is deposited close to the terminal silanols on SiO_2. This is not observed in the Ni_2P/SiO_2-L samples. Also, the increase in P content of the Ni_2P precursor does not affect the SiO-H stretching mode but does increase the intensity of the phosphorus O-H stretching mode. This implies that the P precursor in the preparation of Ni_2P does not form PO_x on the support, but that the P-OH groups are generated on the Ni_2P particles (Fig. 5.11).

The spectra of 2-methylpiperidine taken in a reactive 10% H_2S/H_2 gas stream on Ni_2P/SiO_2-L are very similar to those obtained with He (Fig. 5.9). Again, all the features due to the piperidinium ion are reproduced, albeit with small shifts, including the shoulder at 3247 cm^{-1} due to the N-H stretches, the bands at 3000-2700 cm^{-1} due to the C-H stretches, the strong band at 1616 cm^{-1} due to the NH_2 scissors mode, and the feature at 1456 cm^{-1} due to C-C and C-N stretches. Although diminished in intensity the bands persist without change up to 573 K, close to the temperature at which the reactivity studies were made. This suggests that the reactive intermediate is a piperidinium ion.

Exactly the same situation is found for the adsorption of 2-methylpiperidine on Ni-Mo-S/Al_2O_3 with the 10% H_2S/H_2 stream. Although slightly shifted, the same peaks are observed on this catalyst up to reaction temperature, suggesting again that a piperidinium ion is a reactive intermediate.

For Ni-Mo-S/Al_2O_3, a single negative peak is observed at 3675 cm^{-1} with a small shoulder at 3735 cm^{-1}. This commercial catalyst incorporates phosphorus as a promoter, and the peak is due to O-H modes associated with the phosphorus. However, the precise location of the phosphorus is uncertain. It is likely to be on the support as the peak has been

observed for phosphorus-doped Al_2O_3 supports, for which it is reported that two main bands occur in the O-H stretching region at 3750-3710 cm^{-1} and 3675 cm^{-1} corresponding to Al O-H and P O-H stretching modes, respectively (48, 49). This indicates that the commercial Ni-Mo-S/Al_2O_3 has an $AlPO_4$ phase on the surface. In his review of HDN Prins has suggested that a nickel phosphide might form on P-promoted Ni-Mo-S/Al_2O_3 catalysts (13), and this remains a possibility.

The 2-mepiperidinium ion is also formed on the Ni-Mo-S/Al_2O_3 catalyst but the relative intensity of the peak at 1455 cm^{-1} due to the piperidine ring relative to the peak at 1598 cm^{-1} is much higher than that on the Ni_2P/SiO_2-L samples at temperatures below 473 K. This can be attributed to weak adsorption of 2-methylpiperidine on Lewis acid sites on the Al_2O_3 support.

Overall, the FTIR study suggest that the P-OH group located either on Ni_2P particles in Ni_2P/SiO_2-L or on the support $AlPO_4$ phase or a phosphide phase in commercial Ni-Mo-S/Al_2O_3 plays a key role to protonate 2-methylpiperidine to form 2-methylpiperidinium ion as an intermediate species.

5.4.5. Mechanistic Steps

The findings about the nature of the catalyst surface (Fig. 5.11), the elimination reaction pathway, and the likely piperidinium ion intermediate can be used to propose a reaction mechanism. The steps are presented in Scheme 5.11.

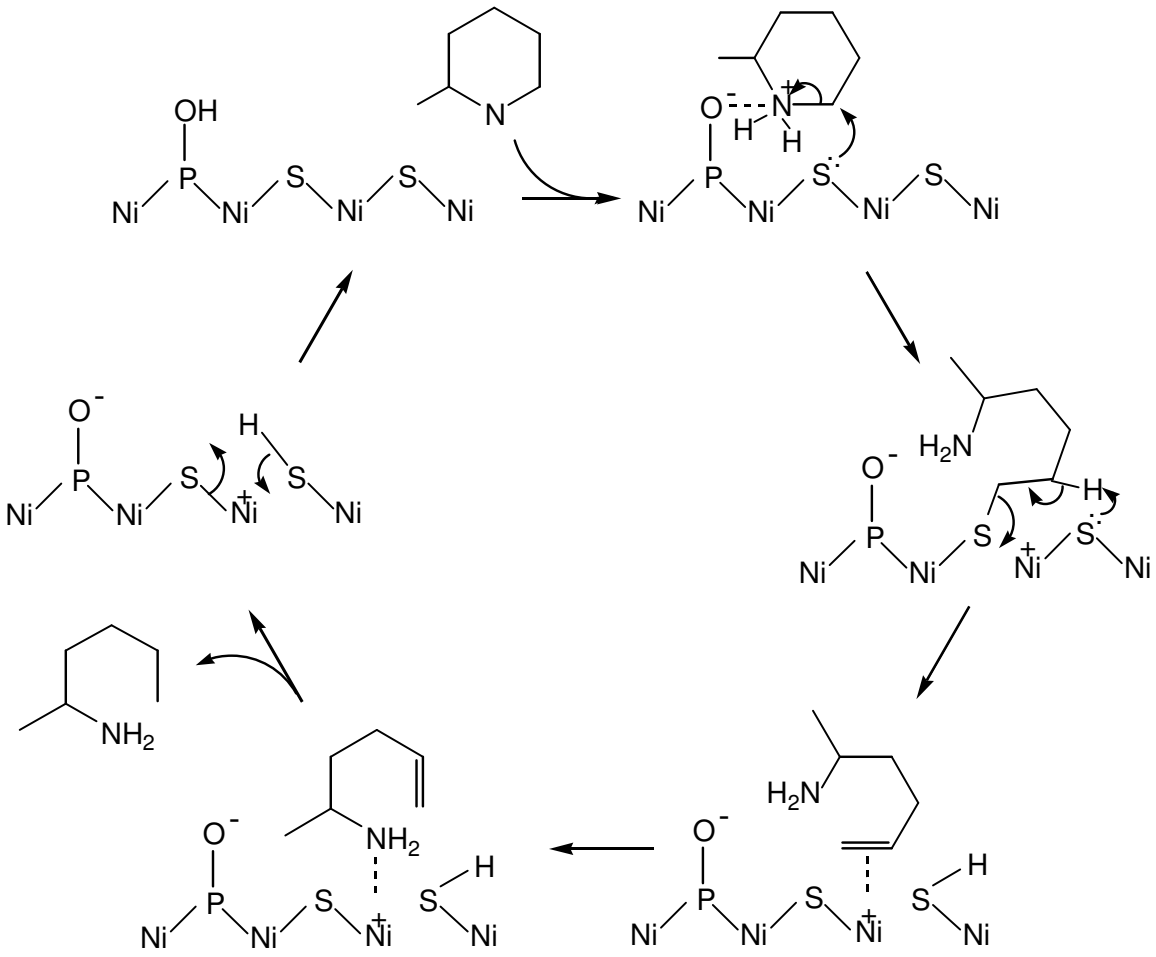

Scheme 5.11. Proposed Mechanism for Denitrogenation

At the top left of the scheme is a depiction of the nickel phosphide surface. It illustrates the presence of hydroxyl groups associated with phosphorus, and the coverage of part of the nickel sites with sulfur. As discussed earlier, evidence for the presence of sulfur is provided by EXAFS studies of the catalyst after HDN (45). A 2-methylpiperidine molecule interacts with this surface to form an adsorbed piperidinium ion, the species that is observed by FTIR. The lone pairs on a suitably positioned sulfur atom carry out a nucleophilic attack on the open side of the piperidinium ring. This causes bond

displacement that results in formation of a secondary amine tethered to the surface through a C-S bond. This ring-opening reaction is a substitution reaction (Scheme 5.3), deduced to occur in the product distribution studies. It is likely to be the rate-determining step, since the piperidinium ion involved is the main species observable, and its high concentration is consistent with its participation in a slow reaction. The C-S bond in the resulting amine intermediate is weak and the species can react rapidly in a variety of ways, including direct hydrogenation. Another possibility is discussed below, but it's features are not important kinetically, since they occur after the rate-determining step.

The surface bound amine can undergo an elimination reaction by attack of another sulfur atom, this time acting as a base, to abstract a β-hydrogen. Elimination reactions on sulfur species are much easier than in nitrogen compounds because of the weakness of the C-S bond. As shown on the bottom right of Scheme 5.11, the resulting olefin is weakly coordinated to the metal center, but undergoes an intermolecular displacement by the more strongly basic amine. This species is held fairly strongly, and the free double bond is hydrogenated on another site (not shown), and the 2-aminohexane desorbs. This is the initial intermediary species observed in the reactivity studies. The reactions depicted thus far, leave a surface with an ionized P-O^- group and a proton. A number of bond shifts readily regenerate the fresh surface.

The mechanism shown in Scheme 5.11 should be considered schematic, as other representations of surface atoms exist. Nevertheless, the scheme captures the essential features of the reaction process: the involvement of a piperidinium ion intermediate, the occurrence of a nucleophilic substitution reaction, and the production of 2-aminohexane as a

primary product. The complex nature of the site is consistent with the observed structure-sensitivity of the HDN reaction on nickel phosphide (43,44).

Regardless of the interpretation of the mechanism, one of the fundamental findings of this study is that the behavior of the nickel phosphide catalyst is very similar to that of Ni-Mo sulfide catalyst. Like the sulfide the phosphide is well able to carry out the substitution mechanism. What remains to be accounted for is the remarkable activity of the phosphide in HDN in the presence of sulfur compounds which surpasses that of the sulfide on an active site basis (43,44).

5.5. Conclusions

The mechanism of hydrodenitrogenation in the presence of sulfur was studied on silica-supported nickel phosphide (Ni_2P/SiO_2-L) and a commercial promoted sulfide (Ni-Mo-S/Al_2O_3) in a three-phase packed-bed reactor at 3.1 MPa and 450-600 K. The product distribution as a function of contact time showed that the primary product was 2-aminohexane in both catalysts, indicating that the preferred pathway was an S_N2-type substitution reaction. The Ni_2P/SiO_2-L catalyst was also used to study the relative rates of denitrogenation of a series of methyl-substituted piperidines of different structure. It was found that the order of reactivity was 4-methylpiperidine ~ piperidine > 3-methylpiperidine > 2,6-dimethylpiperidine > 2-methylpiperidine. The primary factor determining the reactivity of the molecules was the accessibility of the α-carbons next to the N atoms. A secondary factor was the availability and reactivity of the β-H atoms. Overall, the reaction of the substituted piperidines could be explained by the occurrence of independent mechanisms involving S_N2 substitution for unhindered piperidines or E2 elimination for

hindered piperidines. FTIR measurements of 2-methylpiperidine adsorption on the Ni_2P/SiO_2-L and Ni-Mo-S/Al_2O_3 catalysts at close to reaction conditions indicated the formation of a piperidinium ion intermediate associated with P O-H groups on the surface of both catalysts. A reaction mechanism was deduced involving initial quarternization of piperidine followed by nucleophilic attack on an open α carbon by a surface sulfur atom.

References

1. P. Zeuthen, K. G. Knudsen, and D. D. Whitehurst, Catal. Today, 65 (2001) 307.
2. J. R. Katzer, R. Sivasubramanian, Catal. Rev.-Sci. Eng. 20 (1979) 155.
3. C. N. Satterfield, M. Modell, R. A. Hites, and C. J. Declerck, Ind. Eng. Chem. Proc. Des. Dev. 17 (1978) 141.
4. A. Olalde and G. Perot, Appl. Catal. 13 (1985) 373.
5. T. C. Ho, Catal. Rev.-Sci. Eng. 30 (1988) 117.
6. S. C. Kim and F. E. Massoth, Ind. Eng. Chem. Res. 39 (2000) 1705.
7. M. G. McIlvried, Ind. Eng. Chem. Proc. Des. Dev. 10 (1971) 125.
8. R. T. Hanlon, Energy Fuels 1 (1987) 424.
9. A. Kherbeche, R. Hubaut, J. P. Bonnelle, and J. Grimblot, J. Catal. 131 (1991) 204.
10. M. Cerný, Collec. Czech. Chem. Commun. 47 (1982) 928.
11. G. C. Hadjiloizou, J. B. Butt, and J. S. Dranoff, Ind. Eng. Chem. Res. 31 (1992) 2503.
12. G. Perot, Catal. Today 10 (1991) 447.
13. R. Prins, Adv. Catal. 46 (2001) 399.
14. M. Cattenot, J. Portefaix, J. Afonso, M. Breysse, M. M. Lacroix, and G. Perot, J. Catal. 173 (1998) 366.
15. V. Schwartz, V. T. da Silva, and S. T. Oyama, J. Mol. Catal. A, 163 (2000) 251.
16. K. S. Lee, H. Abe, J. A. Reimer, and A. T. Bell, J. Catal. 139 (1993) 34.
17. N. Nelson and R. B. Levy, J. Catal. 58(1979) 485.
18. J. A. Marzari, S. Rajagopal, and R. Miranda, Prepr. - Am. Chem. Soc., Div. Pet. Chem. 38 (1993) 669.
19. P. Clark, X. Wang, and S. T. Oyama, J. Catal. 207 (2002) 256.

20. J. A. Marzari, S. Rajagopal, and R. Miranda, J. Catal. 156 (1995) 255.

21. M. Jian and R. Prins, J. Catal. 179 (1988) 18.

22. F. Rota and R. Prins, J. Catal. 202 (2001) 195.

23. F. Rota, V. S. Ranade, and R. Prins, J. Catal. 200 (2001) 389.

24. M. Egorova, Y. Zhao, P. Kukula, and R. Prins, J. Catal. 206 (2002) 263.

25. S. Rundqvist, Acta Chem. Scand. 16 (1962) 992.

26. S. Ted Oyama and Y.-K. Lee, J. Phys. Chem. B in print.

27. A. P. Legrand, H. Hommel, and A. Tuel, Adv. Col. Interface Sci., 33 (1990) 91.

28. M. J. Ledoux, in Catalysis, Vol. 7, The Chemical Society, London, 1988, pp. 125-148.

29. A. W. Hofmann, Ber. Dtsch. Chem. Ges. 14 (1881) 659.

30. C. N. Satterfield and S. Gültekin, Ind. Eng. Chem. Proc. Des. Dev. 20 (1981) 62.

31. S. H. Yang and C. N. Satterfield, J. Catal. 81 (1983) 168.

32. G. Perot, S. Brunet, C. Canaff, C. and H. Toulhoat, Bull. Soc. Chim. Belg. 96 (1987) 865.

33. R. H. Fish, J. N. Michaels, R. S. Moore, and H. Heinemann, J. Catal. 123 (1990) 74.

34. M. J. Ledoux, and M. Sedrati, J. Catal. 83 (1983) 235.

35. S. Rajagopal, T. L. Grimm, D. J. Collins, and R. Miranda, J. Catal. 137 (1992) 453.

36. R. M. Laine, Catal. Rev.-Sci. Eng. 25 (1983) 459.

37. R. M. Laine, J. Molec. Catal. 21 (1983) 199.

38. R. M. Laine, Ann. N. Y. Acad. Sci. 415 (1983) 271.

39. J. Sonnemans, W. J. Neyens, and P. Mars, J. Catal. 34 (1974) 230.

40. J. L. Portefaix, M. Cattenot, M. Guerriche, J. Thivolle-Cazat, and M. Breysse, Catal. Today 10 (1991) 473.

41. F. de Angelis, I. Grgurina, and R. A. Nicoletti, Synthesis 1 (1979) 70.

42. Y. Zhao and R. Prins, J. Catal. 222 (2004) 532.

43. S. T. Oyama, X. Wang, .Y.-K. Lee Bando, and F. G. Requejo, J. Catal. 210 (2002) 207.

44. X. Wang, P. Clark, and S. T. Oyama, J. Catal. 208 (2002) 321.

45. S. T. Oyama, X. Wang, Y.-K. Lee, and W.-J. Chun, J. Catal. 221 (2004) 263.

46. S. E. Stein, "Infrared Spectra " in NIST Chemistry WebBook, NIST Standard Reference Database Number 69, Eds. P.J. Linstrom and W.G. Mallard, March 2003, National Institute of Standards and Technology, Gaithersburg MD, 20899 (http://webbook.nist.gov).

47. D. Lin-Vien, N. B. Colthup, W. G. Fateley, and J. G. Grasselli, The Handbook of Infrared and Raman Characteristic Frequencies of Organic Molecules, Academic Press, Boston, 1991, pp 155-178.

48. J. A. R. van Veen, P. A. J. M. Hendriks, R. R. Andrea, E. J. G. M. Romers, and A. E. Wilson, J. Phys. Chem. 94 (1990) 5282.

49. C. Morterra, G. Magnacca, and P. P. De Maestri, J. Catal. 152 (1995) 384.

Chapter 6

Conclusions

A number of nickel phosphide (Ni_2P) catalysts supported on siliceous supports of different surface area ranging from SiO_2-L (90 $m^2 g^{-1}$), SiO_2-H (350 $m^2 g^{-1}$) to MCM-41 (789 $m^2 g^{-1}$), and KUSY (784 $m^2 g^{-1}$) were prepared by reduction of phosphate precursors. Surface and structural properties of the supported Ni_2P catalysts were examined by Fourier transform infrared (FTIR) spectroscopy, X-ray diffraction (XRD), and X-ray absorption spectroscopy. Catalytic activities of the supported Ni_2P catalysts and a commercial Ni-Mo-S/Al_2O_3 catalyst were tested for hydrodesulfurization (HDS) of 4,6-DMDBT, hydrodenitrogenation (HDN) of quinoline, and hydrogenation (HYD) of tetralin.

Study of the products of HDS of 4,6-DMDBT at 573 K and 3.1 MPa showed that the hydrogenation pathway was dominant for both nickel phosphide catalysts and a reference Ni-Mo-S/Al_2O_3 catalyst. However, the Ni_2P/SiO_2-H (240 $cm^2 g^{-1}$) catalyst exhibited much higher activity in the HDS of 4,6-DMDBT and better resistance to nitrogen (quinoline) than the Ni-Mo-S/Al_2O_3 catalyst, indicating substantial potential for nickel phosphide catalysts in the deep HDS area. The surface properties of the Ni_2P/SiO_2-H and Ni-Mo-S/Al_2O_3 catalysts were examined by FTIR measurements of CO and pyridine. The results revealed that the Ni_2P catalyst had a high electron density and was able to form π-back bonded CO species on the Ni site, while the Ni-Mo-S/Al_2O_3 catalyst adsorbed CO only weakly. The Ni_2P catalyst also had moderate acidity in the form of PO-H sites able to protonate pyridine species, which

were not observed for the Ni-Mo-S/Al_2O_3 catalyst. It was concluded that the bifunctional nature of the Ni_2P catalyst contributed to the higher activity in the hydrotreating reaction.

The effect of dispersion of Ni_2P particles supported on different surface area SiO_2-L (90 $m^2 g^{-1}$), SiO_2-H (350 $m^2 g^{-1}$), and MCM-41 (789 $m^2 g^{-1}$) supports was studied. The presence of the Ni_2P phase on the SiO_2 supports was confirmed by X-ray diffraction (XRD) measurements, but no Ni_2P peaks were observed for the Ni_2P/MCM-41 sample due to the high dispersion of the Ni_2P particles. However, EXAFS measurements showed the formation of the Ni_2P phase on this support. The activity in the HDS of 4,6-DMDBT at 613 K and 3.1 MPa was higher on the more dispersed catalysts in the order Ni_2P/MCM-41 (487 $m^2 g^{-1}$) > Ni_2P/SiO_2-H (240 $m^2 g^{-1}$) > Ni_2P/SiO_2-L (88 $m^2 g^{-1}$), which correlated well with the number of active sites measured by CO chemisorption. Also, smaller Ni_2P particles showed better resistance to sulfur (dimethyldisulfide) and did not suffer loss of active sites during reaction. EXAFS line shape analysis revealed that smaller Ni_2P particles had shorter Ni-P distances and higher Ni-P coordination together with longer Ni-Ni bond distances, indicating a stronger interaction of Ni-P between Ni and P in dispersed Ni_2P particles. Larger particles had shorter Ni-Ni distances which led to sulfidation, particularly under high S condition in the feed and at relatively high temperature.

The effect of Ni_2P loading and initial Ni/P ratio on the hydroprocessing performance of Ni_2P catalysts supported on potassium ion-exchanged ultra stable Y zeolite (KUSY) were investigated at 3.1 MPa and 603 K. The Ni_2P/KUSY catalyst with a loading level of 12 wt % Ni_2P gave rise to the formation of homogeneous particles of size 1–4 nm, which were likely situated in the mesoporous cavities or at the external surface of the zeolite crystal, and showed high and stable activity in HDS of 4,6-DMDBT. A sample with higher loading of

23 wt % Ni_2P led to the formation of larger particles of size over 20 nm and showed lower activity due to poor dispersion and pore blocking. The initial Ni/P ratio in the preparation of Ni_2P had a significant effect on the catalyst structure and its activity. Use of Ni/P ratio = 1/0.5 led to a deficiency of P in the Ni_2P phase and resulted in deactivation in the HDS. Use of a Ni/P ratio = 1/2 resulted in high and stable catalytic activity. EXAFS analysis of the catalysts revealed that the addition of extra P led to an increase in Ni-P coordination and lengthening in Ni-Ni bond distances, indicating a strong interaction between Ni and P components in Ni_2P. Lower P content led to a decrease in Ni-Ni distances and favored sulfidation during reaction.

The mechanism of hydrodenitrogenation (HDN) of 2-methylpiperidine was studied over a Ni_2P/SiO_2-L (88 $m^2 g^{-1}$) catalyst and a commercial Ni-Mo-S/Al_2O_3 catalyst at 3.1 MPa and 603 K. Analysis of the product distribution as a function of contact time indicated that the reaction proceeded in both cases predominantly by a substitution mechanism. Fourier transform infrared spectroscopy (FTIR) of the 2-methylpiperidine indicated that a piperidinium ion intermediate was formed on both the sulfide and the phosphide. It was concluded that the mechanism of HDN on nickel phosphide is very similar to that on sulfides.

Nickel phosphides exhibit increased catalytic activities and higher stability to sulfur and nitrogen compounds over commercial sulfide catalysts on a site basis. For further application it is desirable to develop well dispersed phosphides on high density support materials for effective catalyst loading. Additional metal phosphides could be developed into hydroprocessing catalysts. For example, it is interesting and relevant to apply bimetallic phosphides such as NiMoP, $NiMoP_2$, and $NiMo_2P_3$.

The kinetic expression for the HDS of 4,6-DMDBT needs to be developed considering the nature of the active sites on the catalysts. It is also necessary to consider the effect of nitrogen and aromatic compounds to clarify their competitive adsorption on the active sites. Careful analysis of the rates of each reaction type as a function of the presence of the other molecules could reveal a general governing kinetic theory.

Vita

Yong-Kul Lee

The author, Yong-Kul Lee was born in Seoul, Korea in 1973. Upon graduation with a B.S. degree in Chemical Engineering at Inha University in 1996, he enrolled in a master program in the Chemical Engineering Department of the Seoul National University. After graduating in 1998, he was employed as a researcher at the Institute of Chemical Processes. In early 2000, he started work on his Ph.D. degree in the Chemical Engineering Department at Virginia Polytechnic Institute and State University.